THESIS

submitted to

THE FACULTY OF SCIENCE OF ROUEN UNIVERSITY

for the degree of Doctor of Philosophy

Discipline: Physics

Speciality: Energy

by

Keli JIANG

Theoretical Study of Light Scattering by an Elliptical Cylinder

Defense on June 24, 2013

Supervisor

Professor Kuan Fang REN

Composition of Jury:

Reviewers:	
Fabrice ONOFRI	Director of research at CNRS, IUSTI, Marseille, France
Xiang'e HAN	Professor at Xidian University, School of Science, Xi'an, China
Examiners:	
Denis LEBRUN	Professor at Rouen University, CORIA-UMR 6614, Rouen, France
Loïc MÉÈS	Research fellow at CNRS, LMFA, Ecole centrale de Lyon, France
Bernard POULIGNY	Director of research at CNRS, CRPP, Bordeaux, France
Claude ROZÉ	Professor at Rouen University CORIA-UMR 6614, Rouen, France
Kuan Fang REN	Professor at Rouen University, CORIA-UMR 6614, Rouen, France
Invited member:	
Richard Lee PANETTA	Professor at Texas A&M University, USA

THESE

présentée

A LA FACULTE DES SCIENCES DE L'UNIVERSITE DE ROUEN

en vue de l'obtention du Doctorat

Discipline : Physique

Spécialité: Energétique

par

Keli JIANG

Etude Théorique de Diffusion de la Lumière par un Cylindre Elliptique

Soutenue le 24 Juin 2013

Directeurs de thèse

Professeur Kuan Fang REN

Membres du jury:

Rapporteurs:	
Fabrice ONOFRI	Directeur de recherche au CNRS, IUSTI, Marseille, France
Xiang'e HAN	Professeur à l'Université de Xi'an, Chine
Examinateurs:	
Denis LEBRUN	Professeur à l'Université de Rouen, CORIA-UMR 6614, Rouen, France
Loïc MÉÈS	Chargé de recherche au CNRS, LMFA, Ecole centrale de Lyon, France
Bernard POULIGNY	Directeur de recherche au CNRS, CRPP, Bordeaux, France
Claude ROZÉ	Professeur à l'Université de Rouen, CORIA-UMR 6614, Rouen, France
Kuan Fang REN	Professeur à l'Université de Rouen, CORIA-UMR 6614, Rouen, France
Invite:	
Richard Lee PANETTA	Professeur à de Texas A&M University, Etats-Unis

.

L'arc-en-ciel est une merveille de la Nature si remarquable, et sa cause a été de tout temps si curieusement recherchée par les bons esprits, et si peu connue, que je ne saurais choisir de matière plus propre à faire voir comment, par la méthode dont je me sers, on peut venir à des connaissances que ceux dont nous avons les écrits n'ont point eues.

Les Météores
René Descartes

Acknowledgements

This thesis is supported by the China Scholarship Council. This work was also partially supported by the French National Research Agency under the grant ANR-09-BLAN-023-02 “CARMINA”.

My deepest gratitude goes first and foremost to Professor Kuan Fang REN, my supervisor, for his constant encouragement and excellent guidance. His creative idea and excellent insight into the physical phenomenon bring me a open mind to do research work. Without his consistent and illuminating instruction, my thesis could not have reached its present form.

Second, I would like to express my heartfelt gratitude to Professor Xiang'e HAN. It is her encouragement and supports, which give me confidence to study abroad. Moreover, her attitude of work triggers my love for science since I follow her for my master supervisor.

Thanks are also due to the members of the jury, Dr. Fabrice ONOFRI, Professor Denis LEBRUN, Dr. Loïc MÉÈS, Professor Bernard POULIGNY and Professor Claude ROZÉ for examining. I would like to thank all of them for their patience in reading the manuscript as well as for their precious comments.

Most of all, I would like to thank my family and friends for their unwavering support and encouragement. Those are my greatest source of strength and inspiration.

Contents

List of Symbols and Abbreviations

Abbreviations

DDA	:	Discrete Dipole Approximation
FDM	:	Finite Difference Method
GLMT	:	Generalized Lorenz-Mie Theory
GO	:	Geometrical Optics
LMT	:	Lorenz-Mie Theory
MOM	:	Method of Moment
SVM	:	Separation of Variable Method
VCRM	:	Vectorial Complex Ray Model

Roman Symbols

a	:	radius of particle
A	:	rotation matrix
$\boldsymbol{b}$	:	base vector perpendicular to the incident plane
$\boldsymbol{c}$	:	base vector perpendicular to the incident wave vector $\boldsymbol{k}$ and $\boldsymbol{b}$
$\boldsymbol{c}'$	:	base vector perpendicular to the refracted wave vector $\boldsymbol{k}'$ and $\boldsymbol{b}$
$\boldsymbol{c}^l$	:	base vector perpendicular to the reflected wave vector $\boldsymbol{k}^l$ and $\boldsymbol{b}$
C	:	curvature matrix of dioptric surface
$\mathcal{D}$	:	the divergence factor in VCRM
D	:	divergent factor in GO
$\boldsymbol{E}^i$	:	incident electric field
$\boldsymbol{E}^{int}$	:	internal electric field
$\boldsymbol{E}^s$	:	scattering electric field
E_0	:	amplitude of incident electric field
F	:	implicit function of isophase of wave
$\boldsymbol{H}^i$	:	incident magnetic field
$\boldsymbol{H}^{int}$	:	internal magnetic field
$\boldsymbol{H}^s$	:	scattered magnetic field
H_n	:	Hankel function
H	:	Hessian function
$H*$	:	adjoint of Hessian function
I	:	scattered intensity
J_n	:	Bessel function
k_n	:	component of wave vector in normal direction
k_τ	:	component of wave vector in tangent direction
$\boldsymbol{k}$	:	incident wave vector
$\boldsymbol{k}'$	:	refracted wave vector
$\boldsymbol{k}^l$	:	reflection wave vector
l_u	:	Rayleigh length in u direction
l_v	:	Rayleigh length in v direction

m_0	:	refractive index of surrounding medium
m	:	refractive index of particle
m_i	:	imaginary part of the refractive index of particle
$\boldsymbol{n}$	:	the normal of surface
p	:	order of ray
Q	:	curvature matrix of incident wave
Q'	:	curvature matrix of refracted/refleced wave
R_1	:	one of the curvature radii of a wavefront
R_2	:	one of the curvature radii of a wavefront
R'_{11}	:	one of the curvature radii of the refracted/reflected wavefront
R'_{12}	:	one curvature radius of refracted/reflected wavefront
R_u	:	the curvature of wave front in u direction
R_v	:	the curvature of wave front in v direction
r	:	Fresnel reflection coefficient
S	:	scattered amplitude
S_G	:	complex amplitude of incident beam
S_d	:	complex amplitude of diffraction wave
$\boldsymbol{s}_1$, $\boldsymbol{s}_2$	:	principal directions of the dioptric surface
$\boldsymbol{t}_1$, $\boldsymbol{t}_2$	:	principal directions of the wavefront
w_0	:	waist radius of a circular Gaussian beam
w_u	:	waist radius an elliptical Gaussian beam in u direction
w_v	:	waist radius of an elliptical Gaussian beam in v direction

Greek Symbols

α	:	parameter size of the particle
ζ	:	angle between the incident wave and z axis
θ_i	:	incident angle
θ_r	:	refracted angle
θ'	:	deviation angle
θ	:	scattering angle
θ_{rg}	:	geometrical rainbow angle
Θ	:	projection matrix
κ_G	:	Gaussian curvature
κ_M	:	mean curvature
λ	:	wavelength
ξ	:	absorbing factor or angle between the incident wave and x axis
ρ_1	:	one of curvature radius of a dioptric surface
ρ_2	:	one of curvature radius of a dioptric surface
τ	:	angle between incident ray and dioptric surface
τ'	:	angle between refracted ray and dioptric surface
$\boldsymbol{\tau}$	:	unit vector tangent to the cylinder surface
ϕ_F	:	phase shift due to Fresnel coefficient
ϕ_T	:	phase shift due to total reflection
ϕ_{PH}	:	phase shift due to optical path
ϕ_{FL}	:	phase shift due to focal lines
ϕ_p	:	total phase shift
φ	:	phase function of the incident wave

Subscripts or superscripts

X	:	1 for perpendicular state and 2 for parallel state
$\perp$	:	electric field perpendicular to the incident plane
$\parallel$	:	electric field parallel to the incident plane

Chapter 1

Introduction

In nature, light can be observed directly from its source, such as the light from stars, lamps or fire. However, most of the light we see arrive at our eyes indirectly: the light from the moon is just the reflection of the light emitted by the sun, the blue sky is due to the scattering of sun light by molecules constituting the atmosphere, the marvel of rainbow is nothing more than the refraction of light by raindrops.

The human has being always interested in those phenomena because of two main reasons. The first is due to the curiosity. From antiquity, we are anxious to understand the mysteries of nature. As early as the seventeenth century, Descartes gave a very satisfactory mathematical explanation of the rainbows with his newly established geometrical optics [1]. The multicolored arches often found in the east in the afternoon are due to the refraction and the internal reflection of light rays on the surface of water droplets. The dependence of the refractive index of the particle on the wavelength (color) of the sunlight makes the different colors at different directions, so forming the multicolored arches. The red (or orange) color of the sun in the morning or in the evening as well as the blue sky can both be explained by the Rayleigh theory: the scattering efficiency of molecules and very small particles in the air decreases dramatically with the wavelength of the light. So the red color light (i.e. large wavelength) is easy to go through the thick atmosphere than the blue one while the later is more scattered in the sky.

The second reason is that the knowledge acquired in understanding those phenomena serves us in the development of new measurement technologies. When the light interacts with particles, or more generally, with any objects, the light scattered from them depends on their properties. By measurement of different quantities of the

scattered light: intensity, polarization, spectrum, etc. we may deduce the characteristics of particle: size, shape, temperature and material (via refractive index). For example, the rainbow refractometry techniques has since long been used to measure the refractive index and the size of spherical particles and circular cylinders. Since the invention of laser, the optical metrology has got a tremendous boom. Many traditional techniques have been considerably improved and much more new techniques are being developed. All these wonderful successes are based on the achievement of the fundamental research on the theory of the interaction of light with particles – this is just the initial motivation of the thesis.

In the environment control, the biochemistry, the fluid mechanics and the combustion fields, it is essential to measure the characteristics of particles whose size often ranges from a few tens of nanometers to several hundreds of micrometers. According to the characteristics of the particles to be measured, various optical techniques have been developed. For example, the diameter of wires can be measured by diffraction. Most of these instruments use, as a scattering model, the Fraunhofer diffraction, the measurement precision can be improved by more rigorous theory – Lorenz-Mie theory (LMT) [2, 3, 4]. Thus the size of the fibers of wool or metals in industry can be measured with same techniques by supposing the cylinder to be circular. In fluid mechanics, especially what concerns the injection of oil in the internal combustion motor, the instability and the breakup of the liquid jets are an essential problem in the atomization since the structure of jet is often very complex [5, 6, 7, 8]. A free jet is not circular cylindrical even in the most stable case. The size, the temperature and the composition of individual droplets or droplet system generated in such process can be measured by rainbow refractometry techniques [9], the Phase Doppler Interferometry [10] or some hybrid techniques. However, almost in all cases, the particles are supposed to be perfectly spherical or circular cylindrical while the real shape of the particles have rarely so ideal shapes. The research on the interaction of complex shaped (non-spherical / non-circular cylindrical) particles is a challenge in the development of optical metrology in very large scope of applications.

Among the non-spherical particles, the infinite circular cylinder is the simplest and the associated scattering problem can be dealt with by the similar manner as for the spherical case. Many researchers have contributed to the research work for circular cylinder scattering [11, 12, 2, 6, 13, 14, 15]. However, most particles in the nature and in industrial process are neither spherical nor circular cylindrical. In the ink-jet printing for instance, it is very important to understand the physics involved in

the precise manipulation of liquid jets and droplets [16]. In the atomization process, the instability and the breakup of the jet depend much on the structure of injector and also the properties of the liquid (temperature, viscosity, pressure). The precise measurement of the 3D structure of jets are essential to understand the mechanism of atomization and for the design of more efficient injectors. The elliptical shape is the first order approximation of real non-circular cylinder and can provide good understanding of the influence of the non-circularity on the scattering properties. Moreover, the elliptical cylinder is also an useful model in the design of antennas and the detection of objects by radar [17, 18, 19]. The scattering of acoustic waves by an elliptical cylinder finds also important applications [20, 18]. Therefore, the study of the scattering of cylinder of elliptical section is fundamental not only in the development of optical metrology, but also in the electromagnetism theory and in the acoustics theory.

Particles light scattering theories and models

Many theories and models have been developed to describe the elastic interaction between light and particles, which provide the basis for optical metrology. They can be categorized into three groups: rigorous theories, approximate models and numerical methods.

Rigorous theories are based on the solution of the Maxwell equations with a method of a separation of the varieties. The most classical one is the Lorenz-Mie theory (LMT) which deals with the scattering of a plane wave by a homogeneous isotropic spherical particle. LMT is often used as a reference to validate other methods. Similar theories are also developed for regular shaped particles whose surface corresponds to a mathematical coordinates system: spheroid, ellipsoid, infinite circular or elliptical cylinder. One of the most important advantages of those theories is that they provide rigorous solutions for scattering problem. However, the special functions involved in such theories are often difficult to evaluate. Except for the spherical particle and infinite circular cylinder, the size of the particle which can be calculated with the algorithms and computers can rarely reach a hundred wavelengths of the incident light.

On the other hand, approximate models, though not rigorous, are very flexible and permit to deal with the scattering of complex shaped particles. The geometrical optics

(GO), the physical optics, the geometrical theory of diffraction [21] and the physical theory of diffraction are often used separately or in complementary each other to allow predicting the scattering of particles which are relatively large compared to the incident wavelength. In GO, the light wave is considered as bundles of rays and the interaction of the light with the particle is just the refraction and reflection of the rays on the surfaces of the particle. It can be applied to large particles of complex shape and allows isolating the contributions of different orders of rays and the effects of interferences. It helps to understand the mechanism of scattering. Effects such as absorption and interference can be taken into account separately and the diffraction can be added to improve its precision in forward direction. Furthermore, fast calculations and direct understanding are two other advantages over the rigorous theories. In the case of the scattering by a spherical particle, or a infinite circular cylinder, the GO is proved to be able to predict very accurately the scattering diagram in almost all directions. But, though theoretically possible, it is rarely applied to the scattering of irregular shaped particles.

Alternatively, the scattering problem of arbitrary shaped particles can be dealt with by direct numerical solution of Maxwell's equations. There exist two classes of numerical methods. The first one uses a differential form of the governing equations and requires the discretization (meshing) of the entire domain in which the electromagnetic fields reside, two of the most common approaches in this class are the finite difference method (FDM) and finite element method(FEM). The second class is the integral equation methods which require instead a discretization of only the sources of electromagnetic field, such as the discrete dipole approximation(DDA) and the method of moment (MoM). These methods are very flexible in the shape of the particle, but they are very costly in term of computer resources and the size parameter of the scatter is also severely limited [22].

We can conclude, therefore, that there are few means to deal with the scattering of large complex shaped particles. The ambition of this thesis is consequently to try to make a step forward in this direction by using the Vectorial Complex Ray Model (VCRM) recently developed at CORIA. Among the complex shaped (non-spherical / non-circular cylindrical) particles, the infinite elliptical cylinder is the simplest but it will permit already to examine the effect of non-circularity and also the scattering of a shaped beam at different incident directions. The PhD thesis is dedicated therefore to the scattering of an infinite cylinder of elliptical section. We will give in the following the state of arts in the field of the scattering of a cylinder for both the rigorous theories

and the approximate models.

Rigorous theories for light scattering by a cylinder

During the past decades, many researchers have devoted to rigorous theories of light scattering by cylinders, and more particularly with the Lorenz-Mie theory (LMT).

When the light illumination on the particle is homogeneous, the incident wave is considered as a plane wave. As early as the middle of the last century. Wait has studied the light scattering of a plane wave by a circular dielectric cylinder at oblique incidence [23]. Van de Hulst has then given the formulation of the scattering field coefficients for perpendicular and obliquely incidence [3]. Bohren and Huffman presents a very complete and elegant form in their book [4]. Then the formulation and program of light scattering for a circular cylinder have been given by Barber and Hill [24]. In the case of elliptical cylinder, the study has been stated by using exact solutions in terms of Mathieu functions to predict the back scattering under normal incidence in 1965 [17]. By considering the scattering by elliptic cylinders on various configuration, a complete set of solutions is provided by Sebak and Safai [25]. The evaluation for the scattering of a plane wave by an infinite elliptical metallic cylinder is used by two different methods, elliptical-cylindrical wave functions and a shape perturbation method [26]. The study for multilayered circular cylinders has also been documented. Lock and Adler [27], and Li et al [28, 29] have contributed to the Debye-series analysis of the scattering of an homogeneous and multilayered cylinders.

With the emergence of laser and new light sources, the collimated beams are widely used in optical metrology. The scattering of a collimated beam by a cylinder has also been well documented in the past years. By considering amplitude and phase distribution, Kozaki have analyzed the scattering of a two dimension Gaussian beam by a conducting cylinder [30] and a dielectric cylinder [31]. In 1979, Kojima et al have treated the scattering of an off-axis Gaussian beam from a circular cylinder by the Fourier-series-expansion method [32]. Then E. Zimmermann investigated the scattering of an off-axis incident two dimensional Gaussian beam by a homogenous dielectric cylinder at normal incidence based on the exact solution of the Helmholtz equation and compared the results with experiments [33]. Later, Gouesbet has tried different methods for the scattering of a Gaussian beam by circular cylinder (see [34] and references therein), but he has not given numerical results. Ren et al have used the plane wave expansion for the scattering of Gaussian beam by a cylinder at

normal incidence in the framework of the Generalized Lorenz-Mie Theory (GLMT) [35] and introduced the Localized Approximation for the calculation of the beam shaped coefficients in the cylindrical coordinate system[35, 36]. They have given numerical results of scattered intensity in the region as far as 8mm from a cylinder of 1μm of radius [35]. About at the same time, Lock used similar method to study the light scattering of a diagonally incident focused Gaussian beam by an infinite cylinder [37, 38]. This approach has later been extended to the scattering of shaped beam by an elliptical cylinder [39, 40, 41]. The research groups of Wu [42, 43] and Caorsi et al [44] used also the Mathieu functions to study the scattering of a homogeneous anisotropic and multilayered elliptical cylinder. However, this theory cannot be applied to large particles due to the difficulty in the evaluation of the elliptical functions.

The scattering of an elliptical cylinder illuminated by a Gaussian beam is much more difficult. There exist theoretical solutions for the elliptical infinite cylinder, but, the numerical implementation is very difficulty due to the calculation of the related special functions. Gouesbet et al have devoted to scattering of an elliptical cylinder by shaped beam by using partial wave expression [45, 46]. Then they employed a plane wave spectrum approach [35] to describe arbitrary shaped beam [41]. After that, they extended the localized approximation to the elliptical coordinate system [40] and exploited Generalized Lorenz-Mie theory for elliptical infinite cylinders [47, 39]. In all aforementioned work, only a little numerical results are provided. Although many authors devoted to study the light scattering of a circular or an elliptical cylinder, the size of the cylinder is always seriously limited, often to several wavelengths.

In the case of elliptical cylinder illuminated diagonally by a wave, due to the cross polarization, the scattering problem is more difficult. Yeh has provided in 1964 exact solutions for the elliptical fiber scattering, but no any numerical results are given [48]. Then the impedance elliptical cylinder was studied by the use of two methods [49]. One is based on the transformation of the elliptical cylinder into circular cylinder in polar coordinates, the other is the finite difference method(FDM) in the elliptical coordinate system. The integral-integrodifferential equations was also employed to study dielectric cylinders having arbitrary shaped with smooth boundaries [50]. Recently, Grigorios has given numerical results of light scattering by elliptical dielectric cylinders using the separation of variable method (SVM) [51].

Approximate methods for light scattering by a cylinder

Although the rigorous theories can describe the interaction between waves and particles, the numerical calculation is difficult or impossible for larger non-spherical / non-cylindrical particles. Therefore, the geometrical optics (GO), or a ray model is expected to be able, instead of the rigorous theories, to deal with the scattering of large and irregular shaped particles.

In the case of an infinite cylinder illuminated by a plane wave, the tracing of rays is simple and very similar with the sphere [3]. Marcuse has obtained the cross section of an elliptical fiber by ray tracing [52]. Holoubek predicted the back scattering of a unclad fibers with the circular cross section [53]. Steinhardt and Fukshansky calculated the intensity distribution in finite circular cylindrical media in 1987 [54]. Adler et al studied the rainbow scattering by a cylinder of nearly elliptical cross section also by using the geometrical optics [55]. But usually the interference effect is not taken into account, especially when the cylinder is not circular. The group of Yang has combined the geometrical optics with integral equation [56, 57] to calculate the scattering properties of different kinds of particles [58, 59, 60]. Hovenac [61] has shown that in the case of a spherical particle, by taking into account correctly interference phenomenon, GO can predict very precisely the scattering in almost directions.

For the scattering of a shaped beam by a spherical particle, Xu et al have studied the GO for spheroid particle in end-top illumination case [62]. However, as soon as we want to extend the GO to a non spherical or non circular cylindrical particle, the evaluation of the divergence/convergence [63] and the phase shift due to the focal line [3] become a very difficult or impossible task. Based on the scattering theory by spherical particle, Xu et la then evaluated the scattering diagrams of a spheroidal particle [64]. There is much less work on GO for the scattering of cylinder illuminated by shaped beams. For the circular cylinder, we find only that Krattiger used the interference of reflected and transmitted rays in a far field for the measurement of the refractive index of capillary eletrophoresis [65]. Unfortunately, we have not found the study for Gaussian beam scattering by an elliptical cylinder.

In order to improve the geometrical optics, Ren et al have integrated the wave property in the ray model and developed the Vectorial Complex Ray Model (VCRM) [66, 67]. This model permits to take into account the interference and the divergence/ convergence of the wave when it encounters an arbitrarily shaped particle. In this model, all waves are described by vectorial complex rays and the scattering intensities

are computed by the superposition of the complex amplitudes of the vectorial rays. The significant merit of this approach is that the wave properties are integrated in the ray model, the divergence/convergence of the wave is deduced by the wavefront equation and the phase shifts due to the focal lines are determined directly by the curvature of the wavefront.

Diffraction plays a important role in the light scattering. Bohren and Huffman [4] have formulated the diffraction of a cylinder in the case of plane wave incidence. Although we found several reference for diffraction of a Gaussian beam by a cylinder [68, 69], we have not found simple expression for numerical calculation. So the part of diffraction of the Gaussian beam will not be taken into account in the chapter 4.

Structure of the thesis

The body of the PhD thesis manuscript is organized as follows: The classical theories and models on the scattering of an infinite cylinder are presented in Chapter 2. They are used as references for the validation of the models developed in the thesis and provide fundamental concepts and formulae useful in the chapters which follow. In Chapter 3, the Vectorial Complex Ray Model (VCRM) is introduced and applied to the scattering of an infinite cylinder of elliptical section illuminated by a plane wave perpendicular to the cylinder axis. The propagation direction of the incident wave can be oblique relative to the axis of the ellipse. VCRM is then extended in Chapter 4 to the scattering of an elliptical cylinder illuminated by three kinds of Gaussian beams: two dimensional Gaussian beam, circular Gaussian beam and astigmatic elliptical Gaussian beam. But in this chapter the direction of the incident beam is still supposed to be perpendicular to the axis of the cylinder and, for sake of simplicity, we are interested only the scattering in the plane perpendicular to the cylinder axis and containing the incident beam axis. In all the scattering process, the rays remain always in this plane. In Chapter 5, we are trying to study the light scattering of an elliptical cylinder illuminated diagonally by a plane wave. This is the first tentative to deal with the 3D ray tracing and the problem of cross polarization. The last Chapter is dedicated to the conclusions and perspectives of the work.

Chapter 2

Classical methods for light scattering by a cylinder

In this chapter, the classical theories and models for the scattering of plane wave by an infinite cylinder will be presented.

The most well-know particle light scattering theory is the Lorenz-Mie theory (LMT or its equivalents). It is based on the rigorous solution of the Maxwell's equations, but only valid for the particles whose shape corresponds to a coordinate system, such as sphere, spheroid, ellipsoid, circular or elliptical infinite cylinder, where the mathematical solutions of the differential equations are possible. In this theory, the incident $\boldsymbol{E}^i$, internal $\boldsymbol{E}^{int}$ and scattered electromagnetic fields $\boldsymbol{E}^s$ are expanded in the corresponding special functions (i.e. eigenfunctions). The expansion coefficients of the incident wave, called beam shaped coefficients, are calculated by the incident wave expressions, while the expansion coefficients of the scattered field and internal field are determined by the boundary conditions. Once these coefficients obtained, all physical quantities can be obtained accordingly. The scattering coefficients in LMT also can be expanded in Debye series in order to study the contribution of different order of wave in rigorous regime. Remarkable work has been done for the spherical particle [70], the infinite circular cylinder at normal [29]or oblique incidence [71]. But we have not found published work on the scattering of an infinite elliptical cylinder.

Geometrical optics(GO) is, on the other hand, an approximate model to deal with the interaction of light with an object. It is simple and intuitive, only valid for the particle of size much larger than the wavelength [3]. In this model, a light beam is considered as bundles of rays and a ray is characterized by its direction, its

amplitude, its phase and its polarization. When a ray hits the particle surface, it is, in general, split in a reflected ray and a refracted ray. The directions of these two rays are governed by the Snell-Descartes laws and their amplitudes are determined using the Fresnel formulas. The total scattered field in a given direction is, therefore, the superposition of the complex amplitudes of all emergent rays in that direction.

This chapter is organized in four sections. First, the rigorous theory is presented and scattering diagrams of a large infinite circular cylinder given. Main profiles characteristics of the scattered intensity can be observed and the role of polarization is also shown. The geometrical optics for the scattering of an infinite circular cylinder is described. In this special case, the analytical expressions for the amplitude and the divergence/convergence factor for all orders can be given as function of the scattering angle. Finally, a short description is also given to the Generalized Lorenz-Mie theory and the diffraction method.

2.1 Lorenz-Mie theory for circular cylinder

We consider an infinite circular cylinder illuminated by a plane wave of wavelength λ. The Cartesian coordinate system $(O; xyz)$ is chosen such that z axis is along the axis of the cylinder and the incident wave propagating in x direction. (see Fig. 2.1). The scattering angle θ is the angle between the direction of the scattered wave and the x axis. The cylinder radius is denoted by a and its refractive index by m. The refractive index of surrounding medium is 1.

When the incident electric field is polarized parallel to the cylinder axis, it has only z component, such that

$$E_z^i = E_0 e^{-ikx} \tag{2.1}$$

where $k = 2\pi/\lambda$ is the wave number and E_0 the amplitude of the incident field. Since the exponential function in the above equation can be expanded as the first kind Bessel functions $J_n(kr)$

$$e^{-ikx} = \sum_{-\infty}^{\infty} i^n J_n(kr) e^{in\theta} \tag{2.2}$$

The incident wave reads therefore as

$$E_z^i = E_0 \sum_{-\infty}^{\infty} i^n J_n(kr) e^{in\theta} \tag{2.3}$$

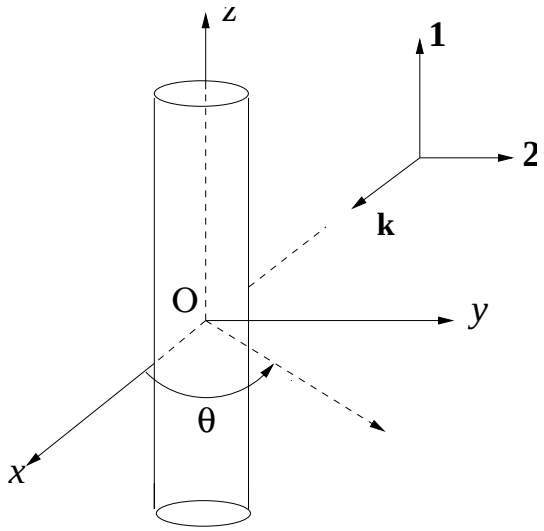

Figure 2.1: Schematic of an infinite circular cylinder illuminated by a plane wave propagating in the x direction. We distinguish two polarizations: perpendicular (1) and parallel (2) to the scattering plane(i.e. xy) .

Similarly, the scattered and internal electric fields can also be expanded as the first kind Hankel functions H_n

$$E_z^s(kr) = -E_0 \sum_{n=-\infty}^{\infty} i^n b_n H_n^{(1)}(kr) e^{in\theta} \tag{2.4}$$

$$E_z^{int}(mkr) = E_0 \sum_{n=-\infty}^{\infty} i^n d_n H_n^{(1)}(mkr) e^{in\theta} \tag{2.5}$$

where b_n and d_n are the scattering and internal field coefficients. The scattered and the internal magnetic fields can be obtained according to the relation between $\boldsymbol{E}$ and $\boldsymbol{H}$ [4].

Since the particle under consideration is free of charge and current, the tangential components of the electric and magnetic fields on the particle surface must be continuous and satisfy the following boundary conditions:

$$\hat{\boldsymbol{n}} \times (\boldsymbol{E}^i + \boldsymbol{E}^s) = \hat{\boldsymbol{n}} \times \boldsymbol{E}^{int} \tag{2.6}$$

$$\hat{\boldsymbol{n}} \times (\boldsymbol{H}^i + \boldsymbol{H}^s) = \hat{\boldsymbol{n}} \times \boldsymbol{H}^{int} \tag{2.7}$$

When the incident electric field is polarized in z direction, the magnetic field is in the xy plane. So by application of the boundary conditions on the cylinder surface at

$r = a$, we obtain

$$E_z^i + E_z^s = E_z^{int} \tag{2.8}$$

$$H_\theta^i + H_\theta^s = H_\theta^{int} \tag{2.9}$$

The scattered and internal field expansion coefficients can be solved from the Eq. (2.8) and Eq. (2.9)

$$b_n = \frac{mJ'(m\alpha)J_n(\alpha) - J_n(m\alpha)J_n(m\alpha)J_n'(\alpha)}{mJ_n'(m\alpha)H_n^{(1)}(\alpha) - J_n(m\alpha)J_n(m\alpha)H_n^{(1)}(\alpha)} \tag{2.10}$$

$$d_n = \frac{1}{J_n(m\alpha)}[J_n(\alpha) - b_n H_n^{(1)}(\alpha)] \tag{2.11}$$

where $\alpha = ka$ is the size parameter. The prime indicates the derivation of the function to its argument.

When the incident magnetic field is along the cylinder axis, similarly as the perpendicular polarization case describe above, the incident magnetic field can be expressed as

$$H_z^i = H_0 e^{-ikx} = H_0 \sum_{-\infty}^{\infty} i^n J_n(kr) e^{in\theta} \tag{2.12}$$

The scattered and internal magnetic fields can be expanded as

$$H_z^s(kr) = -H_0 \sum_{n=-\infty}^{\infty} i^n a_n H_n^{(1)}(kr) e^{in\theta} \tag{2.13}$$

$$H_z^{int}(mkr) = H_0 \sum_{n=-\infty}^{\infty} i^n c_n H_n^{(1)}(mkr) e^{in\theta} \tag{2.14}$$

Similarly as for perpendicular polarization case, the scattered and internal electric fields can be obtained by the relation between $\boldsymbol{E}$ and $\boldsymbol{H}$.

In this case, the electric field is polarized perpendicularly to the cylinder axis, i.e. in xy plane (also called parallel polarization because the electric field is always in the scattering plane).

According to the boundary conditions (2.6) and (2.7), the tangential components of the electric and the magnetic fields on the particles at $r = a$ satisfy the following relations

$$H_z^i + H_z^s = H_z^{int} \tag{2.15}$$

$$E_\theta^i + E_\theta^s = E_\theta^{int} \tag{2.16}$$

So, the scattering and the internal field coefficients are given by

$$a_n = \frac{J'(m\alpha)J_n(\alpha) - mJ_n(m\alpha)J'_n(\alpha)}{J'(m\alpha)H_n^{(1)}(\alpha) - mJ_n(m\alpha)H_n^{(1)}(\alpha)} \tag{2.17}$$

$$c_n = \frac{1}{J_n(m\alpha)}[J_n(\alpha) - a_n H_n^{(1)}(\alpha)] \tag{2.18}$$

When kr is very large, the Hankel function tends to

$$H_n(kr) \sim \left(\frac{2}{\pi kr}\right)^{1/2} e^{-ikr+i(2n+1)\pi/4} \tag{2.19}$$

Therefore, in far field and for perpendicular polarization, the scattering field in Eq. (2.4) simplifies to

$$E_z^s(kr) = E_0 \left(\frac{2}{\pi kr}\right)^{1/2} e^{-ikr-i3\pi/4} T_1(\theta) \tag{2.20}$$

where,

$$T_1(\theta) = \sum_{n=-\infty}^{\infty} b_n e^{in\theta} = b_0 + 2\sum_{n=1}^{\infty} b_n \cos n\theta \tag{2.21}$$

is the amplitude function [3]. The scattered intensity in the far field is then given by

$$I = \frac{2}{\pi kr}|T_1(\theta)|^2 I_0 \tag{2.22}$$

Similarly, the amplitude of the scattered field for the parallel polarization can be written as

$$T_2(\theta) = \sum_{n=-\infty}^{\infty} a_n e^{in\theta} = a_0 + 2\sum_{n=1}^{\infty} a_n \cos n\theta \tag{2.23}$$

The scattered intensity is the same as the perpendicular polarization (Eq. (2.22)) with T_1 replaced by T_2.

To give a idea about the profile of the scattered diagrams of a infinite cylinder and provide reference for the study in the near chapters, we show in Fig. 2.2 and Fig. 2.3 the scattering diagrams of circular cylinders with respectively radius 10 μm and 50 μm. The wavelength of the incident plane wave is 0.6328 μm and the refractive index of particle is 1.33.

We can observe in forward direction that the scattering diagram is rather regular. This is due to, in term of the geometrical optics, the interference of the reflected and the first order refracted waves which are dominant compared to the other high orders. This can be highlighted by the ray model and will be discussed in next section and

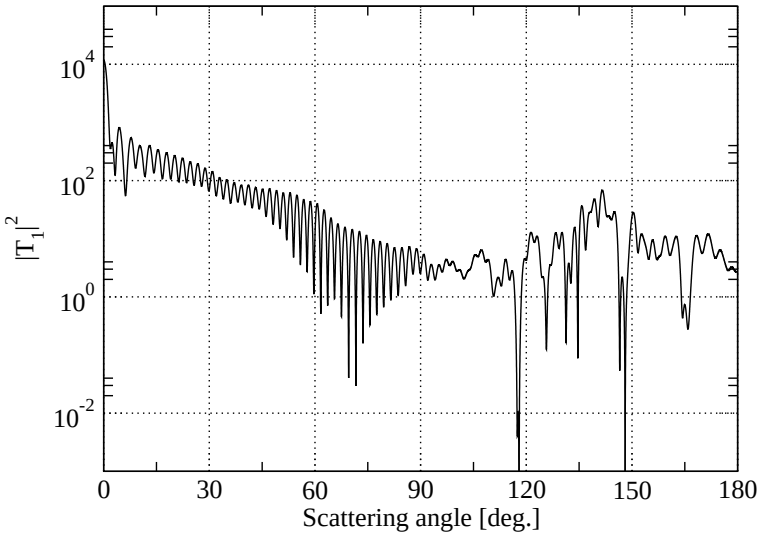

(a). Perpendicular polarization.

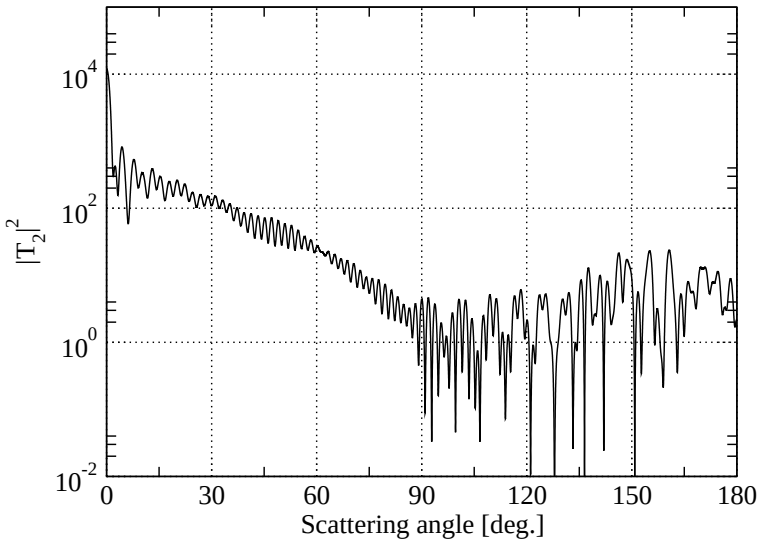

(b). Parallel polarization.

Figure 2.2: Scattering diagrams computed with LMT for an infinite circular cylinder of refractive index $m = 1.33$ and radius $a = 10$ μm illuminated by a plane wave of wavelength $\lambda = 0.6328$ μm.

later in the thesis. The scattering profile in the backward direction is, however, not as such regular, especially for the particle of 10 μm at perpendicular polarization because the contributions of different orders change very much as function of scattering angles.

For the particle of 50 μm (Fig. 2.3), we can see two obvious peaks located around 140° and 130°, that are more pronounced for the perpendicular polarization (Fig.

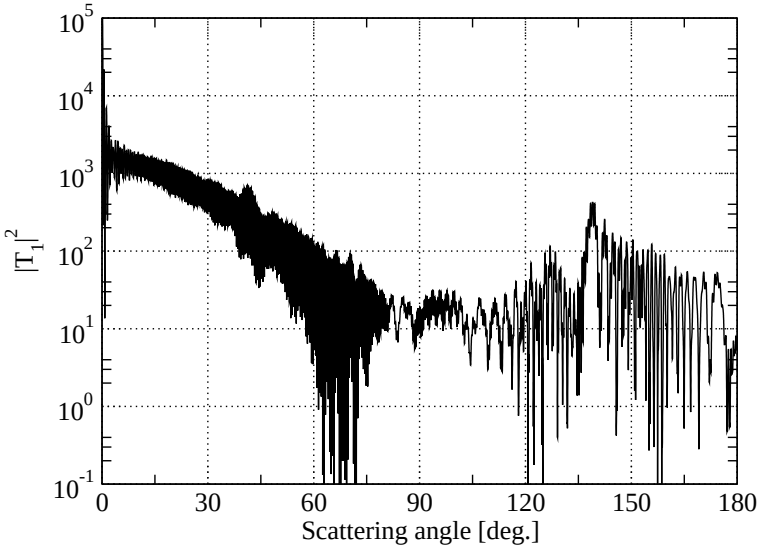

(a). Perpendicular polarization.

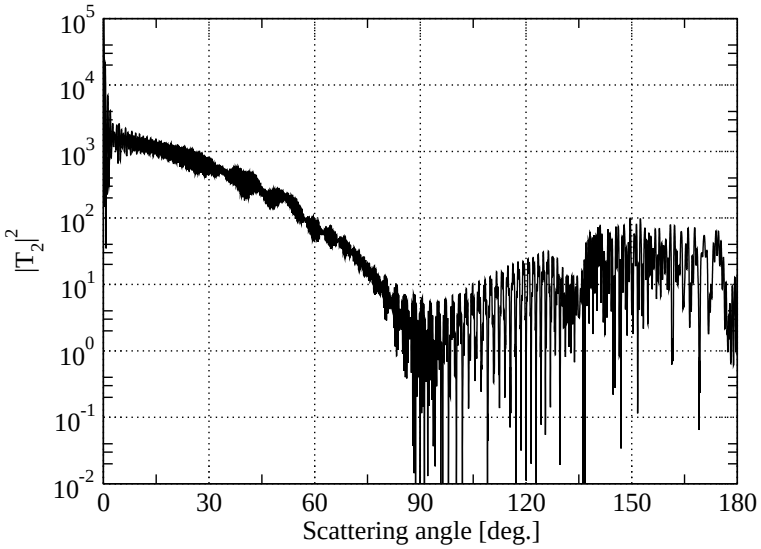

(b). Parallel polarization.

Figure 2.3: Scattering diagrams computed with LMT for an infinite circular cylinder of refractive index $m = 1.33$ and radius $a = 50$ μm illuminated by a plane wave of wavelength $\lambda = 0.6328$ μm.

2.3(a)) than for the parallel polarization (Fig. 2.3(b)). These are the well known rainbows of the first and second orders and will be discussed in details by ray model.

2.2 Generalized Lorenz-Mie theory for cylinder

When a particle is illuminated by an electromagnetic wave or a light beam, if the size of the particle is much smaller than the variation scale of the wave (both the amplitude and the phase), the incident wave can be considered as a plane wave and LMT can be applied. But if it is not the case, LMT is no longer valid and the inhomogeneous illumination must be considered. Ren et al [35] have developed a so-called plane wave expansion method for the scattering of a shaped beam by an infinite circular cylinder. The principle of this method is outlined in the following.

The main idea of the plane wave expansion method is to consider the incident wave as composition of an infinite number of plane waves propagating in different directions. For the perpendicular polarization case, for instance, instead of Eq. (2.3), the incident field is expanded as

$$E_z^i = \frac{E_0}{kr}\sum_{n=\infty}^{\infty}(-i)^n e^{in\theta}\int_{-1}^{1}(kr)^2(1-\gamma^2)I_n(\gamma)J_n(kr\sqrt{1-\gamma^2})e^{-i\gamma kz}d\gamma \qquad (2.24)$$

where $I_n(\gamma)$ is the beam shape coefficients and γ can be regarded as the cosine of the incident angle Γ of the plane wave ($\gamma = \cos\Gamma$) [35]. So the physical meaning of Eq. (2.24) is that a shaped beam can be considered as the superposition of plane waves of propagation direction defined by γ and $I_n(\gamma)$. When a incident electric field, $E_z^i(z, r, \theta)$ for example, is given, the beam shape coefficients can be calculated by :

$$I_n(\gamma) = \frac{i^n}{4\pi(1-\gamma^2)J_n(kr\sqrt{1-\gamma^2})}\int_0^{2\pi} e^{-in\theta}\int_{-\infty}^{\infty}\frac{E_z^i(z,r,\theta)}{E_0}e^{i\gamma kz}kdzd\theta \qquad (2.25)$$

Evidently, the scattered field and the internal field depend also on the beam shape coefficients. It has been proved that the scattered field expansion coefficients for a shaped beam is a linear combination of the beam shape coefficients and the scattering coefficients. But the scattering coefficients a_n and b_n are independent of the beam shape coefficients since they are determined only by the properties of the scatterer.

Based on the above method, Ren et al have calculated the scattering diagrams of an infinite circular cylinder illuminated by a Gaussian beam. But the numerical calculations remain still a problem because, in the case of shaped beam, the scattering field is, in general, neither circular nor spherical. The asymptotic relations of the special functions can not be used to simplify the calculation in far field. The formulation of this theory is very tedious and we will not be presented here. For further details we can refer to the concerned papers [35] and [37].

2.3 Geometrical optics

In the geometrical optics, all waves are described by bundles of rays. Rays possess four properties: direction of propagation, amplitude, phase and polarization of the wave they present.

Fig. 2.4 illustrates the schema of ray when it interacts with a circular cylinder. When a ray arrives on the surface of the particle, it is partially reflected and refracted. The direction of the reflected and refracted rays are given by the Snell-Descartes law:

$$m_0 \sin\theta_i = m \sin\theta_r \tag{2.26}$$

where θ_i and θ_r are respectively the incident angle and the refraction angle. For convenience we introduce also the complementary angles $\tau = \frac{\pi}{2} - \theta_i$ $\tau' = \frac{\pi}{2} - \theta_r$. m and m_0 are respectively the refraction index of the particle and the surrounding medium. Without lose of generality, we suppose in this thesis that $m_0 = 1$ and m is the particle relative refractive index.

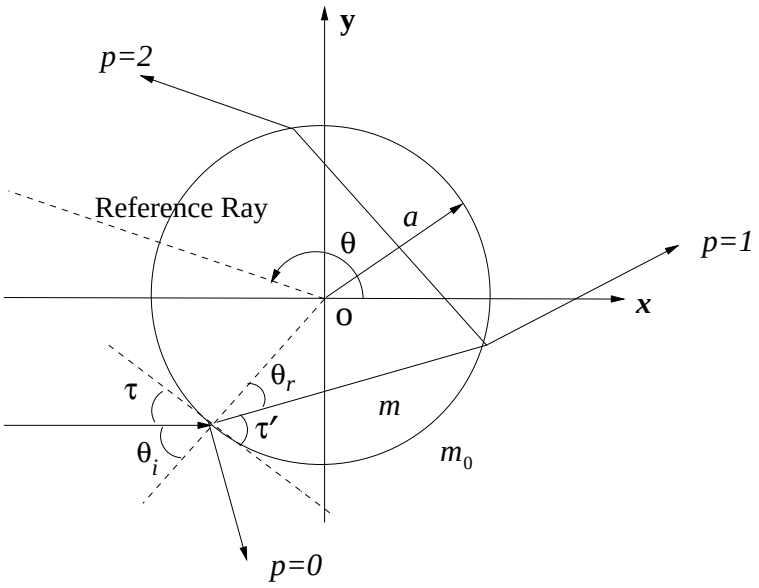

Figure 2.4: Schema of ray interaction with a circular cylinder.

For an incident ray, there is an infinite series of emergent rays, noted usually by p, called the order of ray. $p = 0$ stands for the reflection ray and $p = 1$ for the first order refracted ray. When $p \geq 2$, p designates an emergent ray undergoes $p - 1$ times internal reflections.

If a ray propagating in direction of x axis and impinges on a cylinder of radius a (Fig. 2.4), the coordinates of the incident point are given by

$$x = -a\cos\theta_i \tag{2.27}$$

$$y = a\sin\theta_i \tag{2.28}$$

According to the law of Snell-Descartes, the refraction angle is given by

$$\theta_r = \arcsin(\sin\theta_i/m) \tag{2.29}$$

Since the angle between the emergent/internal ray and the normal of the the particle surface (θ_i/θ_r) is constant, the total deviation angle of a ray of order p from the x axis is given by

$$\theta' = 2\tau - 2p\tau' \tag{2.30}$$

The scattering of a circular cylinder is symmetric about x axis, the scattering angle θ is often reported to the interval $(0, \pi)$ and is related to the total deviation angle by

$$\theta' = 2k\pi + q\theta \tag{2.31}$$

where k is a integer representing the times the emergent ray crosses the x axis. q takes $+1$ or -1.

When a pencil of light arrives on the surface of the particle, it can be converged or diverged and the amplitude of the emergent beam will be more or less important accordingly. This effect can be counted by energy balance between the incident flux and the emergent flux. Consider an incident beam of section $dA = a\sin\tau d\tau dz$. All the flux is emergent to an area dA^s at a far distance r from the particle such that $dA^s = rd\theta dz$. So the relation between the incident intensity I_0 and the emerging intensity I of a ray of order p is given by

$$I(p,\tau) = \frac{\varepsilon^2 I_0 a\sin\tau d\tau dz}{rd\theta dz} \tag{2.32}$$

$$= \frac{a}{r} I_0 \varepsilon^2 D \tag{2.33}$$

where ε is the coefficient related to the reflection on and transmission through the particle surface determined by the Fresnel formula. We will discuss it later. D is referenced as the divergence factor with

$$D = \frac{\sin\tau}{d\theta/d\tau} \tag{2.34}$$

The derivative $d\theta/d\tau$ is evaluated according to the Eq. (2.30) and Eq. (2.26):

$$\frac{d\theta}{d\tau} = 2 - 2p\frac{\tan\tau}{\tan\tau'} \tag{2.35}$$

For low orders, very simple analytical expressions can be obtained for the divergence factors, $p = 0$ with for

$$D_0 = \frac{\cos\theta_i}{2} \tag{2.36}$$

and for $p = 1$

$$D_1 = \frac{m\cos\theta_r\cos\theta_i}{2(\cos\theta_i - m\cos\theta_r)} \tag{2.37}$$

On the other hand, each time a ray hits the surface of the particle, it is reflected and refracted. The ratio of the amplitude of the reflected wave to the incident wave amplitude are given by following Fresnel formulas according to the polarization states:

$$r_1 = \frac{\sin\tau - m\sin\tau'}{\sin\tau + m\sin\tau'} \tag{2.38}$$

$$r_2 = \frac{m\sin\tau - \sin\tau'}{m\sin\tau + \sin\tau'} \tag{2.39}$$

It is worth to point out that the Fresnel coefficients are constants for all order rays in the circular cylinder. The reflected fractions of the intensity are r_1^2 and r_2^2. The fraction of the internal reflected are the same as the first reflection, but the sign of both r_1 and r_2 are reversed. The refracted parts of intensity are $1-r_1^2$ and $1-r_2^2$. The term ε in Eq. (2.33) is then calculated by the Fresnel coefficients. Because ε depends on the order and the polarization of the ray, so from now it will be noted as $\varepsilon_{X,p}$ and given by

$$\varepsilon_{X,p} = \begin{cases} r_{X,0} & p = 0 \\ (1 - r_{X,0}^2)(-r_{X,0})^{p-1} & p \geq 1 \end{cases} \tag{2.40}$$

where $r_{X,0}$ represents the Fresnel coefficient of reflection. The subscript $X = 1$ or 2 stands for perpendicular or parallel polarization. Usually, the dimension of the particle is much smaller than the coherent length of the incident beam, the interference should be taken into account and therefore the phase of the rays must be counted. The phase shifts can be classified into three kinds [3]:

1. *Phase due to reflection and refraction* ϕ_F: It is well known that the reflected wave changes of sign compared with the incident wave. When a wave is reflected on the surface from optically thinner medium ($m_2 < m_1$)to optically denser medium ($m_2 > m_1$), there is an addition a half-wave loss. In fact, this is true

only when the incident angle is small. In more general case, this kind of phase shift is accounted in the Fresnel coefficients. The half-wave loss is just due to that ε may change the sign and is in equality that a phase shift π is added accordingly. In the cases of total reflection or absorbing medium, the Fresnel coefficients are complex and the phase shift can be deduced from the complex Fresnel formulae.

2. *Phase due to optical path*: This type of phase shift is due to the optical path of a ray, usually compared to a reference ray, which arrives at the center of the particle in the same direction of the incident ray and emerges in the same direction as the emergent ray as if there is no particle (no refraction). Therefore, the optical paths of the reflected ray ($p = 0$) has a shorter path than the reference ray, thus it has the positive phase shift. The refraction rays ($p = 1, 2, \cdots$) have longer optical path and the phase shifts are negative. Referring to Fig. 2.1, we can find that the phase shift due to the optical path is

$$\phi_{p,PH} = 2\alpha(\sin\tau - pm\sin\tau') \tag{2.41}$$

3. *Phase due to focal lines*: When a ray passes through a focus, its phase advances by $\pi/2$. Van de Hulst pointed out two types of phase shifts (type a and type b). Type a indicates the phase shift due to the crossing of two adjacent rays in the scattering plane. Type b occurs when a ray crosses the central optical axis. For the infinite circular cylinder, the rays can not intersected in a plane containing the axis of the cylinder, so the total phase shift attributed to focal line is

$$\phi_{p,FL} = \frac{\pi}{2}[p - \frac{1}{2}(1 - s)] \tag{2.42}$$

where s is the sign of the divergence factor and q is determined from Eq. (2.31).

By combining the three kinds of phase shifts, the total phase of a ray of order p is given by

$$\phi_p = \phi_F + \phi_{p,PH} + \phi_{p,FL} \tag{2.43}$$

By comparison of the intensity of GO given in Eq. (2.33) and that of LMT given in Eq. (2.22), we find that a factor of $\sqrt{\pi/2}$ must be added so that the amplitude of GO is consistent with LMT. The amplitude of GO is revised accordingly and the complex amplitude is therefore given by

$$S_{X,p}(\theta) = \sqrt{\frac{\pi\alpha D}{2}}\varepsilon_{X,p}e^{i\phi_p} \tag{2.44}$$

The total field in far region at angle θ is calculated by the summation of the complex amplitudes of all order rays arriving at the same angle as well as that of the diffraction:

$$S_X(\theta) = S_d(\theta) + \sum_{p=0}^{\infty} S_{X,p}(\theta) \tag{2.45}$$

where $S_d(\theta)$ is the amplitude of diffraction which will be discussed in next section.

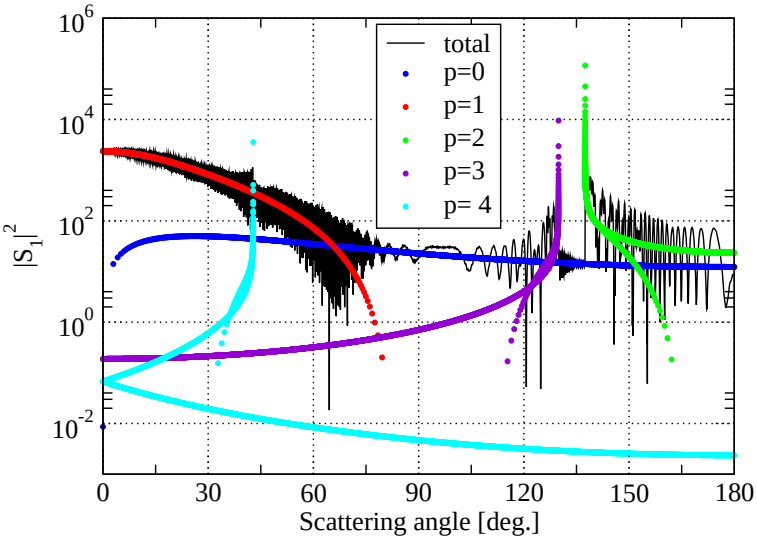

(a). Perpendicular polarization.

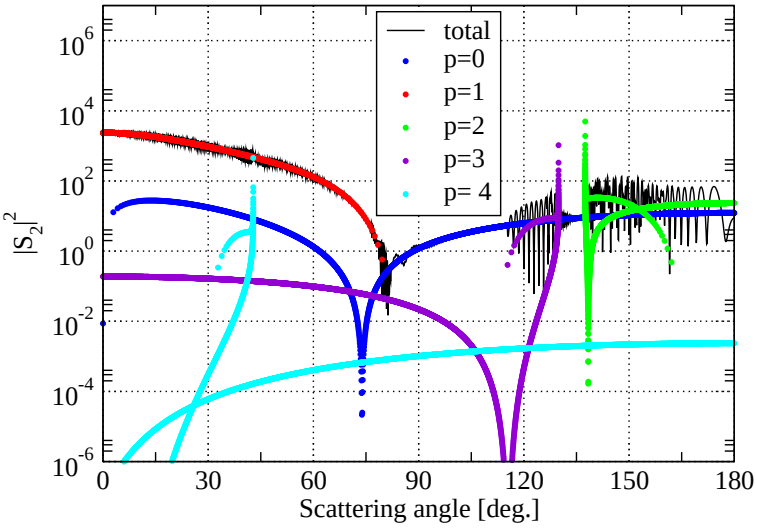

(b). Parallel polarization.

Figure 2.5: Scattering diagrams of the same particle as in Fig.2.3.

GO allows to decompose the contribution of different orders of rays and gives a clear physical picture of mechanism of light scattering. This is one of the most

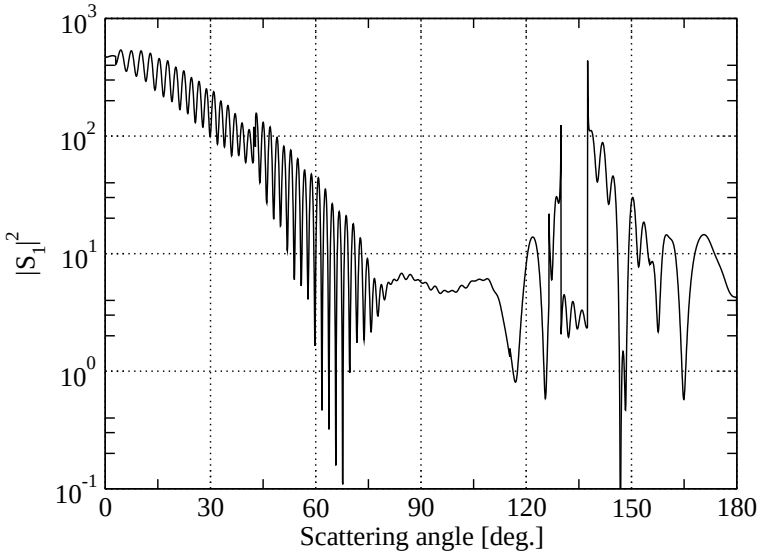

(a). Perpendicular polarization.

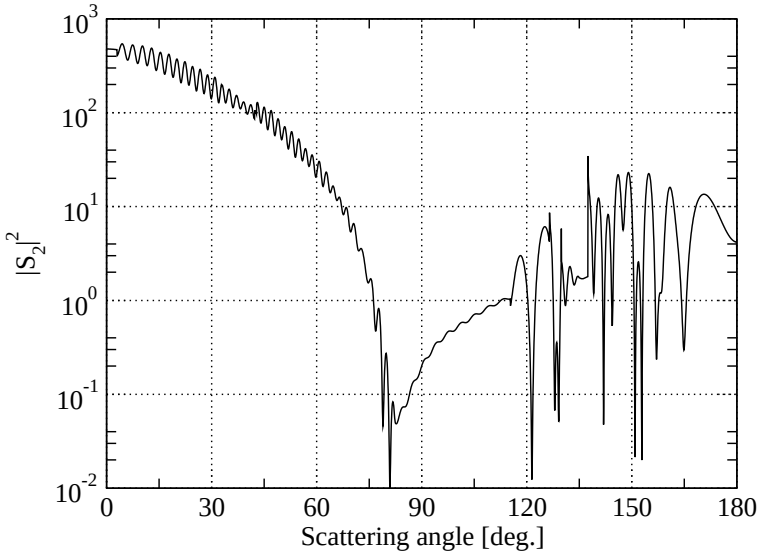

(b). Parallel polarization.

Figure 2.6: Scattering diagrams of the same particle as in Fig.2.2.

attractive advantages of GO. Fig. 2.5 shows the contribution of each order of rays as well as the total scattering phase function.

We can find that the first and the second rainbows, respectively at 137.5° and 129.9°, as well as the Alexander dark region are clearly visible, especially for perpendicular polarization. Compared with the results of LMT, differences in this region are more significant because wave effects have not been taken into account. This can be

remedied by Airy theory in the case of circular cylinder.

The scattering diagram of a small particle ($a = 10\mu$m) is also given in the Fig. 2.6. The global profile is very similar as that obtained by LMT, even the detailed structure near 150°. But the agreement between GO and LMT is obviously not as good as for the particle of 50 μm. The first and the second rainbows as well as Alexander dark region are still clearly observable in Fig. 2.6 but they are not discernable at all for LMT in Fig. 2.2.

Theoretical explanation of rainbow phenomenon is a very interesting subject and has been studied as early as 17th century by Snell and Descartes by using the geometrical optics. The refractometry of rainbow is also an important optical measurement technique. We will give a short description of the rainbow for a circular cylinder. From the point of view of GO, the rainbow formation of a circular cylinder is the same as that of a spherical particle, but the amplitude is different.

In the geometrical optics, the rainbow is a phenomenon of emergent ray converged at an angle such that the intensity tends to infinity. Mathematically, this corresponds to the convergence factor tends to zero, or

$$\left.\frac{d\theta}{d\tau}\right|_p = 0 \tag{2.46}$$

By using Eq. (2.29) and Eq. (2.30), we find that the geometrical optics rainbow angle can be computed by

$$\theta_{rg} = 2\tau_{rg} - 2p \arccos\left(\frac{\cos\tau_{rg}}{m}\right) \tag{2.47}$$

with

$$\sin\tau_{rg} = \sqrt{\frac{m^2-1}{p^2-1}} \tag{2.48}$$

Therefore, the first and the second order rainbows of the rain droplets ($m = 1.33$) are located respectively at the 137.5° ($p = 2$) and 129.9° ($p = 3$).

However, when the particle is not a circular cylinder or a sphere, the rainbow position is much difficult to determine. We will use the new developed ray model to investigate the rainbow of elliptical cylinder, and in the framework of Vectorial Complex Ray Model, the determination of rainbow positions for non-circular cylinder or non-sphere is just a very easy task.

2.4 Diffraction

Theoretically, the diffraction effect is important when the scatterer is not very big compared to the wavelength and the geometrical optics is applicable for large particle. Therefore, bigger the scatter is, better the result of the geometrical optics and less diffraction effect. We have seen in the above two sections that the scattering diagrams of big particle ($a = 50$ μm) predicted by GO are in very good agreement with the rigorous theory – LMT, except in the near forward and around rainbow angles. Especially, the scattered intensity in forward direction is very important and it takes about 50% scattered energy.

In the case of an infinite cylinder illuminated by a plane wave, the cylinder can be considered as an infinite opaque strip. According to the Babinet's principle, the diffraction field is the complementary of that for an infinite slit of the same width and the diffraction patterns of a cylinder and a slit are the same in amplitude but opposite in phase. The term of $3\pi/2$ should therefore be added for sake of the consistency with diffracted phase of the cylinder [72]. In the far field, the Fraunhofer diffraction is considered, so the amplitude is written by [4]

$$S_d = \frac{1+\cos\theta}{2}\frac{\sin(\alpha\sin\theta)}{\sin\theta} \tag{2.49}$$

It is worth pointing out that Eq. (8.44) in [4] is the normalized phase function while Eq. (2.49) is the amplitude which is to be added directly to Eq. (2.45) for obtaining the total scattered field.

Now we can anticipate the results of comparison between LMT, GO and VCRM presented in Chapter 3 (Figs. 3.4, 3.5, 3.6 and 3.7) that by adding the diffraction, the agreement between the LMT and GO is very satisfactory even for a particle as small as 10 μm. On the other hand, by comparison of Figs. 2.5 and 2.6 we can note that diffraction plays only an important role in the forward direction.

In the case of shaped beam illumination, we can infer that the profile of the diffraction contribution should be similar as for the plane wave. The contribution of diffraction of a shaped beam would be smaller than the plane wave and not symmetric when the cylinder is off-axis of the beam. Nevertheless, we will not deal with the term of diffraction in chapter 4 since the accurate calculation should take into account the Gaussian profile of the incident beam, the beam waist radius and the position of the cylinder in the beam.

2.5 Conclusion

In this chapter, we recalled the Lorenz-Mie theory (LMT), the Generalized Lorenz-Mie theory and the geometrical optics (GO) for the scattering of a circular cylinder. They will be used in the next chapter to validate our new developed method in the case of infinite circular cylinder. The basis on GO presented in this chapter is essential for its extension to the scattering of an infinite elliptical cylinder in the following chapters. But even theoretically possible, the classical GO is not apt to deal with particles of shape more complicate, a spheroid with oblique illumination for example [63]. The Vectorial Complex Ray Model (VCRM) will be applied in the following chapters to deal with the scattering of an infinite elliptical cylinder illuminated perpendicularly by a plane wave (Chapter 3) or a Gaussian beam (Chapter 4), and diagonally by a plane wave (Chapter 5).

Chapter 3

VCRM for plane wave scattering by an elliptical cylinder

The geometrical optics is, in principle, very flexible and can be applied to deal with the interaction of light with any shaped object. But in reality, the things are not so simple. Though it has been applied largely in the imaging system and no-imaging (illumination) system design, it is rarely used in quantitative study of particle scattering and optical metrology for non-spherical, non-circular cylindrical particles. It is very probably due to the three reasons:

1. *the tracing of rays in a complex shaped particle:* This is always possible in principle, but the realization is not so easy, especially for 3 dimensional ray tracing. The use of the vectors simplify considerably the tracing process, has already done by some researchers.

2. *the determination of the divergence or convergence:* This is also, in principle, feasible because we can calculate the convergent center of the rays adjacent to a given ray. Undoubtedly, this is very tedious and we have not found any published work reporting or repeating such method.

3. *the calculation of the phase due to focal lines:* When a bundle of rays cross their focal line or focal point, the phase of the wave should be advanced $\pi/2$ or π according to van de Hulst [3]. To take into account the interference of all orders of rays emergent in the same direction, this phase must be counted correctly. It is a easy task for spherical particle or circular cylinder, for a given incident ray, the deviation angles of all orders can be obtained analytically and the focal lines

and the focal points can be counted accordingly (see section 2.2 in reference [3]). But for an irregular particle, the ray direction can only be determined step by step. The determination of the focal lines or focal points is nearly impossible.

To overcome these difficulties, Ren et al have integrated the wave property in the ray model and developed the Vectorial Complex Ray Model (VCRM) [66, 67]. This model permits us to take into account for the interference and the divergence/convergence of the waves when they encounter the smooth surface of an arbitrarily shaped particle. In this model, all waves are described by vectorial complex rays and the scattering intensities are computed by the superposition of the complex amplitudes of the vectorial rays. The significant merit of this approach is that the wave properties are integrated in the ray model, the divergence/convergence of the wave is deduced by the wavefront equation and the phase shifts due to the focal lines are determined directly by the curvature of the wavefront. The key point of VCRM is the introduction of the wave properties in the ray model and the wave structure is described by the wavefront curvatures in terms of differential geometry. The wavefront equation relates the wavefronts of the reflected or refracted wave with those of the incident wave and of dioptric surface. To ease the explanation, we first introduce the general principle of VCRM and then its formulation for the scattering of an infinite elliptical cylinder. VCRM is then applied to predict the light scattering of an infinite cylinder of elliptical cross section illuminated by the plane wave perpendicular to the cylinder axis, but direction of propagation of the incident wave can be oblique relative to the main axes of the ellipse.

3.1 Vectorial complex ray model

In this section, the general principle of VCRM for the scattering of any smooth surface is presented. In VCRM all waves are described by bundles of vectorial complex rays and each ray is characterized by

- its direction of propagation,
- its polarization,
- its phase,
- its amplitude,

- its wavefront curvature matrix [66, 73].

The direction of a vectorial complex ray is expressed by its wave vector $\boldsymbol{k}$. Then according to the fact that the tangent component of the wave vector is continuous on the interface of a particle, the Snell-Descartes law is written simply as

$$k'_\tau = k_\tau \tag{3.1}$$

where k'_τ and k_τ are respectively the tangent components of the wave vectors $\boldsymbol{k}$ and $\boldsymbol{k}'$ of the rays before and after interaction (reflection or refraction) with the surface of the particle. The normal component of the emergent ray is then given by

$$k'_n = \sqrt{k'^2 - k_\tau^2} \tag{3.2}$$

On the other hand, from the mathematical point of view, the structure of any smooth surface in the vicinity of a given point can be described by a 2×2 matrix. Suppose that the curvature of the surface of the particle in the vicinity of the incident point of a ray is described by matrix C and the curvatures of the incident and refracted/reflected wave fronts are expressed respectively by the matrix Q and Q'(see Fig. 3.1). Thus the relation between the three curvature matrix is given by the following wavefront matrix equation [66]

$$(\boldsymbol{k}' - \boldsymbol{k}) \cdot \boldsymbol{n} C = k' \Theta'^T Q' \Theta' - k \Theta^T \, Q \Theta \tag{3.3}$$

where $\boldsymbol{n}$ is the normal of dioptric surface, the superscript T represents the transposed matrix, the letters with or without the prime represent respectively the values after or before interaction of the ray with the surface. Θ is the projection matrix between the base unitary vectors of the coordinates systems on the planes tangent to the wavefront $(\boldsymbol{s}_1, \boldsymbol{s}_2)$ and to the dioptric surface $(\boldsymbol{t}_1, \boldsymbol{t}_2)$

$$\Theta = \begin{pmatrix} \boldsymbol{s}_1 \cdot \boldsymbol{t}_1 & \boldsymbol{s}_1 \cdot \boldsymbol{t}_2 \\ \boldsymbol{s}_2 \cdot \boldsymbol{t}_1 & \boldsymbol{s}_2 \cdot \boldsymbol{t}_2 \end{pmatrix} \tag{3.4}$$

In the special case where the rays remain always in a plane containing one of the principal directions, the curvature matrices described in the two main directions are diagonal

$$C = \begin{pmatrix} \frac{1}{\rho_1} & 0 \\ 0 & \frac{1}{\rho_2} \end{pmatrix} \tag{3.5}$$

$$Q = \begin{pmatrix} \frac{1}{R_1} & 0 \\ 0 & \frac{1}{R_2} \end{pmatrix} \tag{3.6}$$

$$Q' = \begin{pmatrix} \frac{1}{R'_1} & 0 \\ 0 & \frac{1}{R'_2} \end{pmatrix} \tag{3.7}$$

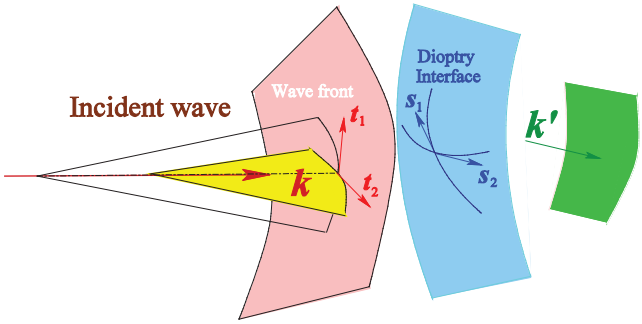

Figure 3.1: Schematic of the interaction between the wavefront and surface.

where ρ_1 and ρ_2 are the two principal curvature radii of the dioptric surface, R_1 and R_2 the principal curvature radii of the wavefront before interaction, and R'_1, R'_2 those of the wavefront after interaction. A example of such case is the scattering of an ellipsoid in the plane defined by an axis of the ellipsoid and the direction of the incident plane wave [66, 67]. In this case Eq. (3.3) is simplified as two scalar equations

$$\frac{{k'_n}^2}{k'R'_1} = \frac{k_n^2}{kR_1} + \frac{k'_n - k_n}{\rho_1} \tag{3.8}$$

$$\frac{k'}{R'_2} = \frac{k}{R_2} + \frac{k'_n - k_n}{\rho_2} \tag{3.9}$$

In the case of reflection, $k'_n - k_n$ in Eqs. (3.8) and (3.9) are replaced by $-2k_n$.

When a bundle of rays encounter the curved dioptric surface, it will be converged or diverged and the intensity of the emergent ray will be more or less important accordingly. In VCRM the divergence factor D is generalized to describe the divergence/convergence of the wave and it is determined directly by the curvature radii of wavefronts as follows

$$\mathcal{D} = \frac{R'_{11}R'_{21}}{R_{12}R_{22}} \cdot \frac{R'_{12}R'_{22}}{R_{13}R_{23}} \cdots \frac{R'_{1p}R'_{2p}}{(r + R'_{1p})(r + R'_{2p})} \tag{3.10}$$

where r is the distance between the origin of the coordinate system and the observation point. The index p is the order of the ray, $p = 0$ for reflection and the other for refracted ray undergone $p - 1$ times internal reflections. R_{1j} and R_{2j} $(j = 1, 2, \cdots, p)$ represent the two curvature radii of the wavefront of incident ray at j^{th} interaction with the surface. R'_{1j} and R'_{2j} are the corresponding curvature radii of the refracted ray. For particles of limited dimension (sphere, spheroid, ellipsoid ...), the term $(r + R'_{1p})(r + R'_{2p})$ in Eq. (3.10) tends to r^2 in far field and often omitted in the

calculation of scattering diagrams. If the particle is infinite in one dimension, as the infinite cylinder, and the incident beam is also infinite in the same direction one dimension divergence factor should be considered, as the case of plane wave incidence as considered in this chapter. But if the cross section of the incident beam is limited in two directions, such as the circular Gaussian beam or the elliptical Gaussian beam, two dimension divergence factors should be used. This case will be dealt with in the next chapter.

Furthermore, in order to take into account the effect of interferences, the phase should be counted correctly. In general, the phase is composed of four parts:

- Phase of the incident wave,
- Phase due to the reflection or refraction,
- Phase due to the optical path,
- Phase shift due to the focal lines.

The first one is calculated directly by the phase function of the incident electromagnetic wave expression (see next section for Gaussian beam as a example). The phase due to the reflection and refraction has already been included in the Fresnel formulae. Then, it is necessary to count the ray path to evaluate the relevant phase. Finally, the phase due to the focal line must be deduced from the wavefront curvature at each stage. If the sign of the curvature changes between two successive interactions, a phase shift of $\pi/2$ is added.

Therefore, the complex amplitude of an emergent ray is calculated by

$$S_{X,p} = \sqrt{\frac{\pi}{2}\mathcal{D}}\ |S_G|\, \varepsilon_{X,p} \exp(i\phi_p) \tag{3.11}$$

where $X = 1$ or 2 corresponds respectively to the perpendicular or parallel polarization, S_G the amplitude of the incident wave, ϕ_p the phase of the p^{th} order ray, $\varepsilon_{X,p}$ stands for the relative amplitude of the X polarized ray of order p calculated by the Fresnel coefficients according to :

$$\varepsilon_{X,p} = \begin{cases} r_{X,0} & p = 0 \\ t_{X,0} t'_{X,p} \prod_{n=1}^{p-1} r'_{X,n} & p \geq 1 \end{cases} \tag{3.12}$$

where $r_{X,0}$ and $t_{X,0}$ are respectively the Fresnel reflection and refraction coefficients for a ray impinging the particle surface from surrounding medium, and $r'_{X,n}$ and $t'_{X,n}$ those coefficients for a ray arriving at the dioptric interface from inside of the particle. In the case of an elliptical cylinder, the Fresnel coefficients vary on each interaction of the ray with the particle since the incident angle changes. The total amplitude of the scattering field at a given angle is just the summation of the complex amplitudes of all emergent rays :

$$S_X = \sum_{p=0}^{\infty} S_{X,p} \tag{3.13}$$

It is worth to point out that the S_X defined by Eqs. (3.11) - (3.13) is the amplitude of the scattered wave and decreases as function of $\sqrt{kr}$ in far field when the particle is illuminated by a very large beam ($w_0 \to \infty$). The scattering phase function of a plane wave is, for example, equal to $kr\|S_X\|^2$.

3.2 VCRM for an infinite elliptical cylinder

3.2.1 Ray tracing

Now we consider an infinite elliptical cylinder illuminated by a plane wave of wavelength λ and choose a Cartesian coordinate system $(O; xyz)$ such that z axis is along the axis of the elliptical cylinder, x and y axis along the two main axis of the ellipse in xy plane (see Fig. 3.2). The propagation direction of the incident wave makes an

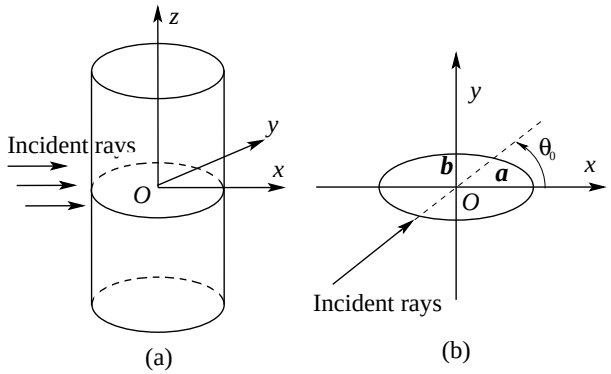

Figure 3.2: Schematic of scattering of a plane wave by an infinite elliptical cylinder.

angle θ_0 with x axis. The cross section of the elliptical cylinder is described by

$$\frac{x^2}{a^2} + \frac{y^2}{b^2} = 1 \tag{3.14}$$

where a and b are respectively the semi-axes of the ellipse in x and y directions. The normal of the surface at given point (x, y) is calculated by

$$\boldsymbol{n} = \frac{b^2 x \boldsymbol{e}_x + a^2 y \boldsymbol{e}_y}{\sqrt{b^4 x^2 + a^4 y^2}} = n_x \boldsymbol{e}_x + n_y \boldsymbol{e}_y \tag{3.15}$$

where $\boldsymbol{e}_x$ and $\boldsymbol{e}_y$ are respectively the unit vectors in x and y directions, and n_x and n_y the components of the normal vector in x and y directions. To simplify the description we define also a unit vector tangent to the surface by

$$\boldsymbol{\tau} = \boldsymbol{n} \times \boldsymbol{e}_z = n_y \boldsymbol{e}_x - n_x \boldsymbol{e}_y \tag{3.16}$$

The curvature radius of the ellipse in xy plane is

$$\rho_1 = a^2 b^2 \left(\frac{x^2}{a^4} + \frac{y^2}{b^4} \right)^{3/2} \tag{3.17}$$

and the curvature radius of the cylinder surface in the plane containing z axis is infinity $\rho_2 = \infty$. We deal with only the orthogonal incident case, the rays remain always in the xy plane and so only one wavefront curvature equation (3.8) is necessary.

When a ray impinges on a circular cylinder, the relation between the refraction and reflection angles of any order is very simple due to the symmetry of the problem. In the case of an elliptical cylinder, we have no longer the circular symmetry and the incident angle of a ray on the surface of the particle changes at each interaction. We describe now how to trace the ray with wave vector and we will see that ray tracing procedure is much simplified by using vectors.

When a ray of wave vector $\boldsymbol{k} = k_x \boldsymbol{e}_x + k_y \boldsymbol{e}_y$ arrives at the cylinder surface (from outside or inside of the cylinder), the components of the wave vector in the normal and tangent directions can be expressed as

$$\begin{aligned} k_n &= \boldsymbol{k} \cdot \boldsymbol{n} = k_x n_x + k_y n_y \\ k_\tau &= \boldsymbol{k} \cdot \boldsymbol{\tau} = -k_y n_x + k_x n_y \end{aligned} \tag{3.18}$$

According to the Snell-Descartes law (3.1), the tangent components are continuous, so the tangent components of the reflected wave vector k_τ^l and the refracted wave vector k'_τ are equal to that of the incident wave vector $k_\tau^l = k'_\tau = k_\tau$. The normal

components of reflected and refracted wave vectors are then given respectively by $k_n^l = -k_n$ and $k_n' = \sqrt{k'^2 - k_\tau^2}$. The refracted wave vector $\boldsymbol{k}'$ and the reflected vector $\boldsymbol{k}^l$ can be finally expressed by

$$\begin{aligned} \boldsymbol{k}' &= k_x' \boldsymbol{e}_x + k_y' \boldsymbol{e}_y = k_\tau' \boldsymbol{\tau} + k_n' \boldsymbol{n} \\ \boldsymbol{k}^l &= k_x^l \boldsymbol{e}_x + k_y^l \boldsymbol{e}_y = k_\tau^l \boldsymbol{\tau} - k_n^l \boldsymbol{n} \end{aligned} \tag{3.19}$$

For the first incident ray (from outside of the cylinder) the normal vector in the above takes the opposite direction of $\boldsymbol{n}$ calculated by Eq. (3.15). Once we know the refracted or internal reflected wave vector, the next incident point is calculated by the intersection of the wave vector with the ellipse. By repeating this procedure, we can trace all the rays until they emerge from the particle.

3.2.2 Convergence or divergence factor

When a wave arrives on a curved surface, it is converged or diverged according to the curvature of the surface and the wavefront curvature of the incident wave. This convergence or divergence must be to determined to evaluate the amplitude of the emergent rays and the phase shift due to the focal line. Since the curvature radius of the cylinder surface in z direction is infinite, only the convergence/divergence of the wavefront on xy plane is to be considered. The divergence factor defined in Eq. (3.10) is then simplified to

$$\mathcal{D} = \frac{R_{11}'}{R_{12}} \cdot \frac{R_{12}'}{R_{13}} \cdots \frac{R_{1p}'}{(r + R_{1p}')} \tag{3.20}$$

Now we will show that in the circular cylinder case, this definition is completely equivalent to the divergence factor in GO Eq. (2.34). In fact, the reflected wave ($p = 0$) curvature can be computed from Eq. (3.8)

$$R_{11}' = -\frac{a \cos\theta_i}{2} \tag{3.21}$$

and the divergence factor is

$$\mathcal{D} = \frac{R_{11}'}{r + R_{11}'} \tag{3.22}$$

In the far field, the term of $r + R_{11}'$ trends to r. Therefore, the divergence factor for $p = 0$ deduces to

$$\mathcal{D}_0 = \frac{a \cos\theta_i}{2r} = \frac{a}{r} D_0 \tag{3.23}$$

Where D_0 is the divergence factor in GO given in Eq. (2.36). In the case of refraction ($p = 1$), the curvature radius of the first refracted wave also can be calculated by Eq. (3.8)

$$R'_{11} = -\frac{am\cos^2\theta_r}{m\cos\theta_r - \cos\theta_i}$$

When the first refracted wave arrives onto the next surface, the curvature of the wave is $R_{12} = 2a\cos\theta_r + R'_{11}$. The curvature radius of the emergent wavefront is finally given by

$$R'_{12} = a\frac{m\cos\theta_r - 2\cos\theta_i}{2(m\cos\theta_r - \cos\theta_i)}\cos\theta_i \tag{3.24}$$

The divergence factor for the refraction $p = 1$ in far field is hereby

$$\mathcal{D}_1 = \frac{R'_{11}}{R_{12}} \cdot \frac{R'_{12}}{r + R'_{12}} = \frac{am\cos\theta_r\cos\theta_i}{2r(\cos\theta_i - m\cos\theta_r)} = \frac{a}{r}D_1 \tag{3.25}$$

D_1 defined in GO is given by Eq. (2.37). We find that with a difference of a factor a/r, the divergence factors in VCRM $\mathcal{D}_0$ and $\mathcal{D}_1$ are equivalent to the divergence factors D_0 and D_1 given in Chapter 2 [Eqs. (2.36) and (2.37)] for circular cylinder as it should be. But the divergence vector defined in VCRM is very general and the dimension of the scatterer is included in the factor. For a circular cylinder the dimension of the particle is well defined by its diameter, while for an arbitrary shaped particle, the divergence factor depends on the curvature of the particle surface where the ray interacts with it and this curvature changes at each interaction. So the divergence factor defined in VCRM reflects well the local curvatures along all the interactions of the ray with the particle surface.

3.2.3 Phase shift

For an elliptical cylinder, the phase shift due to the optical path $\phi_{p,PH}$ can be directly calculated by counting the trajectory distance in and out of the particle. The phase shift due to the reflection or refraction is already included in the Fresnel formulae, but it must be calculated step by step. For total reflection, the Fresnel formulae are complex, the phase shift $\phi_{X,T}$ can be calculated separately [74]

$$\phi_{1,T} = 2\tan^{-1}\left[\frac{(\sin^2\theta_{i,p} - 1/m^2)^{1/2}}{\cos\theta_{i,p}}\right] \tag{3.26}$$

$$\phi_{2,T} = 2\tan^{-1}\left[\frac{m^2(\sin^2\theta_{i,p} - 1/m^2)^{1/2}}{\cos\theta_{i,p}}\right] \tag{3.27}$$

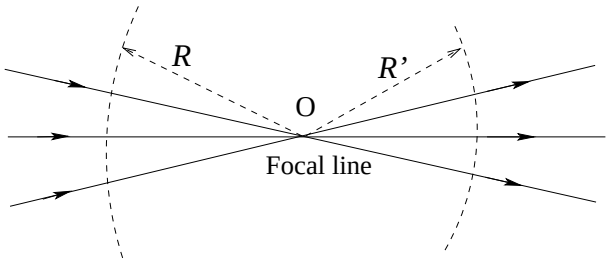

Figure 3.3: Schematic of the change for the curvature radius. O is the center of wavefront.

where the subscript 1 and 2 present the perpendicular and parallel polarizations respectively.

In VCRM, the phase shifts due to the focal lines $\phi_{p,FL}$ are determined by the curvature of wavefront. Each time the sign of curvature radius change, in or out of the cylinder, the phase of the ray advances by $\pi/2$. For a cylinder the convergence/divergence occurs only in one direction, so we have only focal lines as shown in Fig. 3.3, the focal line is perpendicular to the paper sheet. If the convergence in the two directions occurs at the same point, called focal point, it is counted as two focal lines, so the phase advances by π.

By counting all the phase shifts, the total phase shift through the interaction of a ray with the particle is given by

$$\phi_{X,p} = \phi_F(\phi_{X,T}) + \phi_{p,PH} + \phi_{p,FL} \tag{3.28}$$

The total phase shift depends also on the phase of incident wave. If the incident wave does not correspond to a plane wave, the phase of the incident wave varies, therefore, the phase of the incident wave at the incident point is also to be calculated ans added to the total phase of the ray given in Eq. (3.28).

3.2.4 Absorption Factor

When the particle is absorbing, the attenuation should be taken into account too. This can be evaluated by introducing the attenuation factor as function of summating all ray path lengths in the particle [75] according to

$$\xi = \exp\left(-m_i \sum_{q=1}^{p} k'_{n,q} d_q\right) \tag{3.29}$$

where m_i is the imaginary part of particle the refractive index. d_q denotes the length that the ray crosses in the particle and $k'_{n,q}$ is the component of the wave vector normal to the particle surface. It is worth pointing out that the attenuation should not be calculated with real distance but with the wave number in the particle [75]. Eq. (3.29) has been proved to be equivalent to the formula given by Born et Wolf [76], Yang et al Yang [58] and Shen [72] [77].

3.2.5 Amplitude of scattered field

The amplitude of the emergent ray of order p corresponding an incident ray is determined by three factors:

1. the reflection and refraction of the ray on the particle surface, calculated by Fresnel coefficients;
2. the divergence/convergence of the wave on the curved surface, calculated by the divergence factor;
3. and the attenuation for an absorbing particle calculated with Eq. (3.29).

The total complex amplitude of the emergent ray of order p, by counting the phase is therefore given by:

$$S_{X,p}(\theta_j) = \xi \varepsilon_{X,p} \sqrt{\frac{\pi}{2}\mathcal{D}} e^{i\phi_p} \tag{3.30}$$

where $\varepsilon_{X,p}$ has been mentioned in Eq. (3.12). To be convenient and consistent with VCRM, the Fresnel formulae are written as function of the normal components of the wave vectors in and out of the particle (k'_n and k_n respectively)

$$r_1 = \frac{k_n - k'_n}{k_n + k'_n} \tag{3.31}$$

$$r_2 = \frac{m^2 k_n - k'_n}{m^2 k_n + k'_n} \tag{3.32}$$

$$t_1 = \frac{2k_n}{k_n + k'_n} \tag{3.33}$$

$$t_2 = \frac{2mk_n}{m^2 k_n + k'_n} \tag{3.34}$$

This type of the Fresnel coefficient is the same as the expression provided in chapter 2, but it can simplify significantly the calculation, especially for a scattering of particle in 3D.

The total intensity is then just the square of the module of the complex amplitude $|S_X(\theta)|^2$. However, it is important to note that for a given incident ray, each order of emergent rays has its proper direction angle determined by the incident position, the refractive index and the order of the ray. Therefore, if we need the scattered field at a given angle, the amplitude and phase shift are need to be interpolated. In this thesis, the Lagrange interpolation is applied to obtain the complex amplitude at a given angle for each order of emergent rays. All the fields from the different orders as well as the diffraction (Eq. (2.49)) are summed together to obtain the total field. The total intensity is obtained by considering the square of total amplitudes.

In the case of circular cylinder, the incident angle, the refraction angle as well as the Fresnel coefficient remain constant at each interaction of the ray with the particle surface. The calculation described above can be dramatically simplified and analytical expressions can be given for the scattering angle, the phase shifts due to the optical path and the focal lines as well as the divergence factor. These expressions have been given by classical geometrical optics in the last chapter.

3.3 Numerical Results and discussion

A code has been written in Fortran 95 according to the procedure described above. In order to present clearly, we give here the main parameters for numerical calculations in this section. The wavelength of incident wave is $\lambda = 0.6328$ μm. The refractive index of the particle are equal to $m = 1.33$, except for special mention (Fig. 3.13, Fig. 3.14, Fig. 3.15 and Fig. 3.17). In most cases, we find that the maximum order of rays $p_{max} = 6$ is sufficient since the calculation with higher orders gives very similar results [78]. So $p_{max} = 6$ is chosen for the calculation in this section and the number of incident rays is 6000 equal distant and the scattering angular grid is $\Delta\theta = 0.01^\circ$.

Since the ray model is only valid for particles of size much greater than the wavelength, we begin with very large circular cylinders. Fig. 3.4 illustrates the scattering diagrams of a circular cylinder of refractive index $m = 1.33$ and radius $a = 50$ μm illuminated by a plane wave of wavelength $\lambda = 0.6328$ μm calculated by LMT, GO and VCRM for perpendicular and parallel polarizations. The diffraction is taken into account in GO and VCRM. We find that the agreement between GO and VCRM is excellent as expected. In this special case, VCRM is thoroughly equivalent to the classical GO. The results of GO and VCRM are also in very good agreement with

that of LMT in all directions except in the Alexander's dark region and near 90° for parallel polarization. This is the limitation of ray model rather than the numerical methods.

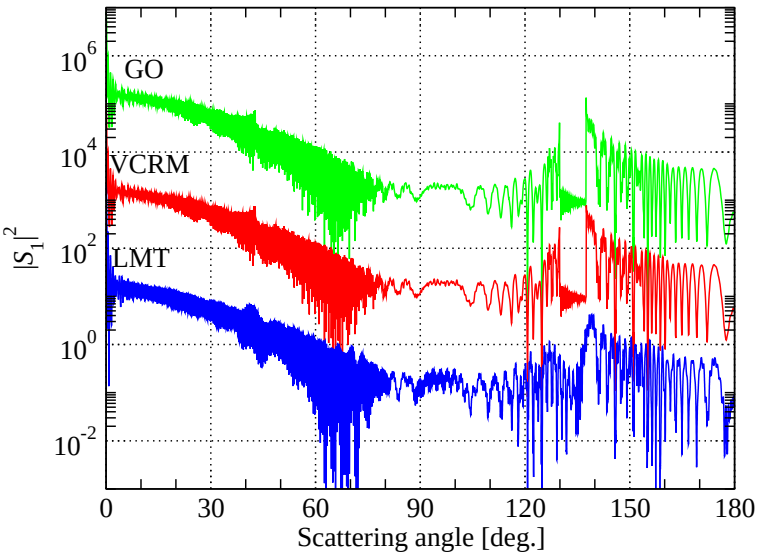

(a). Perpendicular polarization.

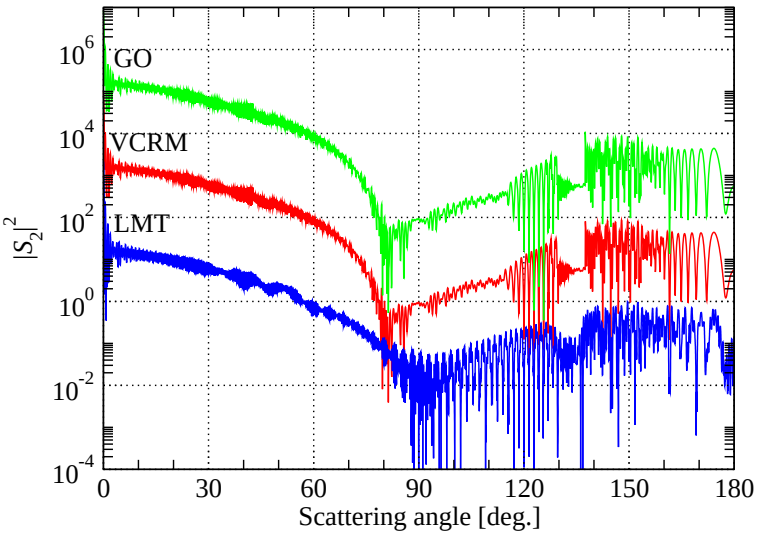

(b). Parallel polarization.

Figure 3.4: Comparison of the scattering diagrams computed by LMT, GO and VCRM for an infinite circular cylinder ($m = 1.33$, $a = 50$ μm) illuminated by a plan wave of wavelength $\lambda = 0.6328$ μm. The results of LMT and GO are shifted by 10^{-2} and 10^2 respectively for clarity.

In order to show the interference effect, the details of the scattering diagram

calculated by the three methods are given in the Fig. 3.5. We find that the profiles of the three curves are in excellent agreement in the near forward direction.

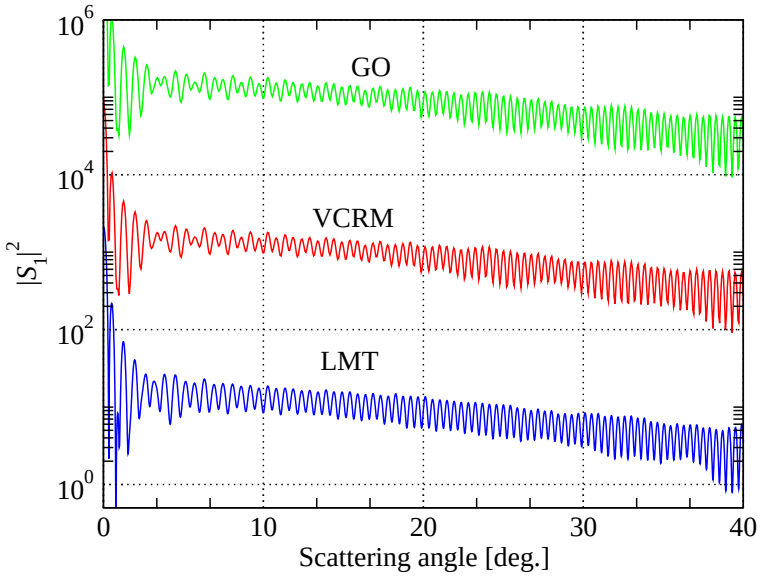

Figure 3.5: Zoom of the scattering diagrams in near forward direction. The parameters are the same as in Fig. 3.4.

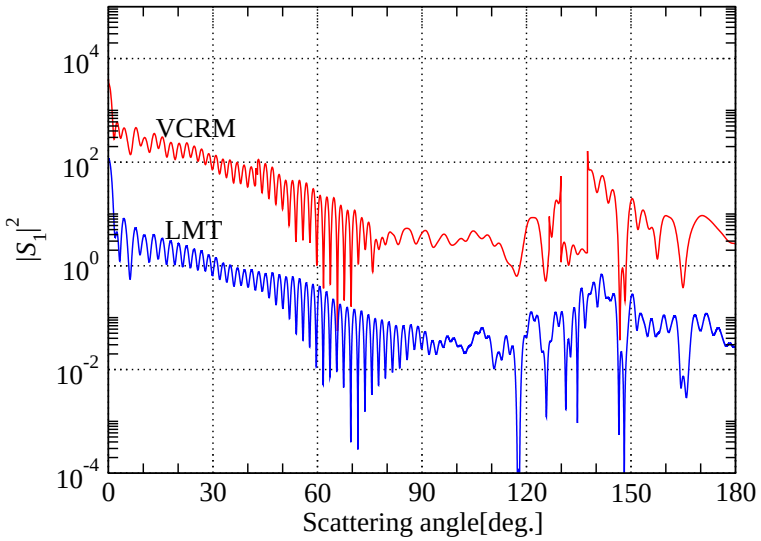

Figure 3.6: Same parameters as in Fig 3.4 (a), but particle radius is $a = 10\mu m$.

Then we examine the effect of particle size on the precision of ray model by comparing the scattering diagrams of a circular cylinder of smaller size calculated by VCRM to those obtained by LMT. Fig. 3.6 shows the scattered intensity by a circular

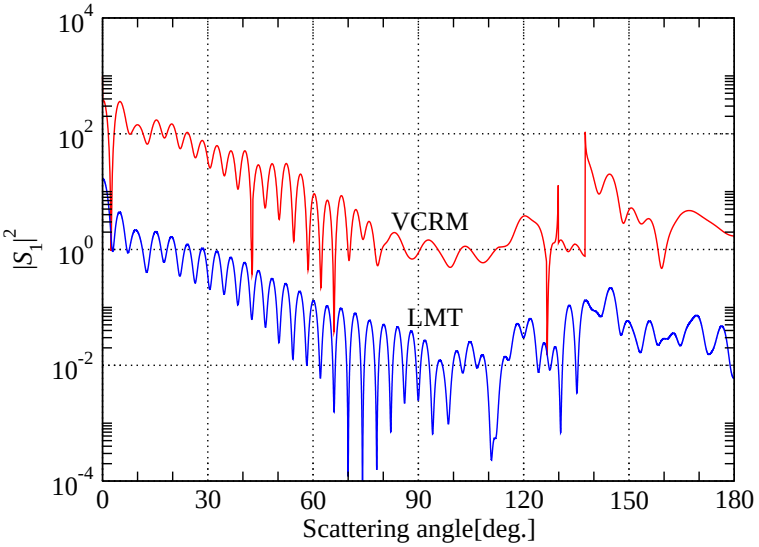

Figure 3.7: Same parameters as Fig 3.4 (a), but with the $a = 5\mu m$.

cylinder with radius of 10 μm illuminated by a perpendicular polarized plane wave. The general agreement between LMT and VCRM may be considered as acceptable, but clearly worse than for the particle of 50 μm of radius. The discrepancy near rainbow angles and around 90° is clearly visible. The difference in the backward direction becomes also perceivable.

If we decrease further the particle size, as shown in Fig. 3.7 for a cylinder of 5 μm of radius, the difference between the diagrams calculated by VCRM and LMT becomes more significant, especially for the scattering angle larger than 80° where the profiles of the two curves are still similar but the details are different.

Now we present the scattering diagrams of elliptical cylinder calculated by VCRM. It should be noted that even many researchers have contributed to the scattering of elliptical cylinder in the framework of rigorous theory as LMT and GLMT [17, 44, 39, 79] or by numerical simulation as DDA and T-matrix [22], we have not found in the literature the scattering diagrams available for large elliptical cylinders. Therefore, to check our code, the scattered intensities of an elliptical cylinder calculated by VCRM will be compared to those of a long ellipsoid by taking one of the ellipsoid semi-axes much longer than the two others. The code for the calculation of the scattered intensity of an ellipsoidal particle is also based on VCRM [66], so it is not a complete independent method, but its programmation is different and it serves at least as a check of the code. Furthermore, in VRCM we can follow the trace and the phase of

each ray and examine its contribution to the amplitude of scattered light.

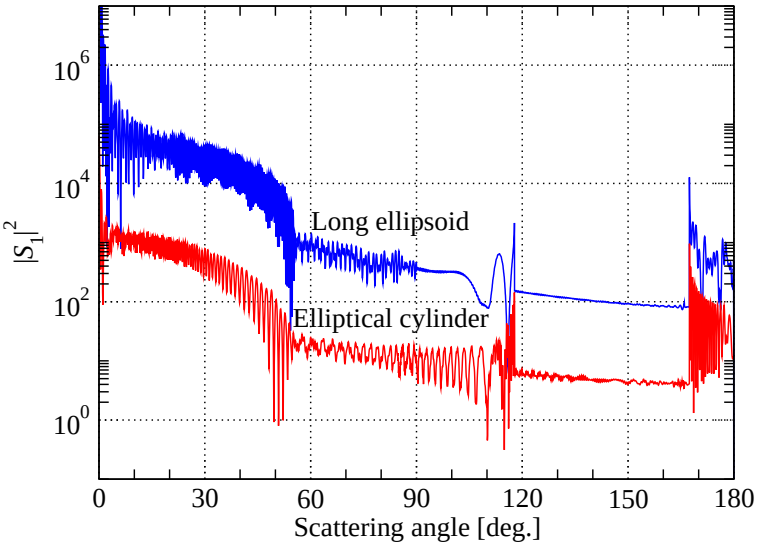

(a). Perpendicular polarization.

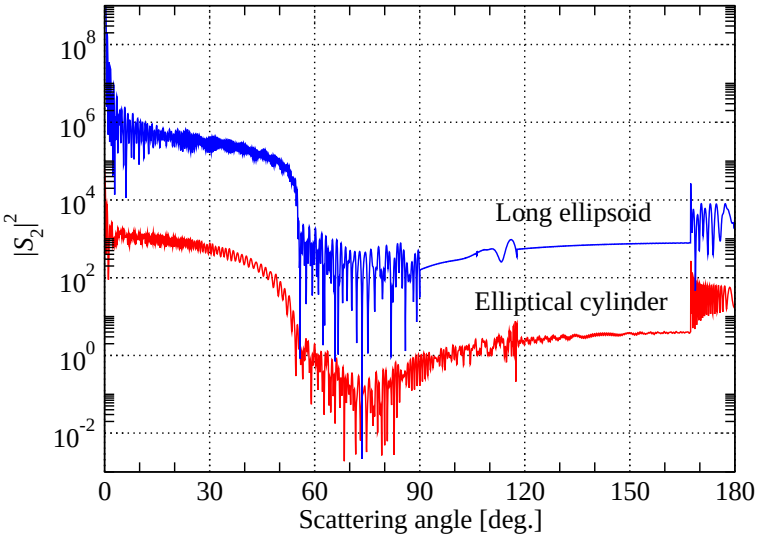

(b). Parallel polarization.

Figure 3.8: Comparison of scattering diagrams of an elliptical cylinder ($a = 50$ μm, $b = 40$ μm) and a long ellipsoid ($a = 50$ μm, $b = 40$ μm, $c = 5$ mm) calculated by VCRM. The refractive index is 1.33. The incident plane wave propagates along x axis. The scattered intensity of the long ellipsoid is offset by 10^{-6} for clarity.

The scattering diagrams of a prolate and an oblate cylinder are compared in Figs. 3.8 and 3.9 with an elliptical cylinder and a long ellipsoid. It can be seen clearly that for two polarizations they are similar in almost all directions. So we can consider

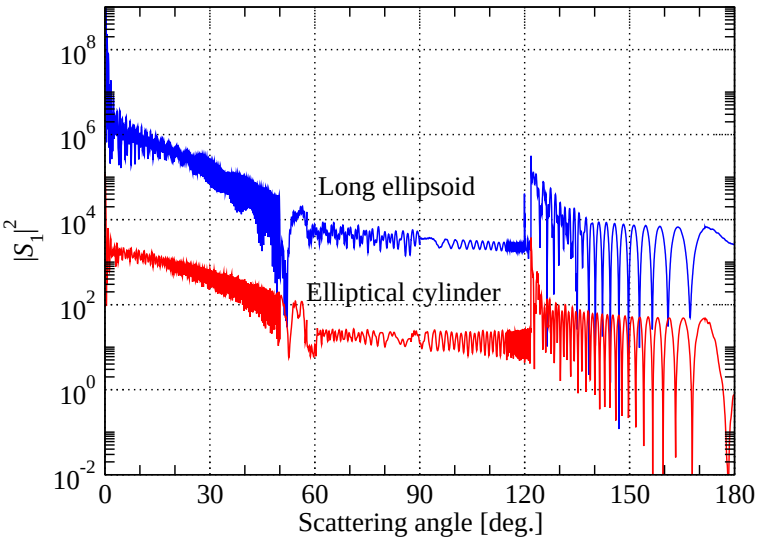

(a). Perpendicular polarization.

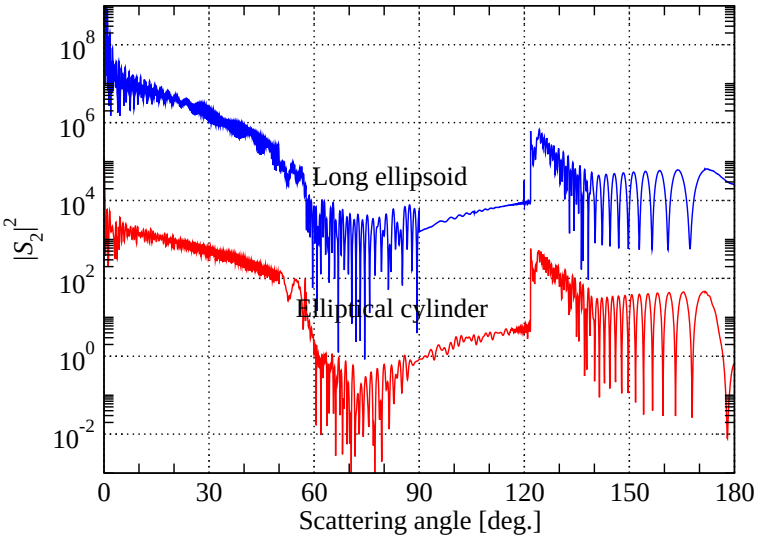

(b). Parallel polarization.

Figure 3.9: Same parameters as Fig 3.8, but with $a = 40$ μm, $b = 50$ μm. The positions of the first and second rainbows respectively locate at 121.8° and 127.0°.

that our code is validated. On the other hand, we observe from the figures that the angular distance between the first and the second rainbows for a prolate elliptical cylinder is 49.57°, much greater than that of a circular or spherical particle of 7.59° (see Fig. 3.4 for example) . While for the oblate elliptical cylinder, only the first rainbow at 121.79° is clearly visible, higher order rainbows are very narrow and week. The fifth order rainbow, for instance, is observable (at 121.79°) when the angle step

in the calculation is small enough. The difference between the two polarizations is similar as for circular cylinder.

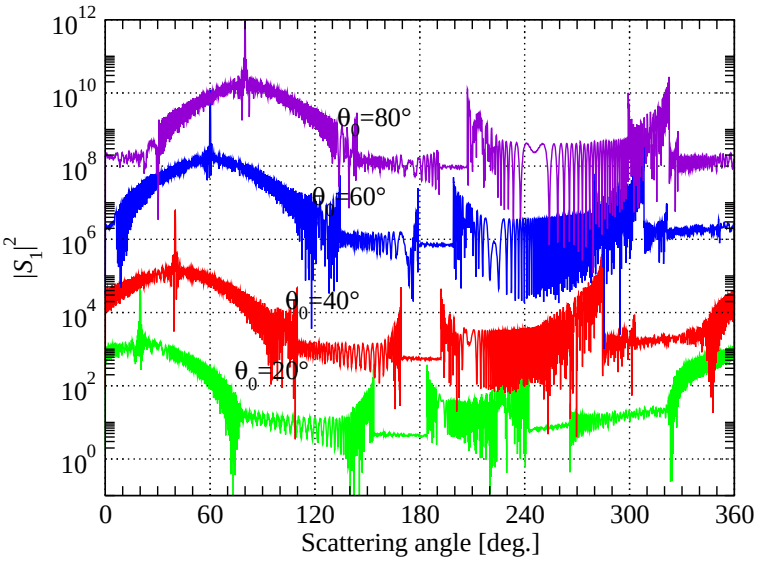

(a). Perpendicular polarization.

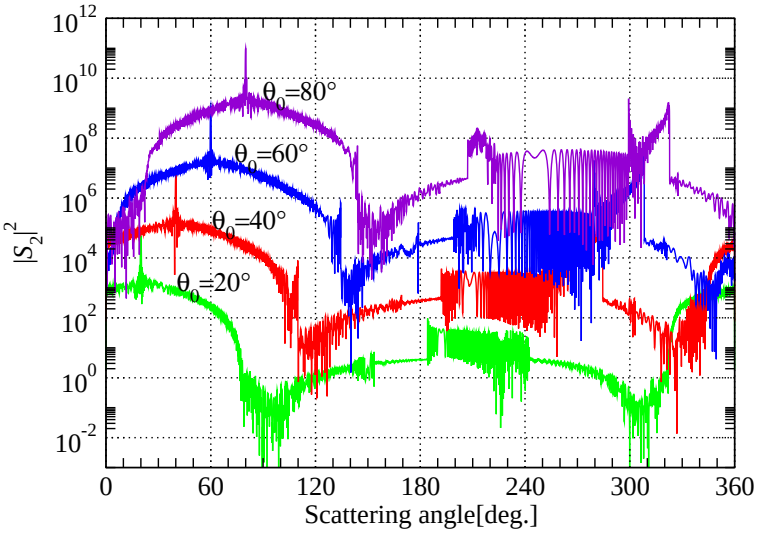

(b). Parallel polarization.

Figure 3.10: Scattering diagrams of an elliptical cylinder illuminated by a plane wave at different incident angles. The other parameters are the same as in Fig. 3.8

.

When an elliptical cylinder is illuminated obliquely by an plane wave, i.e. the incident direction makes an angle with a symmetric axis of the ellipse, due to the asymmetry, the scattering diagrams are much more complicated and depend greatly

on the incident angle and the aspect ratio a/b. The scattering diagrams are no longer symmetric and must be presented for the angles from 0° to 360°.

Fig. 3.10 illustrates the scattering diagrams of an elliptical cylinder illuminated by a plane wave at different angles. The scattering diagrams for $\theta_0 = 0°$ and $\theta_0 = 90°$ correspond respectively to the cases of the prolate and oblate elliptical cylinders shown in Figs. 3.8 and 3.9, and therefore they are not given in this figure. It should be noted that the scattering angle is counted relative to the x axis, so the forward direction is at $\theta = \theta_0$ where we find the most important peak. It can be seen clearly from the Fig. 3.10 that the rainbow positions change with the incident angle and they are not symmetric to the incident direction. Tab. 3.1 compiles the first and the second order rainbow positions extracted from Fig. 3.10. The first rainbow angle in one side ($0 < \theta_1 < 180°$) increases monotonously when the incident angle θ_0 increases, while the first rainbow angle in the other side ($180° < \theta_1 < 360°$) increases until 248.0° for $\theta_0 = 60°$ and then decreases. The second order rainbow exists only for small incident angle util $\theta_0 = 60°$ in one side and $\theta_0 = 20°$ in the other side.

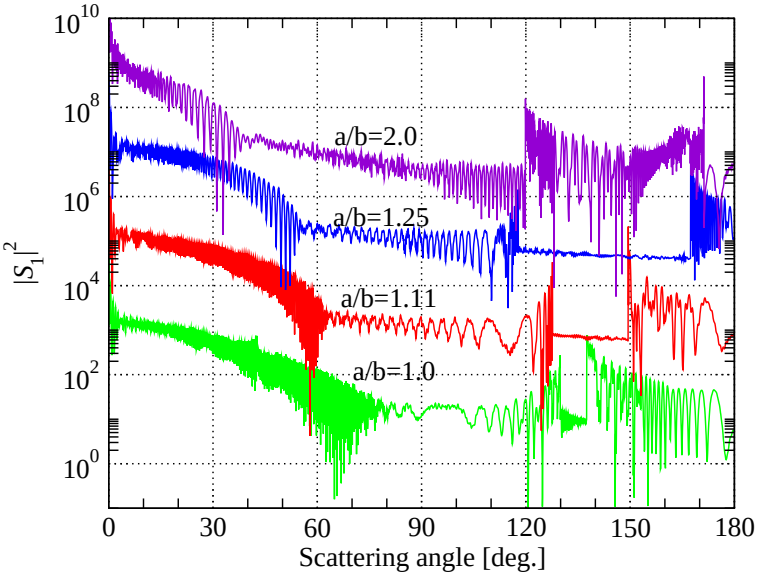

Figure 3.11: Scattering diagrams of an elliptical cylinder illuminated by a plane wave for the different aspect ratios. The perpendicular polarization is chosen.

The scattering diagrams of an elliptical cylinder for perpendicular polarization with aspect ratio as parameter are shown in Fig. 3.11 for $\theta_0 = 0°$. The semi-axis of the ellipse in x direction is 50 μm, while that in y direction is 50 μm, 45 μm, 40 μm or 25 μm. It shows that when the aspect ratio a/b increases from 1 to 1.25, the first

Table 3.1: Rainbow positions of an elliptical cylinder $a = 50$ μm, $b = 40$ μm and $m = 1.33$ illuminated by a plane wave $\lambda = 0.6328$ μm with different incident angles θ_0. θ_1 and θ_1' are the positions of the primary rainbows, and θ_2 and θ_2' are the positions of the second order rainbows.

θ_0	$\theta_1 - \theta_0$	$\theta_2 - \theta_0$	$\theta_1' - \theta_0$	$\theta_2' - \theta_0$
0	167.9	116.8	192.1	243.2
20	164.4	133.3	221.7	247.2
40	152.3	128.9	244.1	-
60	139.4	118.5	248.0	-
80	127.3	-	242.5	-
90	122.0	-	238.0	-

order rainbow goes to larger angle, the second order rainbow to the smaller angle and the Alexander region expands. When the aspect ratio is too big, the positions of the first rainbow (at 119.8°) and the second order rainbow (at 171.2°) are reversed.

To show the dependence of the rainbow positions on both the incident angle and the aspect ratio, Fig. 3.12 depicts the relation of the first rainbow position as function of the incident angle with aspect ratio as parameter. Only the prolate cylinder (aspect ratio larger than 1) is shown in the figure since those for an oblate elliptical cylinder (aspect ratio less than 1) can be deduced directly from this figure. In fact, if we note the rainbow position of a prolate cylinder of aspect ratio $\kappa = a/b$ by θ_r for an incident angle θ_0, then the rainbow angle of an oblate cylinder of aspect ratio $1/\kappa$ with incident angle of $90° - \theta_0$ is at $450° - \theta_r$. For a circular cylinder, the relation between the incident angle and the primary order rainbow position is linear (black solid line). For an elliptical cylinder, the relation is no longer linear. When the aspect ratio increases, the rainbow angle on one side (shown in the high part of Fig. 3.12) decreases until $\theta_0 = 20°$ and then increases, and on the other side (shown in the lower part of Fig. 3.12) the rainbow angle increases until $\theta_0 = 60°$ and then decreases. If the aspect ratio is too small ($\kappa = 0.5$) or too big ($\kappa = 2$) the rainbow structure is very different(blue square symbols in Fig. 3.12). For example, when the incident angle is 0, the rainbow positions do not follow the variation as described above but jump to the other side relative to the rainbow of a circular cylinder. There is only one first rainbow when the incident angle is between 9° and 56° but three first rainbow for the incident angle between 50° and 55°.

The light scattering by an infinite cylinder with refractive index less than unity, called thereafter bubble cylinder for short, can also be calculated with our code.

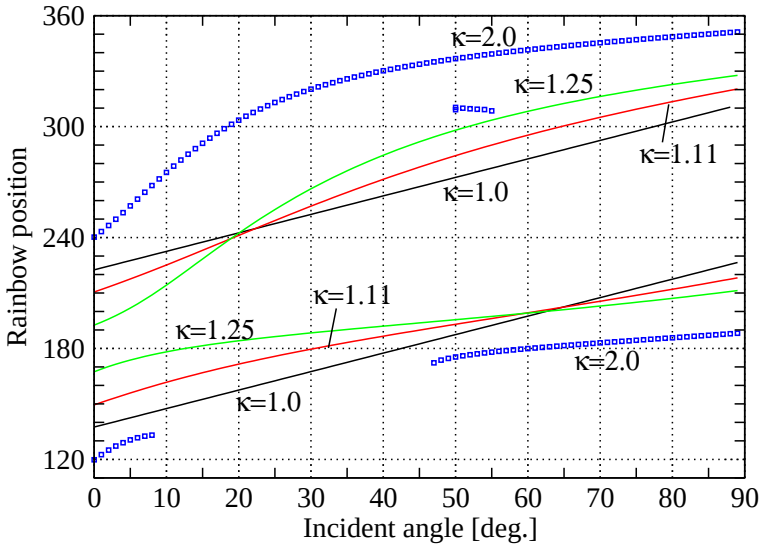

Figure 3.12: Relation of incident angle and the rainbow angle position for different aspect ratios.

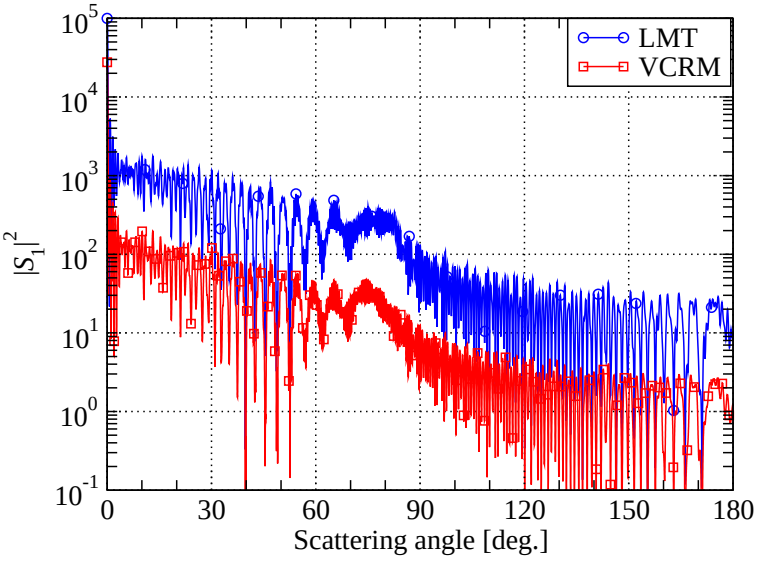

Figure 3.13: Same parameters as Fig. 3.4, but for the refractive index of particle is 0.75.

Still, we first compare the light scattering diagram of a circular cylinder calculated by VCRM and by LMT in order to evaluate its precision. Consider a cylinder of refractive index $m = 0.75$ and radius $a = 50\mu m$ illuminated by the plane wave of wavelength $\lambda = 0.6328\mu m$. The results are shown in Fig. 3.13. We found that agreement is

very good, even better than for the cylinders of refractive index larger than unity. Anyway small differences are still observable in the region near 83°. That is due to the discontinuity of the derivative of the reflected wave amplitude. In fact, when the incident angle on the particle surface is smaller than the critical angle of 48.59°, the amplitude of the reflected ray varies gradually. Once the incident angle is larger than the critical angle, the incident energy is totaly reflected and no rays are refracted into the particle. This difference is expected to be improved by taking into account the wave effect using Huygens-Fresnel integration. But we will not deal with it in this thesis [80, 81].

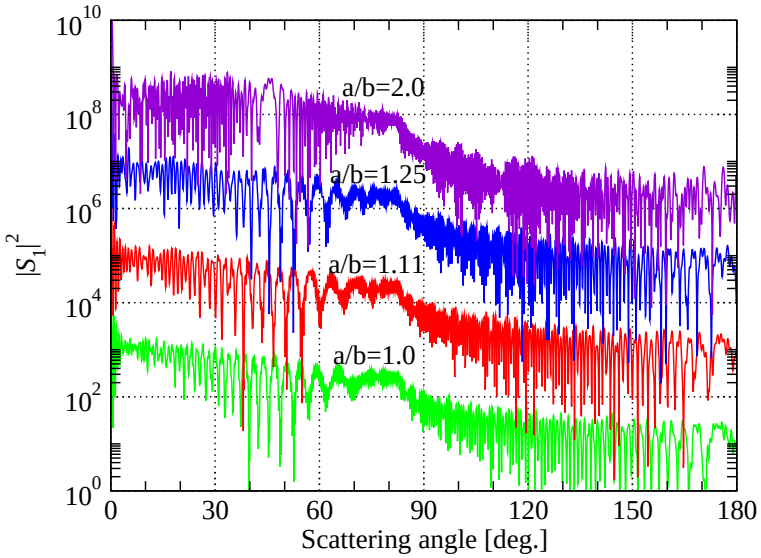

Figure 3.14: The parameters are the same as in Fig. 3.11 but for the refractive index of the particle is 0.75. The incident wave is perpendicular polarization.

To analyze the influence of the aspect ratioκ , the scattering diagrams of elliptical cylinder with κ as parameter are illustrated in the Fig. 3.14. The particle radius is the same as in Fig. 3.11, but the refractive index is now $m = 0.75$. We find that, similar to the spheroidal bubble [78], the scattering diagrams are unsensible to the aspect ratio of the elliptical cylinder.

Furthermore, we can note that when the particle of refractive index is smaller than the surrounding medium, no rainbow phenomenon is observed for a circular bubble cylinder. But for an elliptical bubble cylinder, the rainbows do exist for certain ellipticities and incident angles. An example is given in Fig. 3.15 to show that the rainbow can occur in a bubble cylinder. The second rainbows are formed and locate at 146° and 158°. But the amplitude is weak and difficultly detectable in this example.

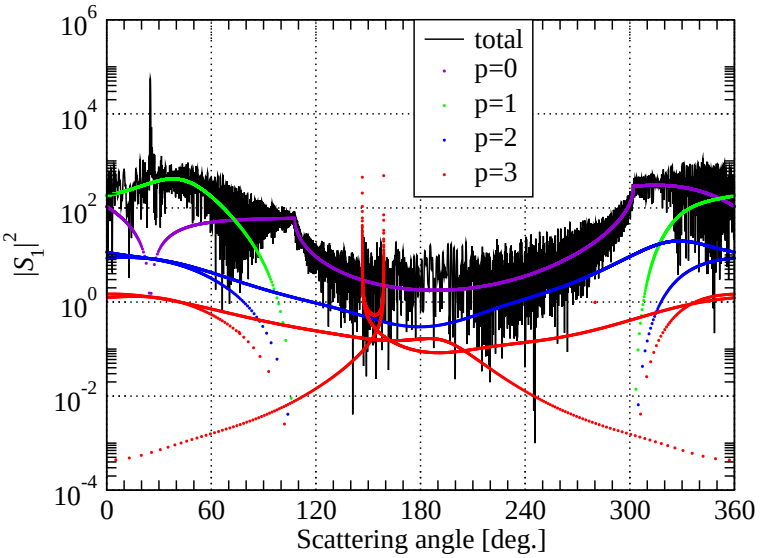

Figure 3.15: Total and individual order scattered intensities of an elliptical bubble cylinder ($m = 0.75, a = 50\mu m, b = 25\mu m$) illuminated by a plane wave of wavelength $\lambda = 0.6328\mu m$ with an incident angle $\theta_0 = 25°$.

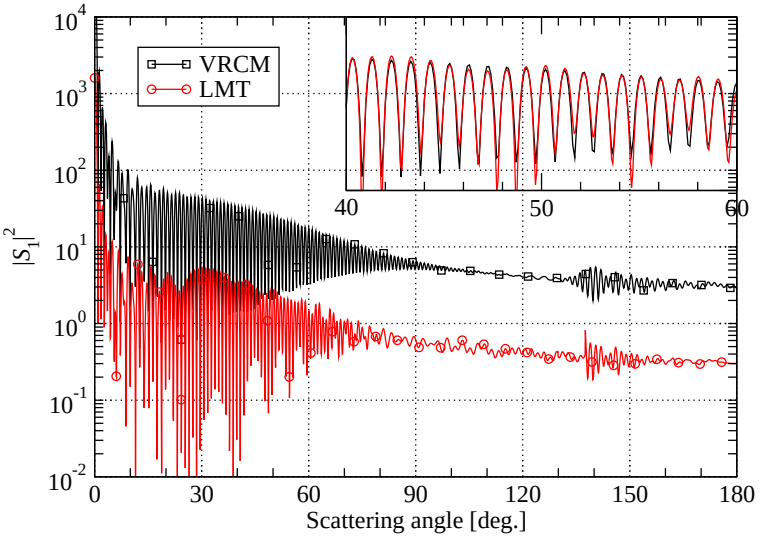

Figure 3.16: The circular cylinder of radius 20μm illuminated by the plane wave of wavelength $\lambda = 0.6328\mu$m. The refractive index of particle is $1.33 + i0.005$.

We have also applied our code to the calculation of the scattering of an absorbing infinite elliptical cylinder. The scattering diagrams calculated by VCRM and LMT for an absorbing circular cylinder of radius $r = 20\mu$m are compared in Fig. 3.16. It can be seen that the agreement is good in almost all directions. Note that the rainbows

are difficult to observe. This is because that for such a large particle, the amplitudes of emergent rays decrease very rapidly as the order of the rays. This can be evaluated by Eq. (3.29) knowing that distance between two successive interactions of a ray on the internal surface of a circular cylinder is

$$d = 2a \sin \tau'$$

τ' for the first and the second rainbows are respectively 49.56° and 44.37° (according to Eq. (2.47)). So the attenuation factor between the two interactions is

$$\xi = \exp(-2pm_i k' a \sin^2 \tau') = \begin{cases} 0.048 & p = 2 \\ 0.015 & p = 3 \end{cases}$$

That is to say that the intensities of the first the second rainbows are reduced respectively to 4.8% and 1.5% of the rainbows of a transparent cylinder.

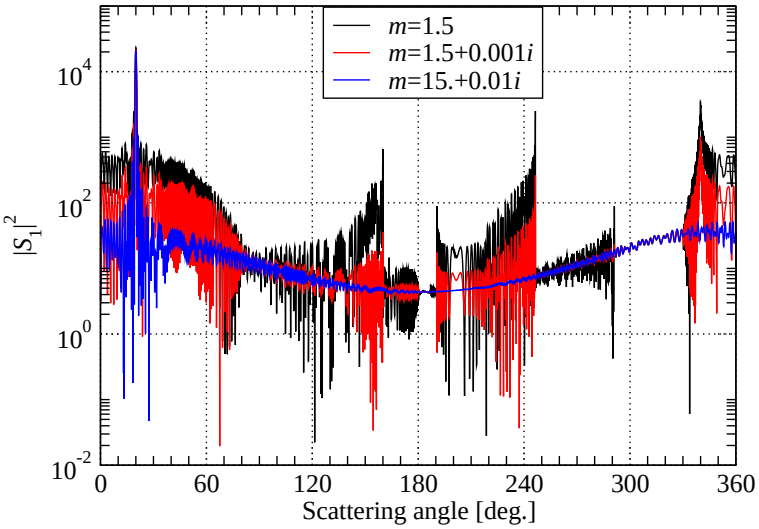

Figure 3.17: Scattering diagram of an elliptical cylinder of semi-axes $a = 30\mu$m,$b = 20\mu$m illuminated by a plane wave of wavelength $\lambda = 0.6328\mu$m and incident angle $\theta_0 = 20°$ with refractive index as parameter.

For an elliptical cylinder, it is not easy to evaluate the attenuation factor as for a circular cylinder and the rainbow structure is also more complicated. Fig. 3.17 shows the scattering diagram of an absorbing elliptical glass fibre. We can note that the absorption effect is more important in both sides (mainly for higher orders) than in the forward (mainly for $p = 1$) and backward (mainly for $p = 2$) regions. Nevertheless, there is a "background" intensity even for a very absorbing particle $m = 1.5 + 0.01i$, this is, in fact, the contribution of pure external reflection.

3.4 Conclusions

In this chapter, Vectorial Complex Ray Model has been applied to the light scattering of an infinite elliptical cylinder illuminated by a plane wave with arbitrary oblique incidence relative to the symmetric axes of the elliptical cross. The model and the code developed have been validated by comparing the results with Mie theory and the classical GO in the case of circular cylinder. A good agreement is found in almost all the directions. It is proved that VCRM can predict with precision the light scattering of a cylinder of size as small as some tens of wavelengths, despite existence of discrepancy in the Alexander's dark region and near the caustics which is caused by the limitation of geometrical optics.

To ensure that the code works well for the elliptical cylinder, the results were also compared with that of a long ellipsoid particle. After the careful validation, our model has been applied to the study of the scattering diagrams as function of the incident angle and the aspect ratio of the ellipse. A special attention has been paid to the rainbow phenomena of an infinite elliptical cylinder. It is found that the scattering diagram is sensible to both the incident angle and aspect ratio. The structure of rainbow of a elliptical cylinder is much more complicated than for a circular cylinder especially when the aspect ratio is important.

Finally, the light scattering of the bubble cylinder (the relative refractive index of the cylinder to the surrounding medium is less than unity) and the absorbing cylinder are also calculated by the code. As a curiosity, we have shown that for particular parameters an elliptical bubble cylinder can produce rainbow like patterns which can not be observed with circular bubble cylinders.

Chapter 4

VCRM for scattering of Gaussian beam by an elliptical cylinder

In the proceeding chapter, VCRM has been applied to the scattering of a plane wave by an infinite elliptical cylinder. The propagation direction of the plane wave is perpendicular to the axis of the cylinder but it can make any angle with the main axes of the ellipse of the cylinder section. This is the most simple case in the light scattering by irregular particles, and all the scattering properties are independent of z axis (along the particle axis) and only the divergence of the wave in one direction is to be considered.

In this chapter we will extend VCRM to the scattering of a shaped beam which introduce new problems:

- *Determination of illumination region:* In the plane wave case, the illumination region is easy to determine, especially for an elliptical cylinder (or a particle of shape well defined by an analytical expression such as spheroid, ellipsoid, etc.). But when the incident wave is a shaped beam, the illumination region can not be determined analytically since the directions of the rays representing the incident beam vary as function of the position in the beam. This problem will be dealt with numerically in the framework of VCRM and the details will be given in Section 4.1.

- *Calculation of wavefront curvature:* As we have seen in the last chapter, VCRM allowing accounting for the divergence/convergence of a wave each time a ray interacts with the particle surface. The curvature of a plane wave is zero, its radii of curvatures in the two principal directions are therefore infinite. But for

a shaped beam, the curvature of wavefront depends not only on the beam shape parameters such as the wavelength, the beam waist radius (for two dimensional Gaussian beam and circular Gaussian beam, or radii for elliptical Gaussian beam), etc. but also the position of the particle in the beam. So to evaluate the convergence in each interaction of a ray with the particle surface, we need to determine the wavefront curvature at the incident point. This can be done according to the phase function of the beam. To express the curvature in the particle coordinate system, a transformation of coordinate systems is necessary. Sections 4.2 and 4.3 will be devoted to the coordinate system transformation and the wavefront curvature calculation. The methods presented herein are general and can be applied to any shaped beam.

As examples of the method, three kinds of Gaussian beam will be considered and the calculation of propagation direction and the curvature radii will be presented in Section 4.4.

We would note also that different from the scattering of a plane wave, when an infinite cylinder is illuminated by a shaped beam, even the curvature of the particle in one direction is zero, the divergence/convergence in two directions must be considered. This is a conventional procedure in VCRM, so only some important remarks will be given with numerical results in section 4.5.

4.1 VCRM for scattering of a shaped beam

We consider here the scattering of a shaped beam by an infinite elliptical cylinder, and more particularly the case where the incident beam axis is perpendicular to the cylinder. We are interested only in the scattering of the beam in the plane containing the beam axis. We suppose also that the beam possesses a symmetry so that the rays remain always in the same plane, such as in the cases of Gaussian beams and Bessel beams. With these assumptions, one principal direction of the wavefront is always parallel to the axis of the cylinder axis, while the other changes its direction each time the ray interacts with the particle surface but it stays in the same plane. We need therefore only to trace the rays in this plane.

The ray tracing in VCRM is relatively straight forward once we know the position and the angle of the incident ray. This is simple for a plane wave since the direction of all the incident rays are the same and is the direction of the wave. The incident

position can be determined by the analytical solution of the equation of the ellipse and the line corresponding to the direction of the incident direction. The lit region can also be determined analytically. For a plane wave of incidence angle θ_0 with respect to x axis, the two limit points A and B between lit region AFB and dark region AGB are given by (see the two dot lines in Fig. 4.1)

$$x_A = -a^2\gamma_0^2/\sqrt{b^2+\gamma_0^2a^2} \tag{4.1}$$

$$y_A = b^2/\sqrt{b^2+\gamma_0^2a^2} \tag{4.2}$$

$$x_B = -x_A \tag{4.3}$$

$$y_B = -y_A \tag{4.4}$$

where $\gamma_0 = \tan\theta_0$. It is evident that the two points A and B are symmetric to the center of the ellipse. We need to trace the incident rays of the x coordinate varying from x_A to x_B.

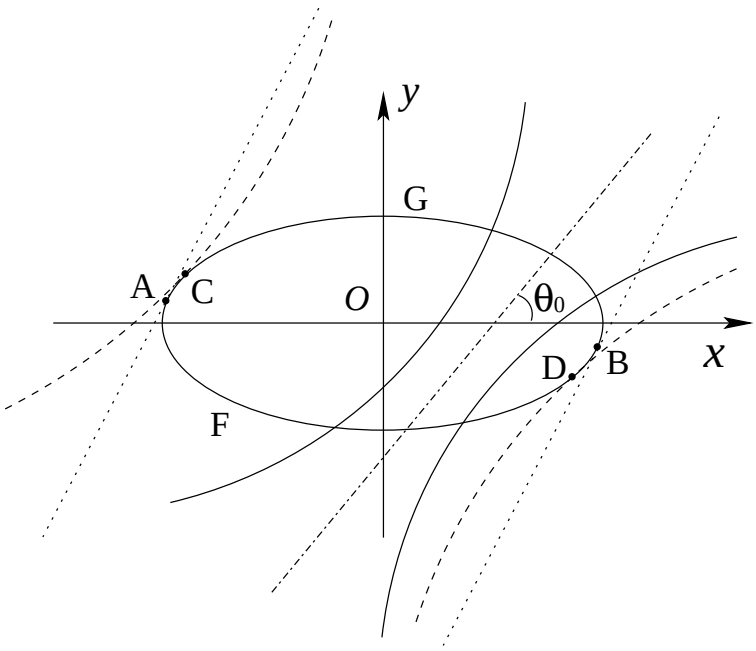

Figure 4.1: Illumination by a shaped beam

When the incident wave is a shaped beam, the determination of the incident point and the lit region are not so easy. Consider a beam as shown in Fig. 4.1 and outlined with solid lines. The beam axis (dot-dashed line) makes an angle θ_0 with respect to x axis. Note that, to avoid mixing with the lit limit points A and B of plane wave,

the incident angle for the shaped beam is different from that of the plane wave in the figure. The two lit limit points are C and D, which are the points corresponding to the rays tangent to the surface of the particle. These points depend on the beam shape parameters, as well as its direction and position relative to the particle. In general, the problem of these points can not be obtained analytically, but relatively easy to be dealt with numerically. In fact, for a given point on the surface of the particle, we can calculate the wave vector of the incident beam $\boldsymbol{k}$ and the out going normal of the particle surface $\boldsymbol{n}$ at that point. If their scalar product $q = \boldsymbol{n} \cdot \boldsymbol{k}$ is negative, then the ray impinges on the particle, otherwise, the ray will not counted.

The second problem to be considered in the scattering of a shaped beam by an elliptical cylinder is the divergence factor. As stated in the section 3.1, in VCRM the divergences of all waves are described with the wavefront curvature step by step. Because we are limited in two dimension scattering problem, the wavefront curvature equation is simplified to two scalar equations (3.8) and (3.9) as stated in chapter 3. Furthermore, the second curvature radius of the cylinder is infinity, so the two scalar equations are given by

$$\frac{{k'_n}^2}{k' R'_1} = \frac{k_n^2}{k R_1} + \frac{k'_n - k_n}{\rho_1} \tag{4.5}$$

$$\frac{k'}{R'_2} = \frac{k}{R_2} \tag{4.6}$$

where ρ_1 is the local curvature radius of ellipse, R_1 and R_2 the curvature radii of the wavefront before the refraction/reflection, R'_1 and R'_2 those after refraction/reflection. For a shaped beam, the two principal curvature radii of the wavefront can be determined by its phase function. The calculation of the curvature of a Gaussian beam will be given in the following subsection.

The divergence factor in VCRM is deduced directly from the curvature radii of the rays. For the scattering of a plane wave by an infinite cylinder, the wave is converged or diverged in one direction and can be treated as a two dimensional scattering. But in the case of shaped beam, the divergence and convergence in two directions must be counted and the two dimension divergence factor definition (Eq. (3.10)) should be used.

When an infinite cylinder is illuminated by a plane wave, the scattering is two dimensional, we have only one term $(r + R'_{1p})$ which tends to r in far field and can be omitted in the calculation of scattering diagram. For the scattering of a shaped beam by an infinite cylinder, the wavefront curvature radius of the emergent wave in

horizontal plane (cross section of cylinder) is similar as for the plane wave (Eq. (4.5)), but that in the vertical plane (infinite direction) is almost the same as the wavefront curvature radius of the incident beam (see Eq. (3.9)). This curvature radius varies from some millimeters for strongly focused beam to some kilometers for very large beam. However, in practical applications, r is in the order of centimeters to meters, so, in general, R'_{1p} is not so small to be neglected nor big enough to replace the term $(r + R'_{1p})$ by R'_{1p}. The scattered wave is therefore neither cylindrical nor spherical.

The phase shift and the complex amplitude calculations are similar as that described in the last chapter. We will deal with in the following sections the specific problems to the scattering of a shaped beam, i.e. the coordinate system transformation, the determination of the ray direction and the wavefront curvature radii of a shaped beam.

4.2 Transformation of coordinate systems

Consider an infinite elliptical cylinder illuminated by a Gaussian beam of waist radius w_0 and wavelength in vacuum λ. We define $(O_G; uvw)$ and $(O; xyz)$ as the beam coordinate system and the particle coordinate system respectively. The relation between them can be given by a translation and three rotations measured by the three Euler angles. Starting with the beam coordinate system $(O_G; uvw)$ overlapping the particle coordinate system $(O; xyz)$, we translate first the beam center to (x_0, y_0, z_0), then rotate around z axis an angle α, around the line of nodes (temporary u axis) an angle β such that the temporary z axis is in the direction of the beam axis w, and finally around w axis an angle γ to obtain the coordinate system $(O_G; uvw)$. The first two angles are to define the propagation direction of the beam and the third one is to determine the polarization. The relation between the two coordinate systems is given by

$$\begin{pmatrix} u \\ v \\ w \end{pmatrix} = A \begin{pmatrix} x - x_0 \\ y - y_0 \\ z - z_0 \end{pmatrix} \tag{4.7}$$

The elements of the transformation matrix A

$$A = \begin{pmatrix} a_{11} & a_{12} & a_{13} \\ a_{21} & a_{22} & a_{23} \\ a_{31} & a_{32} & a_{33} \end{pmatrix} \tag{4.8}$$

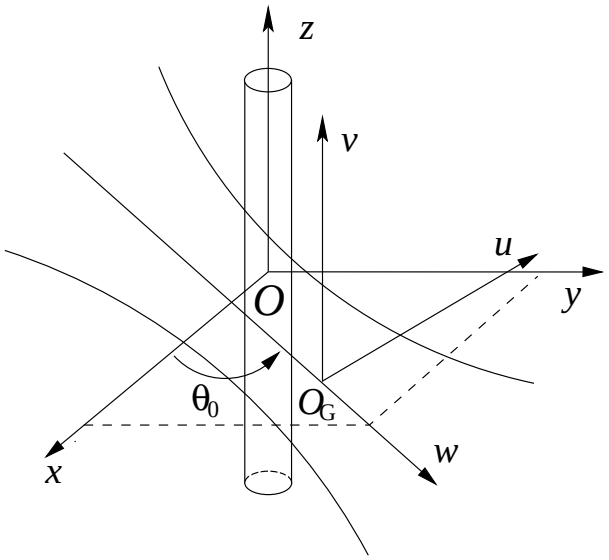

Figure 4.2: Geometry of Cartesian coordinates of the beam and the particle

are defined by

$$a_{11} = \cos\alpha\cos\gamma - \cos\beta\sin\alpha\sin\gamma \tag{4.9}$$

$$a_{12} = \sin\alpha\cos\gamma + \cos\beta\cos\alpha\sin\gamma \tag{4.10}$$

$$a_{13} = \sin\beta\sin\gamma \tag{4.11}$$

$$a_{21} = -\cos\alpha\sin\gamma - \cos\beta\sin\alpha\cos\gamma \tag{4.12}$$

$$a_{22} = -\sin\alpha\sin\gamma + \cos\beta\cos\alpha\cos\gamma \tag{4.13}$$

$$a_{23} = \sin\beta\cos\gamma \tag{4.14}$$

$$a_{31} = \sin\alpha\sin\beta \tag{4.15}$$

$$a_{32} = -\cos\alpha\sin\beta \tag{4.16}$$

$$a_{33} = \cos\beta \tag{4.17}$$

In the case of an elliptical cylinder illuminated by a shaped beam in xy plane with an incident angle θ_0 relative to the x axis, the three Euler angles are respectively $\alpha = \theta_0 + 90°$, $\beta = 90°$ and $\gamma = 0$ for parallel polarization or $90°$ for perpendicular polarization (see Fig. 4.2). The matrix A for $\gamma = 0$ is simplifies to

$$A = \begin{pmatrix} -\sin\theta_0 & \cos\theta_0 & 0 \\ 0 & 0 & 1 \\ \cos\theta_0 & \sin\theta_0 & 0 \end{pmatrix} \tag{4.18}$$

Then the coordinates of a point in the Gaussian beam after rotation are given by

$$u = -(x - x_0)\sin\theta_0 + (y - y_0)\cos\theta_0 \tag{4.19}$$

$$v = z \tag{4.20}$$

$$w = (x - x_0)\cos\theta_0 + (y - y_0)\sin\theta_0 \tag{4.21}$$

The matrix A for the perpendicular polarization ($\gamma = 90°$) is similar. Therefore, when we know the position of the beam center (x_0, y_0, z_0) and its propagation direction, the coordinates of a point in the beam coordinates system (u, v, w) can be obtained from its coordinates in the particle coordinate system (x, y, z).

4.3 Wavefront curvature and propagation direction

Suppose that the phase function of a beam is expressed in its own coordinate system by $\varphi(u, v, w)$. Its isophase surface $\varphi(u, v, w) = C$ is then given in the particle coordinate system as an implicit function

$$F(x, y, z) = \varphi[u(x, y, z), v(x, y, z), w(x, y, z)] - C \tag{4.22}$$

Any beam can be considered as bundles of rays, the propagation direction of each ray is normal to the local wavefront surface of the beam and characterized by the wave vector $\boldsymbol{k}$ in VCRM. It can be calculated by the gradient of the phase function of the beam according to

$$\boldsymbol{k} = k\frac{\nabla F(x, y, z)}{||\nabla F(x, y, z)||} \tag{4.23}$$

where the gradient of the phase function is given by

$$\nabla F(x, y, z) = \left(F'_x, F'_y, F'_z\right) = \left(\varphi'_u, \varphi'_v, \varphi'_w\right) A \tag{4.24}$$

where f'_ξ denotes the first derivative of function f (F or φ) relative to ξ (x, y, z or u, v, w). From Eq. (4.7), we find that the derivatives of u, v, w relative to x, y, z are just the transformation matrix, i.e.

$$\begin{pmatrix} u_x & u_y & u_z \\ v_x & v_y & v_y \\ w_x & w_y & w_z \end{pmatrix} = A \tag{4.25}$$

The curvature of the wavefront of a given beam at any point can be described by its Gaussian curvature κ_G and the mean curvature κ_M. According to the differential geometry, the Gaussian curvature and the mean curvature can be calculated by [82]

$$\kappa_G = \frac{\nabla F \cdot H^*(F) \cdot \nabla F^T}{|\nabla F|^4} \tag{4.26}$$

$$\kappa_M = \frac{\nabla F \cdot H(F) \cdot \nabla F^T - |\nabla F|^2 \mathrm{Trace}(H)}{2|\nabla F|^3} \tag{4.27}$$

where $H(F)$ is the hessian of the function F and defined by

$$H(F) = \begin{pmatrix} F''_{xx} & F''_{xy} & F''_{xz} \\ F''_{yx} & F''_{yy} & F''_{yz} \\ F''_{zx} & F''_{zy} & F''_{zz} \end{pmatrix} \tag{4.28}$$

$H^*(F)$ stands for the adjoint of the hessian. The notation $F''_{\xi\eta}$ in the above equation stands for the second derivative of function F relative to its variable ξ and η. By using the same notation for the phase function φ, the hessian can be expressed as the second derivatives of the phase function φ relative to its variables (u, v, w)

$$H(F) = A^T \begin{pmatrix} \varphi''_{uu} & \varphi''_{uv} & \varphi''_{uw} \\ \varphi''_{vu} & \varphi''_{vv} & \varphi''_{vw} \\ \varphi''_{wu} & \varphi''_{wv} & \varphi''_{ww} \end{pmatrix} A \tag{4.29}$$

where A^T is the transpose of A. Once the Gaussian curvature and the mean curvature are calculated, the two main curvatures can be obtained by

$$\kappa_1, \kappa_2 = \kappa_M \pm \sqrt{\kappa_M^2 - \kappa_G} \tag{4.30}$$

Therefore, the matrix of the incident wavefront Q in its main directions is written by

$$Q = \begin{pmatrix} \kappa_1 & 0 \\ 0 & \kappa_2 \end{pmatrix} \tag{4.31}$$

In the case under study in this chapter, one main direction is always in the z direction (axis of the cylinder) and the other remains in the plane of symmetry, i.e. xy plane.

4.4 Description of Gaussian beams

The procedure described in Sections 4.1-4.3 is general and can be applied to the scattering of any shaped beam. As examples, we apply it to three kinds of Gaussian

beam: two dimensional Gaussian beam, circular Gaussian beam and astigmatic elliptical Gaussian beam. But we limit ourselves to the two dimensional scattering, i.e. the beam axis is perpendicular to the axis of the cylinder and we are interested only in the scattering in the plane perpendicular to the cylinder axis and containing the incident beam axis.

4.4.1 Two dimensional Gaussian beam

A two dimensional Gaussian beam is a beam with an infinite extension in one direction and a Gaussian profile of amplitude (or intensity) in the other direction. It can be obtained by focusing a plane wave with a cylindrical lens.

Consider now a two dimensional Gaussian beam propagating in w direction with a Gaussian amplitude profile in u direction. Then the complex amplitude of its electric field S_G can be expressed in its own coordinate system $(O_G; uvw)$ by [83, 84]

$$S_G(u, v, w) = A_G \exp(i\varphi)$$

where A_G and φ present respectively the amplitude and the phase of the beam with

$$A_G = \frac{w_0}{w_l} \exp\left(-\frac{u^2}{w_l^2}\right) \tag{4.32}$$

and

$$\varphi(u, v, w) = -k\left\{w + \frac{u^2}{2w[1 + (l/w)^2]}\right\} + \tan^{-1}\left(\frac{w}{l}\right) \tag{4.33}$$

where k is the wave number and l is the Rayleigh length, defined by

$$l = \pi w_0^2/\lambda \tag{4.34}$$

w_l is the local radius at w and is related to the beam waist radius w_0 by

$$w_l = w_0[1 + (w/l)^2]^{1/2} \tag{4.35}$$

As mentioned earlier, we know that the propagation direction of the wave at any point in the beam, represented by a ray and characterized by its wave vector, can be determined by the derivatives of the phase function φ of the beam, whereas the curvature radii of the wavefront can be calculated by the second derivatives of the phase function.

From Eq. (4.33) we obtain the first and the second derivatives of a two dimensional Gaussian beam as

$$\varphi'_u = -k\frac{uw}{l^2+w^2} \tag{4.36}$$

$$\varphi'_v = 0 \tag{4.37}$$

$$\varphi'_w = -k - k\frac{u^2(l^2-w^2)}{2(l^2+w^2)^2} + \frac{l}{l^2+w^2} \tag{4.38}$$

and

$$\varphi''_{vv} = 0 \tag{4.39}$$

$$\varphi''_{uv} = \varphi''_{vu} = 0 \tag{4.40}$$

$$\varphi''_{vw} = \varphi''_{wv} = 0 \tag{4.41}$$

$$\varphi''_{uu} = -\frac{kw}{l^2+w^2} \tag{4.42}$$

$$\varphi''_{uw} = \varphi''_{wu} = -\frac{ku(l^2-w^2)}{(l^2+w^2)^2} \tag{4.43}$$

$$\varphi''_{ww} = -\frac{kwu^2(3l^2-w^2)}{(l^2+w^2)^3} - \frac{2lw}{(l^2+w^2)^2} \tag{4.44}$$

Then the wave vector, the Gaussian and the mean curvatures of the wavefront can be calculated by Eqs. (4.23), (4.26) and (4.27).

For the case under study in this chapter, the transformation matrix is given by Eq. (4.8). We can show, as expected, that the z component of the wave vector $\boldsymbol{k}$ in the plane $z = 0$ is zero and one of the main curvature for the Gaussian beam wavefront is zero. In fact, the gradient of the isophase function is

$$\nabla F(x, y, z) = (f_1, f_2, 0) \tag{4.45}$$

where $f_1 = -\sin\theta_0\varphi'_u + \cos\theta_0\varphi'_w$ and $f_2 = \cos\theta_0\varphi'_u + \sin\theta_0\varphi'_w$. The wave vector is therefore given by (Eq. (4.23)):

$$\boldsymbol{k} = \left(k\frac{f_1}{\sqrt{f_1^2+f_2^2}}, k\frac{f_2}{\sqrt{f_1^2+f_2^2}}, 0\right) \tag{4.46}$$

The hessian $H(F)$ and its adjoint $H^*(F)$ of the two dimensional Gaussian beam are given by

$$H(F) = \begin{pmatrix} h_{11} & h_{12} & 0 \\ h_{21} & h_{22} & 0 \\ 0 & 0 & 0 \end{pmatrix} \tag{4.47}$$

where,

$$h_{11} = \sin\theta_0(\sin\theta_0\varphi''_{uu} - \cos\theta_0\varphi''_{wu}) + \cos\theta_0(\cos\theta_0\varphi''_{ww} - \sin\theta_0\varphi''_{uw}) \quad (4.48)$$

$$h_{12} = \cos\theta_0(-\sin\theta_0\varphi''_{uu} + \cos\theta_0\varphi''_{wu}) + \sin\theta_0(\cos\theta_0\varphi''_{ww} - \sin\theta_0\varphi''_{uw}) \quad (4.49)$$

$$h_{21} = \sin\theta_0(\sin\theta_0\varphi''_{uw} - \cos\theta_0\varphi''_{ww}) + \cos\theta_0(\cos\theta_0\varphi''_{uw} + \sin\theta_0\varphi''_{ww}) \quad (4.50)$$

$$h_{22} = \cos\theta_0(\cos\theta_0\varphi''_{uu} + \cos\theta_0\varphi''_{wu}) + \sin\theta_0(\cos\theta_0\varphi''_{ww} + \sin\theta_0\varphi''_{ww}) \quad (4.51)$$

and

$$H^*(F) = \begin{pmatrix} 0 & 0 & 0 \\ 0 & 0 & 0 \\ 0 & 0 & h_{11}h_{22} - h_{21}h_{12} \end{pmatrix} \quad (4.52)$$

By introducing $\nabla F(x, y, z)$, $H(F)$ and $H^*(F)$ given above into Eq. (4.26), we can conclude that the Gaussian curvature of two dimensional Gaussian beam is hereby equal to zero. That reveals one of the principal curvature radius tends to the infinity.

4.4.2 Circular Gaussian beam

Then we consider the circular Gaussian beam which is a beam of circular section with a Gaussian amplitude profile. Suppose that its propagation direction is still in w direction and the beam waist radius is w_0, then the complex amplitude of its electric field S_G and the phase function are given in its own coordinate system $(O_G; uvw)$ by [62]

$$S_G(u, v, w) = \frac{w_0}{w_l}\exp\left(-\frac{u^2+v^2}{w_l^2}\right)\exp(i\varphi) \quad (4.53)$$

$$\varphi(u, v, w) = -k\left\{w + \frac{u^2+v^2}{2w[1+(l/w)^2]}\right\} + \tan^{-1}\left(\frac{w}{l}\right) \quad (4.54)$$

where the Rayleigh length $l = \pi w_0^2/\lambda$ and the local beam radius $w_l = w_0[1+(w/l)^2]^{1/2}$ are the same as for the two Gaussian beam.

The first derivatives of the phase function (Eq. (4.54)) are given by

$$\varphi'_u = -k\frac{uw}{l^2+w^2} \quad (4.55)$$

$$\varphi'_v = -k\frac{vw}{l^2+w^2} \quad (4.56)$$

$$\varphi'_w = -k - k\frac{(u^2+v^2)(l^2-w^2)}{2(l^2+w^2)^2} + \frac{l}{l^2+w^2} \quad (4.57)$$

The second derivatives are

$$\varphi''_{uu} = \varphi''_{vv} = -\frac{kw}{l^2 + w^2} \tag{4.58}$$

$$\varphi''_{uv} = \varphi''_{vu} = 0 \tag{4.59}$$

$$\varphi''_{uw} = \varphi''_{wu} = -\frac{ku(l^2 - w^2)}{(l^2 + w^2)^2} \tag{4.60}$$

$$\varphi''_{vw} = \varphi''_{wv} = -\frac{kv(l^2 - w^2)}{(l^2 + w^2)^2} \tag{4.61}$$

$$\varphi''_{ww} = -\frac{kw(u^2 + v^2)(3l^2 - w^2)}{(l^2 + w^2)^3} - \frac{2lw}{(l^2 + w^2)^2} \tag{4.62}$$

Since the circular Gaussian beam is symmetric about u and v, the two principal curvature on w axis are the same, so we have $\kappa_G = \kappa_M^2$. We will not give the demonstration here because the analytical calculation is very tedious. Our numerical expressions have confirmed well this conclusion.

4.4.3 Astigmatic elliptical Gaussian beam

The laser sheet is a kind of shaped beam widely used in optical metrology, such as the Particle Imaging Velocimetry (PIV). It is in fact a Gaussian beam with an elliptical section, i.e. the beam waist radii in the two directions are different and they can locate at different positions along the propagation direction, so it is really an astigmatic elliptical Gaussian beam. Such beam can be obtained from a circular Gaussian beam by focusing it in one direction with a cylindrical lens.

Consider an astigmatic elliptical Gaussian beam propagating along w axis with the two beam waist radii w_{0u} and w_{0v} and polarized in u direction. Its electric field in the first order approximation (Davis' model) is given in its own beam coordinate system $(O_G; uvw)$ by [85, 83]

$$\boldsymbol{E} = E_0 \psi_0^{sh} \left(\boldsymbol{e}_u - \frac{Q_u u}{l_u} \boldsymbol{e}_w \right) \exp\left(-ikw\right) \tag{4.63}$$

where

$$\psi_0^{sh} = i\sqrt{Q_u Q_v} \exp\left[-iQ_u \frac{u^2}{w_{0u}^2} - iQ_v \frac{v^2}{w_{0v}^2} \right] \tag{4.64}$$

$$Q_u = \frac{1}{-i + (w - w_{du})/l_u} \tag{4.65}$$

$$Q_v = \frac{1}{-i + (w - w_{dv})/l_v} \tag{4.66}$$

In the paraxial approximation, the electric field component in v direction can be neglected and the complex amplitude of the electric field S_G can be expressed by

$$S_G(u,v,w) = |S_G| \exp(i\varphi) \tag{4.67}$$

where $|S_G|$ and φ present the amplitude and the phase of the beam and are given by

$$|S_G| = \sqrt{\frac{w_{0u}}{w_u}}\sqrt{\frac{w_{0v}}{w_v}} \exp\left(-\frac{u^2}{w_u^2} - \frac{v^2}{w_v^2}\right) \tag{4.68}$$

and

$$\begin{aligned} \varphi(u,v,w) &= -k\left\{w + \frac{u^2}{2R_u} + \frac{v^2}{2R_v}\right\} \\ &+ \frac{1}{2}\tan^{-1}\left(\frac{w-w_{du}}{l_u}\right) + \frac{1}{2}\tan^{-1}\left(\frac{w-w_{dv}}{l_v}\right) \end{aligned} \tag{4.69}$$

where

$$w_u = w_{0u}\sqrt{1 + \frac{(w-w_{du})^2}{l_u^2}} \tag{4.70}$$

$$w_v = w_{0v}\sqrt{1 + \frac{(w-w_{dv})^2}{l_v^2}} \tag{4.71}$$

$$R_u = (w-w_{du})[1 + \frac{l_u^2}{(w-w_{du})^2}] \tag{4.72}$$

$$R_v = (w-w_{dv})[1 + \frac{l_v^2}{(w-w_{dv})^2}] \tag{4.73}$$

$$l_u = \frac{\pi}{\lambda} w_{0u}^2 \tag{4.74}$$

$$l_v = \frac{\pi}{\lambda} w_{0v}^2 \tag{4.75}$$

w_{du} and w_{dv} are respectively the coordinates of the beam waists in u and v directions.

The first and second derivatives of the phase function are given by

$$\begin{aligned} \varphi'_u &= -\frac{ku}{R_u} \\ \varphi'_v &= -\frac{kv}{R_v} \\ \varphi'_w &= -k - \frac{1}{2}ku^2\frac{l_u^2 - (w-w_{du})^2}{[(w-w_{du})^2 + l_u^2]^2} - \frac{1}{2}kv^2\frac{l_v^2 - (w-w_{dv})^2}{[(w-w_{dv})^2 + l_v^2]^2} \\ &\quad + \frac{1}{2}\frac{l_u}{l_u^2 + (w-w_{du})^2} + \frac{1}{2}\frac{l_v}{l_v^2 + (w-w_{dv})^2} \end{aligned} \tag{4.76}$$

and

$$\begin{aligned}
\varphi''_{uu} =& -\frac{k}{R_u} \\
\varphi''_{vv} =& -\frac{k}{R_V} \\
\varphi''_{uv} =& \phi''_{vu} = 0 \\
\varphi''_{uw} =& \phi''_{wu} = -\frac{ku[l_u^2 - (w - w_{du})^2]}{[(w - w_{du})^2 + l_u^2]^2} \\
\varphi''_{vw} =& \phi''_{wv} = -\frac{kv[l_v^2 - (w - w_{dv})^2]}{[(w - w_{dv})^2 + l_v^2]^2} \\
\varphi''_{ww} =& \frac{ku^2[3l_u^2 - (w - w_{du})^2]}{R_u[(w - w_{du})^2 + l_u^2]^2} + \frac{kv^2[3l_v^2 - (w - w_{dv})^2]}{R_v[(w - w_{dv})^2 + l_v^2]^2} \\
& - \frac{l_u}{R_u[l_u^2 + (w - w_{du})^2]} - \frac{l_v}{R_v[l_v^2 + (w - w_{dv})^2]}
\end{aligned} \tag{4.77}$$

Evidently, the two kinds of Gaussian beam discussed in the previous sections are the special cases of the astigmatic elliptical Gaussian beam. So the scattering of a two dimensional Gaussian beam can be considered as an astigmatic elliptical Gaussian beam with $w_{du} = w_{dv} = 0$, $w_{0u} = w_0$ and $w_{0v} = \infty$ and the scattering of a circular Gaussian beam is the special case for $w_{du} = w_{dv} = 0$, $w_{0u} = w_{0v} = w_0$. Working in the special case permits to simplify the problem and to isolate different effects. And the results are useful for the validation of the general case. In the following section, we will present the numerical results calculated with three independent codes developed for the scattering of three kinds of Gaussian beam.

4.5 Numerical results and discussion

On the basis of the theories presented above, three codes have been written in Fortran 95. Since there is very few results in the literature for the scattering of large non-circular cylinder, the validation of our method is mainly based on the examination of the physical phenomena, such as the rainbow positions, the rainbow structures, the focusing of the beam by the particle.

Anyway, two "validations" with "independent" results are given. The first is the scattering of a two dimensional Gaussian beam by a fused silica capillary given by Krattiger et al [65]. Their results have been validated by experiment. The second is the comparison with the numerical results of a long ellipsoid particle calculated also

with VCRM. The first is partial since only the orders $p = 0$ and $p = 1$ are considered. The second is not really independent since it is based on the same model. The lack of the results in the literature proves in certain sense the necessity and the difficulty of the problem we are dealing with.

To simplify the presentation, we give at this stage the main parameters used for the calculation in this section. The wavelength of the incident beam and the refractive index of the particle are supposed constant and equal to $\lambda = 0.6328$ μm and $m = 1.33$ respectively except for Fig. 4.3. The number and order of rays as well as the scattering angular grid are chose as same as in the case of plane wave (see Section. 3.3).

4.5.1 Two dimensional Gaussian beam

In all shaped beams, the two dimensional Gaussian beam is the simplest so we start with this case. It is worth to point out that in far field the scattered wave of a two dimensional Gaussian beam is cylindrical (independent of z), the scattering diagrams given in this subsection are the phase function. However, the scattered fields of a circular Gaussian beam and an elliptical Gaussian beam are, in general, neither cylindrical nor spherical, there is not a simple relation between the scattered intensity and observation distance, so the scattering diagrams will be in the intensity at a given distance in the next two subsections.

To validate our theory and code, a capillary is chosen to compare with Fig. 6 in the reference [65] (copied in Fig. 4.3(a)) by setting the same parameters. It should be pointed out that the refractive index of the core ($m = 1.332$) is smaller than that of the capillary wall ($m_0 = 1.457$). The beam waist radius is $w_0 = 8.4$ μm and its center locates at $y_0 = 48$ μm in the y direction. As we found that our results (Fig. 4.3(b)) are in good agreement with that in the reference [65] (copied in Fig. 4.3(a)), we conclude that our code is validated.

We have examined the rainbow positions as function of the ellipticity of the cylinder when it is illuminated by the plane wave in last chapter. But when an elliptical cylinder is illuminated by a two dimensional Gaussian beam, the tracing of the rays are the same. Although the incident angle of the rays on the particle can be different from the propagation direction of the beam, the rainbow positions for Gaussian beam are almost the same as that of plane wave, but their relative intensity varies as function of the beam waist radius and the position of the particle. Fig. 4.4 shows

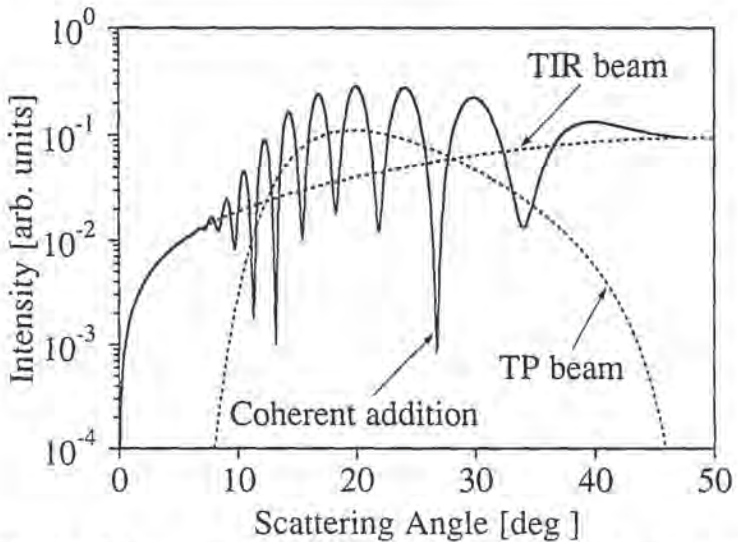

(a). Fig. 6 in the reference [65].

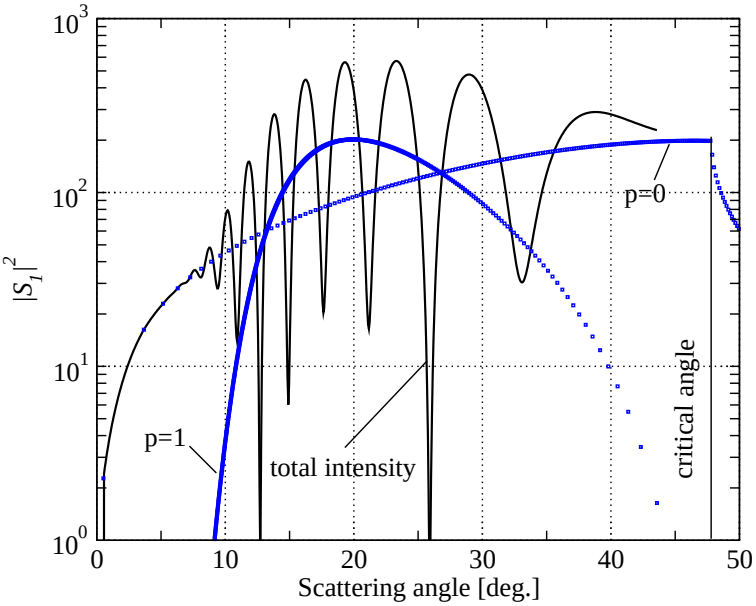

(b). Our results calculated with VCRM.

Figure 4.3: Scattering diagram of a fused silica capillary of radius $a = 50\mu$m filled with water $m = 1.332$, illuminated by a Gaussian beam with waist radius $w_0 = 8.4\mu$m and offset 48μm in y direction. The refractive index of the capillary wall is $m_0 = 1.457$, so is greater than the core(water).

the scattering diagrams of a two dimensional Gaussian beam ($w_0 = 30$ μm) by an elliptical cylinder of major axis $a = 50$ μm with aspect ratio as parameter. The beam center is on the axis of the cylinder. It is shown that the rainbow positions are similar

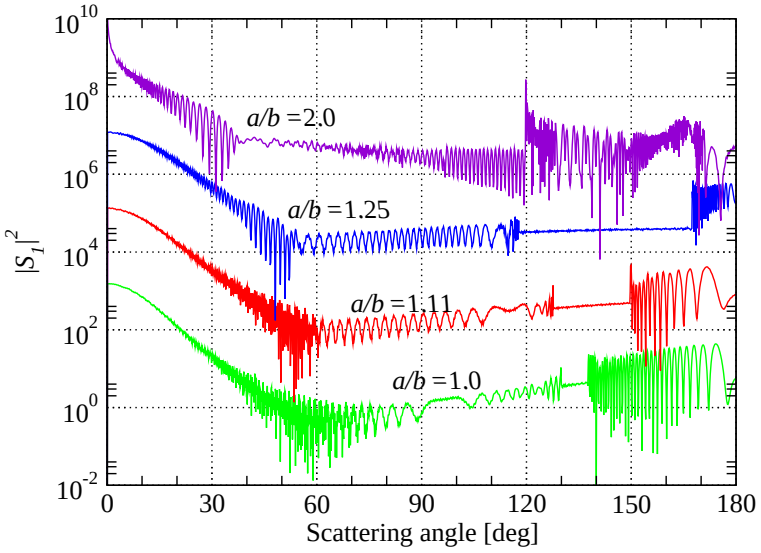

Figure 4.4: Scattering diagrams of an elliptical cylinder illuminated by a Gaussian beam $w_0 = 30$ μm with aspect ratio as parameter. The major axis is 50 μm, the minor axis are 50 μm, 45 μm, 40 μm and 25 μm. The polarization is in xz plane. The results for $\kappa = 1.11$, $\kappa = 1.25$ and $\kappa = 2$ are offset by 10^2, 10^4 and 10^6 for clarity.

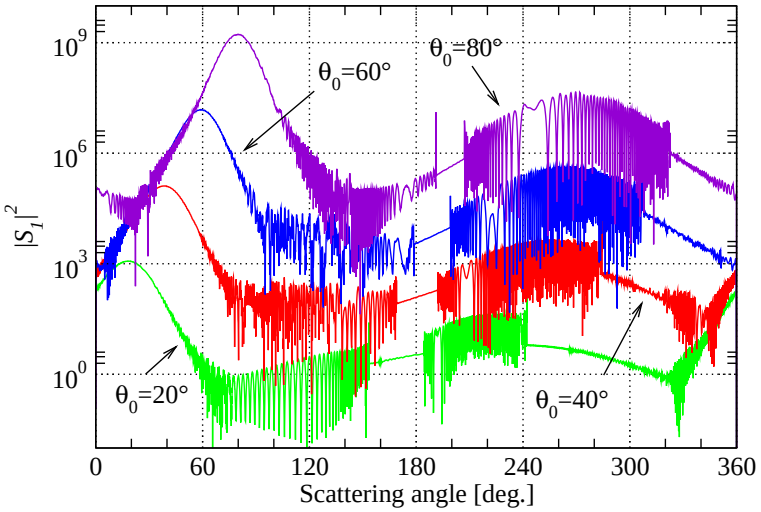

Figure 4.5: Scattering diagrams of an elliptical cylinder $a = 50$ μm and $b = 40$ μm illuminated by a Gaussian beam ($w_0 = 25$ μm) at different angles. The results for $\theta_0 = 40°$, $\theta_0 = 60°$ and $\theta_0 = 80°$ are shifted by 10^2, 10^4 and 10^6 for clarity.

to the plane wave case (Fig. 3.11 in chapter 3) but the amplitudes of the first and the second rainbows are less important. By comparison of the scattering diagrams of a plane wave (Fig. 3.10 (a) in chapter 3) with that of a two dimensional Gaussian

beam (Fig. 4.5), we find that when the particle is illuminated by a two dimensional Gaussian beam of waist radius smaller the particle radius at different angles, i.e. the incident beam axis remains in xy plane but makes an angle θ_0 with x axis, the scattered intensities are focused more in forward direction.

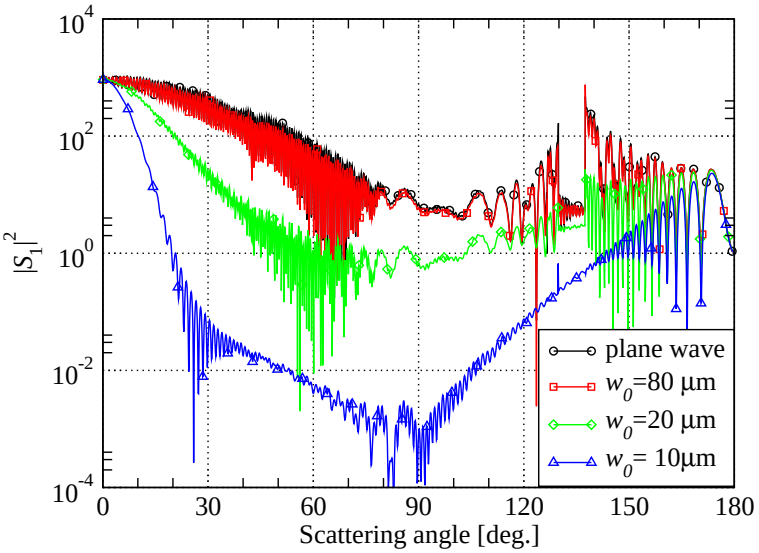

Figure 4.6: Scattered diagrams of a circular cylinder of radius 30 μm illuminated by a plane wave and Gaussian beam of waist radius ($w_0 = 80, 20, 10$ μm). The center of the Gaussian beam is located on the axis of the cylinder. The incident beam is polarized in z direction.

We then compared the scattering diagrams of an infinite circular cylinder of radius $a = 30$ μm illuminated by a plane wave and a two dimensional Gaussian beam of three waist radii 80 μm, 20 μm and 10 μm. We can see from Fig. 4.6 that the scattering diagram of a two dimensional Gaussian beam with large waist radius ($w_0 = 80$ μm) tends to that of a plane wave. This means that when the beam waist radius of a two dimensional Gaussian beam is about three time s larger than the particle radius, the scattering in the plane containing the beam can be considered as the scattering of a plane wave. When the beam waist radius decreases, the general scattered intensities decreases accordingly. With a two dimensional Gaussian beam is strongly focused ($w_0 = 10\mu$m for example), the scattered intensity at sides (around 90°) reduces dramatically while it remains almost the same in forward and backward directions.

Fig. 4.7 shows the scattering diagrams of an elliptical cylinder at oblique incidence with a two dimensional Gaussian beam of different waist radius. The two semi-axes of the elliptical cylinder are respectively $a = 50$ μm and $b = 40$ μm and the incident wave

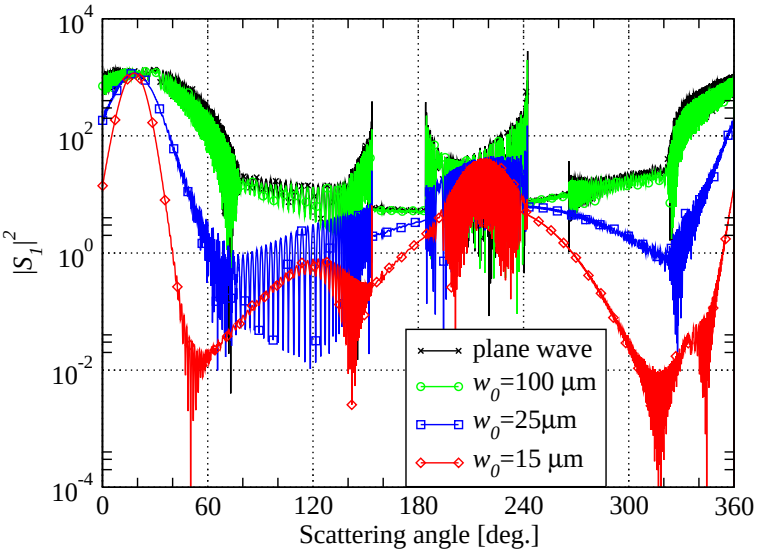

Figure 4.7: Scattered diagrams of an elliptical cylinder of major radius $a = 50$ μm and minor radius $b = 40$ μm illuminated by plane wave and a two dimensional Gaussian beam of three different waist radius ($w_0 = 100, 25, 15$ μm). The incident beam is polarized along z direction and makes an angle $\theta_0 = 20°$ with x axis. The center of the beam is located on the axis of the cylinder.

is the plane wave or a two dimensional Gaussian beam of waist radius $w_0 = 100$ μm, 25 μm or 15 μm. We remark that the profile of the scattering diagrams are very different from those of the circular cylinder. The scattering diagrams are no longer symmetric, so they must be given in all directions (0 to 360°). The rainbow angles and the Alexander dark regions in the two sides of the scattering diagram (0° to 180° and 180° to 360°) are not symmetric neither. This has been discussed in last chapter in the case of plane wave. When a cylinder is illuminated by a two dimensional Gaussian beam of waist radius relatively small, the incident beam intensity at the impact position for rainbow is weak. For example, in the cases $w_0 = 15$ μm, the rainbow phenomena are not visible in two sides relative to the incident direction (20 to 200° and 200° to 20°). If $w_0 = 25$ μm the rainbow is much visible in the side of scattering angle smaller than 200° than in other side.

4.5.2 Circular Gaussian beam

In this subsection, the scattering of a circular Gaussian beam by circular/elliptical cylinders are discussed. The scattering properties as a function of the beam position

and orientation, the beam waist as well as the observation distance will be examined.

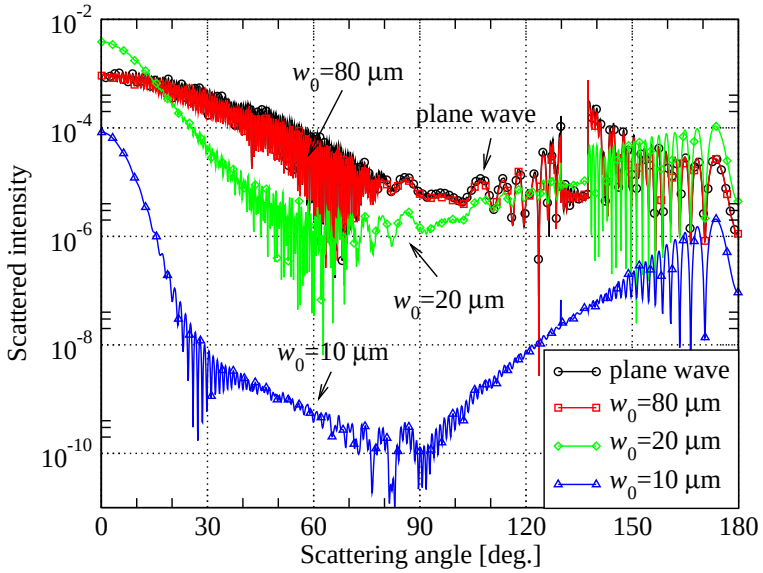

Figure 4.8: Scattered intensities of a circular cylinder of radius 30 μm illuminated by the plane wave and a Gaussian beam of waist radius ($w_0 = 80, 20, 10$ μm). The center of the Gaussian beam is located on the axis of the cylinder. The incident beam is polarized in z direction.

The scattering intensity of an infinite circular cylinder with the same parameters as in Fig. 4.6 are compared firstly. The profile of the scattered intensity in Fig. 4.8 is very similar to Fig. 4.6. But for the waist radius $w_0 = 20$ μm, the scattered intensities in the forward and backward directions are more important than that for the plane wave and the Gaussian beam of $w_0 = 80$ μm and 10 μm. This is due to the focusing of the incident wave. This effect can be explained by the wavefront equation (Eq. (4.6)). In fact, the wavefront radius in xz plane of the Gaussian beam of $w_0 = 20$ μm at the incident point $x = -a, y = 0$ is 131.145 mm, that of the wave just transmitted in the particle is 174.782 mm according to Eq. (4.6) and the wavefront radius of the emergent wave of the first order ($p = 1$) is equal to 131.370 mm. So the emergent wave is focused near the observation distance (0.1 m) in the forward direction. The transformation of the wavefront curvature in the other direction (xy plane) can be evaluated by Eq. (4.5) and we find that the wavefront radius of the emergent ray ($p = 1$) is very small (about 30 μm). Similar calculation can be done for other Gaussian beams. With the same procedure, we find that the focal distance of the beam $w_0 = 80$ μm is 33.6 m and

that of the beam $w_0 = 10$ μm is at about 8 mm. Therefore the scattered intensity at 0.1m in the forward direction for the Gaussian beam $w_0 = 20$ μm are much stronger than the other beams . The fact of the scattering intensity in backward direction for $w_0 = 20$ μm is stronger than the others can also be explained with the same principle.

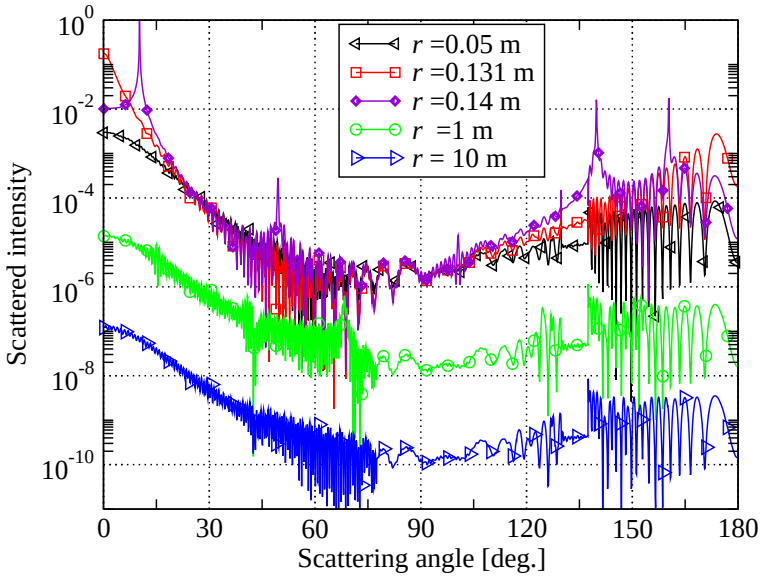

Figure 4.9: Scattering intensities at different observation distances of an circular cylinder of radius 30 μm illuminated by a Gaussian beam of waist radius $w_0 = 20$ μm. The center of the Gaussian beam is on the axis of the cylinder. The incident beam is polarized in xz plane.

To confirm the above reasoning, we examine now the variation of scattered intensities as function of the observation distance. Fig. 4.9 illustrates the scattering intensity observed at different distance from a circular cylinder illuminated by a Gaussian beam. The radius of the cylinder is 30 μm and the Gaussian beam radius is $w_0 = 20$ μm. We find that the scattered intensities at 1 m is about 100 times greater than that at 10 m, i.e. the scattered field is almost spherical. Note that the scattered intensity at 0.131 m is 10,000 times more important than that at 1 m in forward direction, but the mean intensity is not more than 10 times around 60°. This is due to the focusing of the incident wave in the longitudinal direction of the cylinder, an effect already discussed for Fig. 4.8. Furthermore, we can also observe that the scattered intensity at 0.14 m has several peaks. In fact, all these peaks are different orders of the same incident ray due to the focusing of the incident wavefront arrived at $y = 10$ μm in our

case. The corresponding incident angle and refraction angle on the particle surface are respectively about 20° and 15°. The scattering angles are respectively 140°, 10°, 160°, 50° and 100° for the emergent rays at order p from 0 to 4. The scatted intensity will decrease when the observation distance is smaller than the focal distance, such that the intensity at 0.05 m is weaker than at 0.13 m and 0.14 m. This effect of focusing depends on the beam waist radius, the position of the particle in the beam and the size of the particle. These results confirm that the scattered field of a Gaussian beam by an infinite cylinder is, in general, neither cylindrical nor spherical.

Since the measurement distance is usually in the order of tens od centimeters, all the observation distances are fixed to 0.1 m In the following.

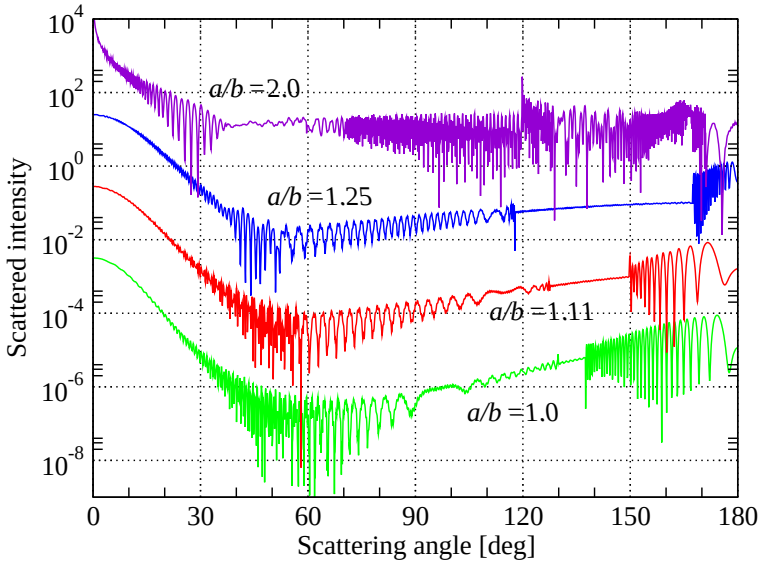

Figure 4.10: Scattered intensities of an elliptical cylinder illuminated by the Gaussian beam $w_0 = 30$ μm with aspect ratio as parameter. The major axis is 50 μm, the minor axis is 50 μm, 45 μm, 40 μm or 25 μm. The polarization is in xz plane. The results for $\kappa = 1.11$, $\kappa = 1.25$ and $\kappa = 2$ are offset by 10^2, 10^4 and 10^6 for clarity.

We have discussed the scattering of an elliptical cylinder at different aspect ratios illuminated by a two dimensional Gaussian beam at different incident angles in the last subsection. When the elliptical cylinders are illuminated by a circular Gaussian beam, the tracing of the rays is almost the same as for two dimensional Gaussian beam and the profile of the scattered intensity predicted by VCRM is also similar. This can be approved by comparing Fig. 4.4 with Fig. 4.10. Due to its similarity with the problem of the scattering of a two dimensional Gaussian beam, the scattering of a circular Gaussian beam by an elliptical cylinder at different incident angles will not

given here.

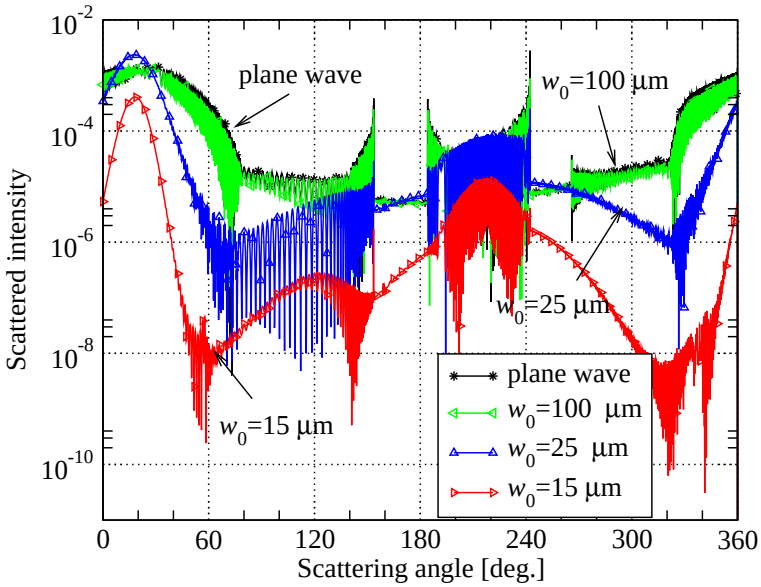

Figure 4.11: Scattered intensities of an elliptical cylinder of major radius $a = 50$ μm and minor radius $b = 40$ μm illuminated by the plane wave and a Gaussian beam of three different waist radius ($w_0 = 100, 25, 15$ μm). The incident beam is polarized along z direction and makes an angle $\theta_0 = 20°$ with x axis. The center of the beam is located on the axis of the cylinder.

Fig. 4.11 shows the scattered intensity of an elliptical cylinder at oblique incidence. The parameter are the same as in Fig. 4.7. We can also observe the similar phenomenon of focusing discussed for Fig. 4.8. Still according to the Eq. (4.6), the position of the focal spot for the beam of waist radius 25 μm is located at approximate 0.2 m. The scattered intensity at the observation distance of 0.1 m is still more important than the other beams. Moreover, the intensity for $w_0 = 15$ μm is obviously lower than that for $w_0 = 100$ μm and also plane wave. That is because the total power of the incident beam is smaller since we assume always that the amplitude of the electric field at the center of beam is unity.

When a narrow Gaussian beam illuminates a very deformed elliptical cylinder, we can observe the separation of scattering orders and total reflection even for a cylinder of refractive index larger than unity. Fig. 4.12 shows the scattering diagrams of an elliptical cylinder of two semi-axes $a = 30$ μm, $b = 12$ μm illuminated by a Gaussian beam ($w_0 = 5$ μm). When the incident beam makes a small angle with the major axis of the elliptical cylinder the scattered waves of different orders interfered ($\theta_0 = 10°$).

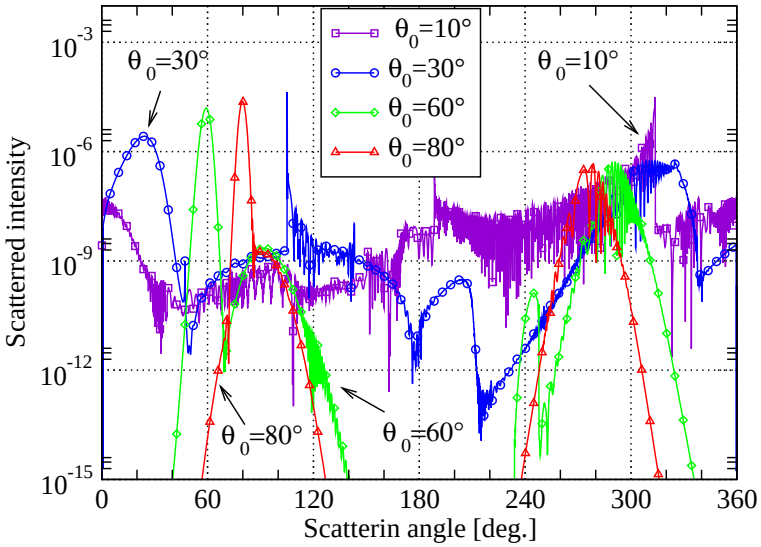

Figure 4.12: Scattered intensities of an elliptical cylinder ($a = 30$ μm, $b = 12$ μm) illuminated by a Gaussian beam ($w_0 = 5$ μm) at different incident angles.

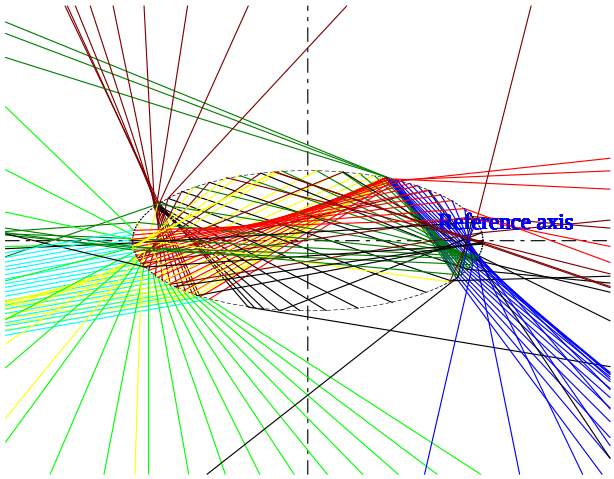

Figure 4.13: Ray tracing for the incident angle $\theta_0 = 10°$ in the Fig. 4.12.

When the incident angle is relatively large, $\theta_0 = 30°$ for example, the scattered wave of different orders begin to separate: $p = 1$ in 25°, $p = 3$ in 100° with rainbow at 105°, $p = 4$ in 205°, but $p = 0$ and 2 interfere around 320°. The scattered waves of different orders become more and more separated when the incident angle increases. When $\theta_0 = 60°$, the orders $p = 1$ at 60° and $p = 3$ at 90°, $p = 4$ at 245° are well separated, while $p = 0$ and $p = 2$ still interfere around 290°. When we increase further the incident angle to near perpendicular to major axis, the deviation of the beam is

small such that the orders 1 and 3 are almost at the same angle and so do $p = 0$, 2 and 4. We can remark that the scattered intensity in forward direction for $\theta_0 = 10°$ is much less than that for other incident angles. This is due to the total reflection of the rays near the axis of the incident beam (see Fig. 4.13).

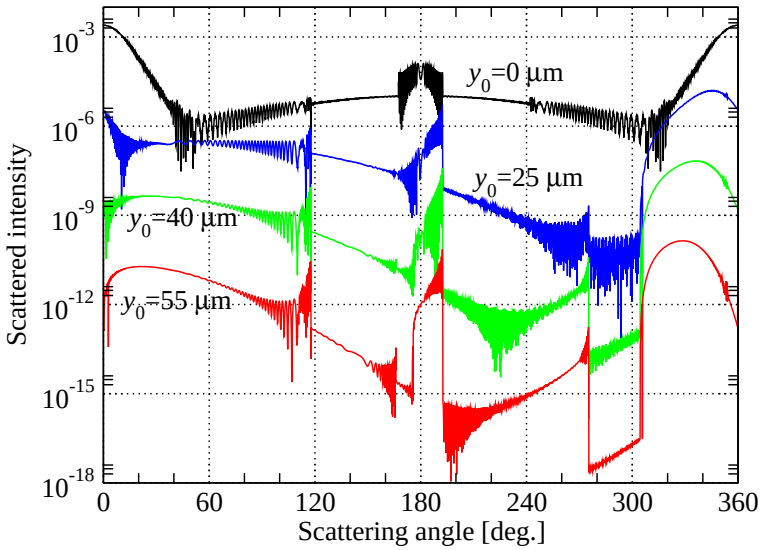

Figure 4.14: Scattered intensities of an elliptical cylinder ($a = 50$ μm, $b = 40$ μm) illuminated by a Gaussian beam ($w_0 = 25$ μm, $z_0 = x_0 = 0$) parallel to x axis with y_0 as parameter. The results of $y_0 = 25$ μm, 40 μm and 55 μm are offset by 10^{-2}, 10^{-4} and 10^{-6} for clarity.

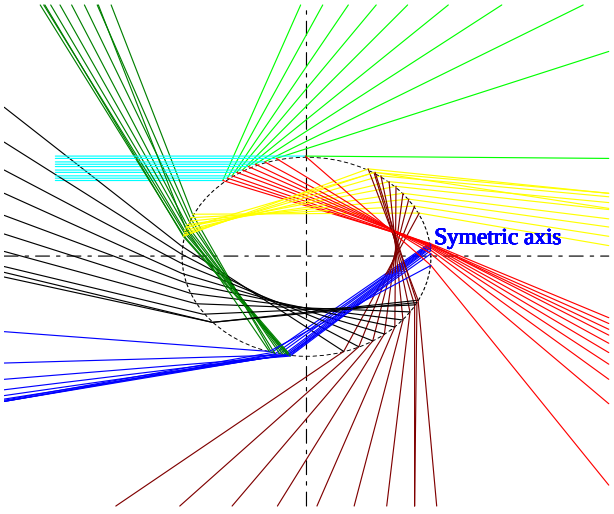

Figure 4.15: Ray tracing for the center of Gaussian beam locate at $y_0 = 55$ μm, a case shown in Fig. 4.14.

We show the scattered intensities in Fig. 4.14 when the incident Gaussian beam shifts in y direction. Evidently, when the beam center is on the axis of the cylinder, the scattering diagram is symmetric. When the beam is shifted from the major axis of the cylinder, the intensities are concentred in several zones corresponding to different orders. For example, there are three main zones well separated when the beam is 55μm off-axis. This phenomenon is very clearly shown in Fig. 4.15: $p = 0$ in $0° - 60°$, $p = 1$ in $310° - 350°$, $p = 2$ around $180°$ and $p = 3$ around $110°$.

4.5.3 Astigmatic elliptical Gaussian beam

In this subsection, the scattering of an astigmatic elliptical Gaussian beam is discussed. We will investigate the influence of the waist radii and the positions of the astigmatic elliptical Gaussian beam in two directions on the scattered intensities. We recall that the observation distance is fixed to 0.1m in this subsection, the polarization of the incident wave is along the axis of the cylinder, v axis in the beam coordinate system is parallel to z axis of the particle coordinate system, and the center of the beam is located on the axis of the cylinder except for Fig. 4.19.

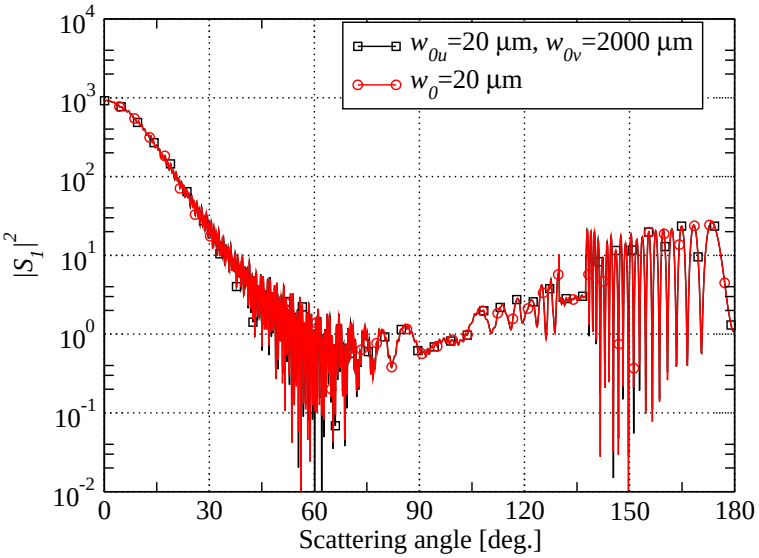

Figure 4.16: Same particle as in Fig. 4.8, but the incident beam is a two dimensional Gaussian beam of waist radius 20μm or an astigmatic elliptical Gaussian beam of waist radii $w_{0u} = 20\mu m$ and $w_{0v} = 2000\mu m$ in the u and v directions respectively.

Fig. 4.16 compares the scattering diagram of a circular cylinder of radius 30μm

and the refractive index 1.33 illuminated by a two dimensional Gaussian beam of waist radii 20μm and an astigmatic elliptical Gaussian beam of waist radius $w_{0u} = 20\mu m$ and $w_{0v} = 2000\mu m$ in u and v directions respectively. An excellent agreement is found in all directions as expected. That is because when the curvature radius of the beam in v direction is much larger than the waist radius in u direction and also much larger than the particle radius, the astigmatic elliptical Gaussian beam can be considered as a two dimensional Gaussian beam.

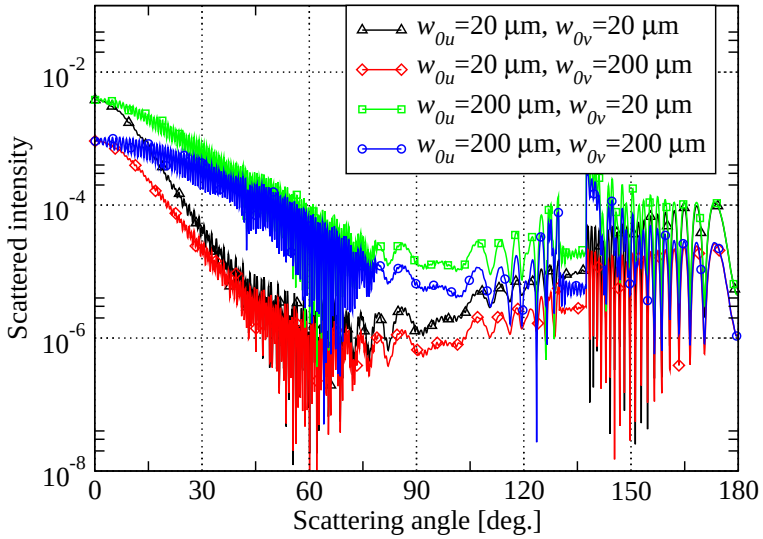

Figure 4.17: Same parameters as in Fig. 4.8, except for the waist radii of the beam.

Then Fig. 4.17 illustrates the scattered intensity by a circular cylinder of radius $a = 30\mu$m illuminated by a Gaussian beam with the waist radius as parameters. We find that the scattered intensity for $w_{0u} = 20\mu$m and $w_{0v} = 20\mu$m is higher than that for $w_{0u} = 200\mu$m, $w_{0v} = 200\mu$m (considered as plane wave) in the forward and backward directions. That is attributed to the focusing effect discussed in the previous subsection, but note that the intensity is lower elsewhere the scattered intensity for the beam $w_{0u} = 20\mu$m, $w_{0v} = 200\mu$m, and that for the beam $w_{0u} = 20\mu$m, $w_{0v} = 20\mu$m in all directions. The latter is higher due to the focusing effect in v direction. For the same reason we can predict that the scattered intensity for the beam $w_{0u} = 200\mu$m, $w_{0v} = 20\mu$m must be similar to that of $w_{0u} = 20\mu$m, $w_{0v} = 20\mu$m in forward and backward directions and it is really true in Fig. 4.17.

We now consider the scattered intensities of an elliptical cylinder (with the same particle as in Fig. 4.11) illuminated by different Gaussian beams. In Fig. 4.18, the

similar focusing effect is observed and the conclusions for a circular cylinder (Fig. 4.17) are still valid, but the angular dispositions are different and dependent on the incident angle.

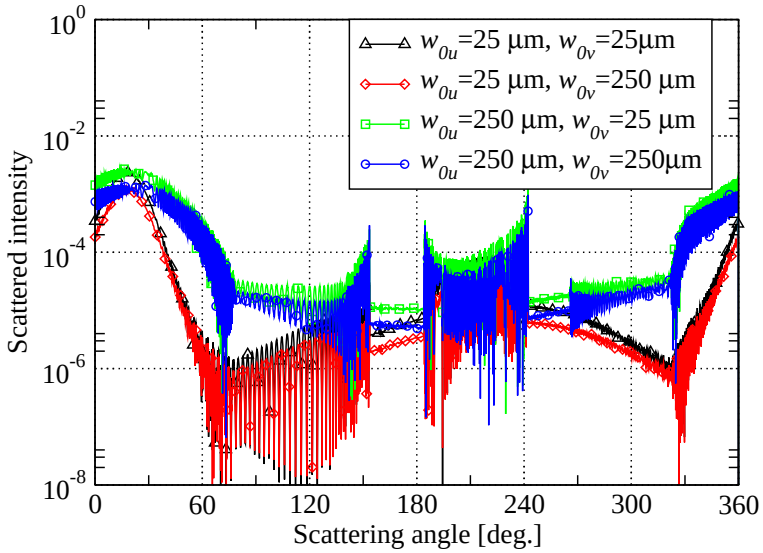

Figure 4.18: Same parameters as Fig. 4.11, except for the waist radii of the beam.

Then the positions of the astigmatic elliptical Gaussian beam center are considered as parameters. Fig. 4.19 illustrates the scattering diagrams of the astigmatic circular Gaussian beams. The beam centers in u direction always locates on the axis of the cylinder, but the beam centers in v direction are shifted on w axis by an elliptical cylinder. Note that $w_{dv} > 0$ means that the center of beam is shifted toward to the propagation direction. From this figure, we can see that the curves of the scattered intensity for $w_{dv} = 0\mu$m and $w_{dv} = -50\mu$m are coincident. That is because that the curvature radius in v direction at the incident point is very large in this case, their scattering intensity is weak.

On the other way, when beam center is shifted toward the propagation direction, the scattering diagrams are different from that the beam center locates after the cylinder axis. This can be explained that when the beam center is before the cylinder axis, the wave arriving on the particle is convergent. We can found this effect in the scattering of $w_{dv} = 50\mu$m. With the beam center in v direction approaches to the axis of cylinder, the focusing effect decreases gradually ($w_{dv} = 25\mu$m for example). The variation of the curvature radius R_v of the refracted ray (p=1) in z direction on the incident point (x=-a,y=0) as function of w_{dv} is compiled in Table 4.1. It is clear that

the focal distance for $w_{dv} = 50\mu$m is the nearest to the observation distance(0.1m), so its intensity is much higher than the scattering intensities for $w_{dv} = 25\mu$m and $w_{dv} = 0\mu$m.

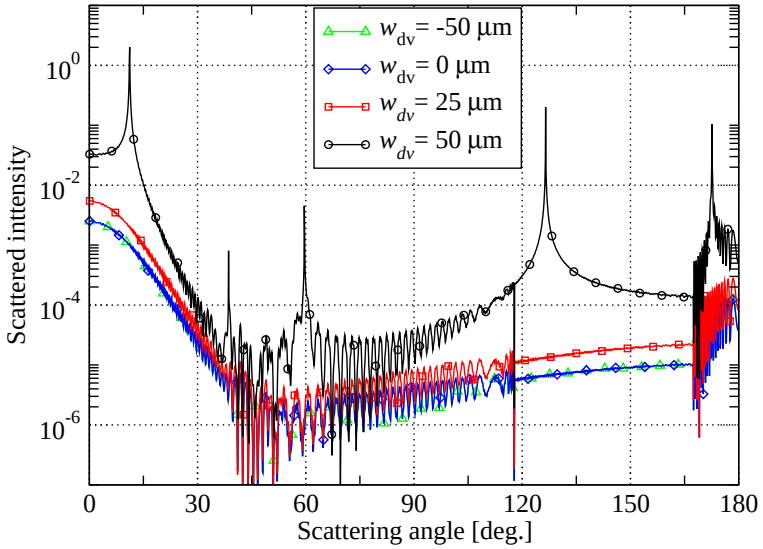

Figure 4.19: Same particle as in Fig. 4.11 illuminated by an astigmatic elliptical Gaussian beam of waist radii of 25μm in u and v directions. The beam waist in u direction is located at center of the particle while the beam waist in v direction moves along the beam axis.

Table 4.1: Evaluation of the wavefront curvature radius in v direction of refracted ray ($p = 1$) of an elliptical cylinder($a = 50\mu$m,$b = 40\mu$m). The beam waist in u direction is located at center of the particle while the beam waist in v direction moves along the beam axis.

$w_{dv}(\mu m)$	-50	0	10	20	30	40	50
$R_v(m)$	0.193	0.193	0.161	0.138	0.120	0.107	0.096

4.6 Conclusion

In this chapter, Vectorial Complex Ray Model has been employed to predict the light scattering of an infinite elliptical cylinder illuminated by three kinds of Gaussian beam. To validate the numerical code, the scattering of a two dimensional Gaussian beam by a capillary is chosen, to compare with data available in the literature. A good agreement is found. Then the scattering properties as function of the observation distance, the waist radii, the orientation and the position of beam were examined.

We discovered important focusing effects at some particular observation distance for a given waist radius. We also observed the separation of scattering orders and total reflection when a very deformed elliptical cylinder is illuminated by a strongly focused beam.

Chapter 5

Plane wave scattering by an elliptical cylinder at diagonal incidence

In the last two chapters, VCRM has been applied to the light scattering of a plane wave and a shaped beam by an elliptical cylinder at normal incidence (in 2D model). In this chapter, we are trying to extend VCRM to the interaction of an elliptical cylinder and a plane wave at diagonal incidence. In this case, the ray tracing is in three dimensions. Adler et al have noted [86]: "There has been much less investigation of the caustic of plane wave/cylinder scattering than there has been of plane wave/sphere and plane wave-spheroid scattering, and perhaps this neglect was due to the expectation that nothing really new would be seen". And their experimental observations have shown that this is in fact not the case. We will show in this chapter that light scattering of a diagonally incident plane wave by a cylinder, especially an elliptical cylinder, is rich in phenomena with clear intuitive interpretation. Here we have two new difficulties compared to the normal incidence cases studied in the previous chapters:

- *Ray trajectories*: At normal incidence, the ray tracing is in a plane (scattering plane), so ray trajectories are relatively easy to determine. But for the diagonal incidence (in 3 dimensional model), the incident rays and refracted rays are no longer in a plane. The emergent rays are along the surface of a cone and can be viewed on the circle C (Fig.5.1), toward the apex of cone [87]. Thanks to the representation of the rays in VCRM, the ray tracing process will be considerably simplified.

- *Cross polarization*: At diagonal incidence, the polarization of the emergent wave will no longer stay in the same direction, or the same plane, as the incident wave polarization. That means that the polarization direction of a ray before and after the p^{th} interaction with the cylinder surface changes. In VCRM, the polarizations of incident, refracted and refracted waves will be decomposed in two directions: perpendicular and parallel to the plane defined by the incident ray and the normal of the particle surface.

5.1 VCRM for an infinite elliptical cylinder at diagonal incidence

5.1.1 Ray tracing

Now, we refer to the ray tracing in an elliptical cylinder illuminated by a diagonally incident plane wave. In this case, the directions of all the incident rays are the same. But the direction of the incident plane varies as a function of the incident point of a ray on the surface of the cylinder, so a special attention should be paid to the application of the Fresnel formulae.

Consider an elliptical cylinder whose center O is located at the origin of the Cartesian coordinate, illuminated diagonally by a plane wave. z axis is along the axis of the elliptical cylinder, x and y axis along the two main axes of the ellipse in xy plane. The propagation direction of the plane wave makes an angle ξ with x axis, an angle ζ with z axis. The geometry is shown in Fig. 5.1. The wave vector of the incident wave is therefore written by

$$\boldsymbol{k} = \sin\zeta\cos\xi\boldsymbol{e}_x + \sin\zeta\sin\xi\boldsymbol{e}_y + \cos\zeta\boldsymbol{e}_z \tag{5.1}$$

when ζ is equal to 90°, the incident wave direction lies in the xy plane and therefore corresponds to the normal incidence.

In order to calculate the curvature matrix of wavefront and resolve the polarization, we define two orthogonal vector base: one at the surface of the cylinder and the other on the surface of the wavefront. For the first one, we choose normal of the cylinder surface $\boldsymbol{n}$ and unit vector along z axis as the two base vector. The third one is defined by

$$\boldsymbol{t} = \boldsymbol{n} \times \boldsymbol{e}_z \tag{5.2}$$

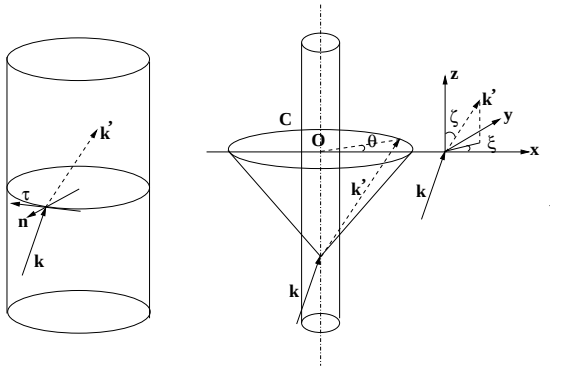

Figure 5.1: Schemata od a cylinder diagonally illuminated by a plane wave.

The unit vectors $\boldsymbol{n}$, $\boldsymbol{e}_z$ and $\boldsymbol{t}$ form triad on the cylinder surface. The base vectors $\boldsymbol{e}_z$ and $\boldsymbol{t}$ are tangent to the surface of cylinder and $\boldsymbol{n}$ is perpendicular to the surface.

Now, we define the base vectors on the wavefront surface. The unit vector $\boldsymbol{b}$ tangent to the wavefront surface and perpendicular to the wave vector $\boldsymbol{k}$ and the normal $\boldsymbol{n}$ is defined by

$$\boldsymbol{b} = \frac{\boldsymbol{k} \times \boldsymbol{n}}{||\boldsymbol{k} \times \boldsymbol{n}||} \tag{5.3}$$

The unit vector $\boldsymbol{b}$ defined in such way is also perpendicular to the refracted wave vector $\boldsymbol{k}'$ and the reflected wave vector $\boldsymbol{k}^l$, so common for the incident wave, refracted wave and reflected wave

$$\boldsymbol{b} = \frac{\boldsymbol{k} \times \boldsymbol{n}}{||\boldsymbol{k} \times \boldsymbol{n}||} = \frac{\boldsymbol{k}' \times \boldsymbol{n}}{||\boldsymbol{k}' \times \boldsymbol{n}||} = \frac{\boldsymbol{k}^l \times \boldsymbol{n}}{||\boldsymbol{k}^l \times \boldsymbol{n}||} \tag{5.4}$$

The base vectors $\boldsymbol{c}$, $\boldsymbol{c}'$ and $\boldsymbol{c}^l$ are then defined by $\boldsymbol{b}$, $\boldsymbol{k}$, $\boldsymbol{k}'$ and $\boldsymbol{k}^l$

$$\boldsymbol{c} = \boldsymbol{b} \times \boldsymbol{k},\ \boldsymbol{c}' = \boldsymbol{b} \times \boldsymbol{k}',\ \boldsymbol{c}^l = \boldsymbol{b} \times \boldsymbol{k}^l \tag{5.5}$$

The orthogonal base vectors are ($\boldsymbol{k}$, $\boldsymbol{b}$, $\boldsymbol{c}$) for the incident wave, ($\boldsymbol{k}'$, $\boldsymbol{b}$,$\boldsymbol{c}'$) for refracted wave and ($\boldsymbol{k}^l$, $\boldsymbol{b}$, $\boldsymbol{c}^l$) for the reflected wave. It is worth to point out that the unit vector $\boldsymbol{b}$ is perpendicular to the incident plane, the other base vectors lie in the incident plane.

We also define the unit vector tangent to the surface of the cylinder and lying in the incident plane:

$$\boldsymbol{\tau} = \boldsymbol{n} \times \boldsymbol{b} \tag{5.6}$$

According to Snell-Descartes law, the tangent components of the electric field on the interface are continuous, so the tangent components of the reflected wave vector

k_τ^l and the refracted wave vector k_τ' are equal to that of the incident wave vector $k_\tau^l = k_\tau' = k_\tau$. The difference with respect to the section 3.2.1 is that the components of the refracted/reflected waves in the z direction are determined by incident angle ζ and counted for a specific value . The refracted wave vector $\boldsymbol{k'}$ and the reflected vector $\boldsymbol{k}^l$ can be finally expressed by

$$\boldsymbol{k'} = k_x' \boldsymbol{e}_x + k_y' \boldsymbol{e}_y + k_z' \boldsymbol{e}_z = k_\tau' \boldsymbol{\tau} + k_n' \boldsymbol{n} \tag{5.7}$$

$$\boldsymbol{k}^l = k_x^l \boldsymbol{e}_x + k_y^l \boldsymbol{e}_y + k_z^l \boldsymbol{e}_z = k_\tau^l \boldsymbol{\tau} - k_n^l \boldsymbol{n} \tag{5.8}$$

where the normal and tangent components of any vector $\boldsymbol{k}$ can be calculated accordingly to the projection law: $k_n = \boldsymbol{k} \cdot \boldsymbol{n} = k_x n_x + k_y n_y + k_z n_z$ and $k_\tau = \boldsymbol{k} \cdot \boldsymbol{\tau} = k_x \tau_x + k_x \tau_y + k_z \tau_z$ respectively.

Once we know the refracted wave vector $\boldsymbol{k'}$, the coordinate of the former intersection point x_0, y_0, z_0 and the equation of the ellipse, it is easy to obtain the coordinate of the next intersection point,

$$x_p = -\frac{x(b^2 - a^2 k_1^2) \pm 2abk_1\sqrt{a^2 - x^2}}{b^2 + a^2 k_1^2} \tag{5.9}$$

$$y_p = k_1 x_p + y_0 - k_1 x_0 \tag{5.10}$$

$$z_p = \frac{\sqrt{(x_p - x_0)^2 + (y_p - y_0)^2}}{\tan[\cos^{-1}(\frac{k_z'}{mk})]} \tag{5.11}$$

where $k_1 = k_y'/k_x'$. k_x', k_y' and k_z' are the components of the first refracted and internal reflected wave in x, y and z directions respectively. By repeating the procedure described above, we can trace all the rays until they emerge from the particle.

5.1.2 Curvature of wavefront

We have seen that the wavefront equation (Eq. (3.3)) can be simplified as two scalar equations in the case of normal incidence for a plane wave and a shaped beam. But in the diagonal case, the principal directions of the wavefront refracted and reflected rays are unknown, we have to use the curvature matrix (in Eq. (3.3)) and to calculate the curvature of the wavefronts step by step.

When a plane wave is incident onto a particle, the curvature matrix of the incident wavefront is given by

$$Q = \begin{pmatrix} 0 & 0 \\ 0 & 0 \end{pmatrix} \tag{5.12}$$

So the term of $k\Theta^T\, Q\Theta$ in the Eq. (3.3) is removed, because the curvature matrix of the incident wave is null.

Now the curvature matrix of the dioptric surface for an infinite cylinder is expressed by

$$C = \begin{pmatrix} \frac{1}{\rho_1} & 0 \\ 0 & 0 \end{pmatrix} \tag{5.13}$$

where ρ_1 is the local curvature radius of the elliptical section of the cylinder.

The projection matrix Θ' between the base vectors of the dioptric surface $(\boldsymbol{t}, \boldsymbol{e}_z)$ and the base vectors for the refracted wavefront $(\boldsymbol{c}', \boldsymbol{b})$ is [73]

$$\Theta' = \begin{pmatrix} \boldsymbol{t}\cdot\boldsymbol{c}' & \boldsymbol{t}\cdot\boldsymbol{b} \\ \boldsymbol{e}_z\cdot\boldsymbol{c}' & \boldsymbol{e}_z\cdot\boldsymbol{b} \end{pmatrix} \tag{5.14}$$

The projection matrix between the reflected wave and the dioptric surface is given by

$$\Theta'_l = \begin{pmatrix} \boldsymbol{t}\cdot\boldsymbol{c}^l & \boldsymbol{t}\cdot\boldsymbol{b} \\ \boldsymbol{e}_z\cdot\boldsymbol{c}^l & \boldsymbol{e}_z\cdot\boldsymbol{b} \end{pmatrix} \tag{5.15}$$

So the curvature matrix of the refracted wavefront can be obtained from Eq. (3.3) as

$$Q' = \frac{1}{k'}(\boldsymbol{k}' - \boldsymbol{k})\cdot\boldsymbol{n}\Theta'^{T-1} C \Theta'^{-1} \tag{5.16}$$

where the superscript represents the inverse of its matrix. Eq. (5.16) can also be written explicitly in a matrix form

$$Q' = A \begin{bmatrix} (\boldsymbol{e}_z\cdot\boldsymbol{b})\,(\boldsymbol{e}_z\cdot\boldsymbol{b}) & (-\boldsymbol{e}_z\cdot\boldsymbol{b})\,(\boldsymbol{t}\cdot\boldsymbol{b}) \\ (-\boldsymbol{e}_z\cdot\boldsymbol{b})\,(\boldsymbol{t}\cdot\boldsymbol{b}) & (\boldsymbol{t}\cdot\boldsymbol{b})\,(\boldsymbol{t}\cdot\boldsymbol{b}) \end{bmatrix} \tag{5.17}$$

where the coefficient

$$A = \frac{k'_n - k_n}{k'\rho_1} \frac{1}{(\boldsymbol{t}\cdot\boldsymbol{c}'\ \boldsymbol{e}_z\cdot\boldsymbol{b} - \boldsymbol{e}_z\cdot\boldsymbol{c}'\ \boldsymbol{t}\cdot\boldsymbol{b})^2} \tag{5.18}$$

To obtain the principal curvature of refracted wavefront, the diagonalization of the matrix is necessary. After the diagonalization, the curvature matrix reads as [88]

$$Q' = A \begin{bmatrix} (\boldsymbol{e}_z\cdot\boldsymbol{b})^2 + (\boldsymbol{t}\cdot\boldsymbol{b})^2 & 0 \\ 0 & 0 \end{bmatrix} \tag{5.19}$$

From the matrix above, we found that one of the curvature radius of refracted wave is infinity because only one element in the matrix is not null. This was expected since

a plane wave becomes locally a cylindrical wave after the first refraction. So, the curvature radius of the wavefront after the first refraction are given by:

$$R'_{11} = \frac{1}{A[(\boldsymbol{e}_z \cdot \boldsymbol{b})^2 + (\boldsymbol{t} \cdot \boldsymbol{b})^2]} \tag{5.20}$$

$$R'_{12} = \infty \tag{5.21}$$

It is necessary to point out that only the refracted wavefront curvature is derived in detail, since the matrix for reflected wave can be obtained directly thanks to the similarity in the derivation for the Θ' and Θ'^T replaced by Θ'_l and Θ'^T_l.

In the case of normal incidence, the formulae of curvature radii are significantly simplified. In fact the term of $(\boldsymbol{e}_z \cdot \boldsymbol{b})^2 + (\boldsymbol{t} \cdot \boldsymbol{b})^2$ in the Eq. (5.19) is simplified to 1 since $\boldsymbol{b}$ and $\boldsymbol{e}_z$ are in the same direction and $\boldsymbol{b}$ is perpendicular to $\boldsymbol{t}$. The term of $(\boldsymbol{t} \cdot \boldsymbol{c}'\ \boldsymbol{e}_z \cdot \boldsymbol{b} - \boldsymbol{e}_z \cdot \boldsymbol{c}'\ \boldsymbol{t} \cdot \boldsymbol{b})^2$ in Eq. (5.18) simplifies to $\cos^2\theta_r$. Therefore, the curvature radius of the refracted wave becomes

$$\frac{k' \cos^2\theta_r}{R'_1} = \frac{k' \cos\theta_r - k \cos\theta_i}{\rho_1} \tag{5.22}$$

This formulation of curvature radius is the same as Eq. (3.8) in chapter 3.

Let us now introduce the concept of eigenvectors, which are used to express the two principal directions of the wavefront surface. The eigenvectors corresponding to Eq. (5.19) are [88]

$$\boldsymbol{s}_1 = \begin{pmatrix} 1 \\ -\boldsymbol{t} \cdot \boldsymbol{b} / \boldsymbol{e}_z \cdot \boldsymbol{b} \end{pmatrix} \tag{5.23}$$

$$\boldsymbol{s}_2 = \begin{pmatrix} 1 \\ \boldsymbol{e}_z \cdot \boldsymbol{b} / \boldsymbol{t} \cdot \boldsymbol{b} \end{pmatrix} \tag{5.24}$$

The normalized eigenvectors are therefore

$$\boldsymbol{s}_1 = \begin{pmatrix} \frac{1}{\sqrt{1+(-\boldsymbol{t}\cdot\boldsymbol{b}/\boldsymbol{e}_z\cdot\boldsymbol{b})^2}} \\ \frac{-\boldsymbol{t}\cdot\boldsymbol{b}/\boldsymbol{e}_z\cdot\boldsymbol{b}}{\sqrt{1+(-\boldsymbol{t}\cdot\boldsymbol{b}/\boldsymbol{e}_z\cdot\boldsymbol{b})^2}} \end{pmatrix} \tag{5.25}$$

$$\boldsymbol{s}_2 = \begin{pmatrix} \frac{1}{\sqrt{1+(\boldsymbol{e}_z\cdot\boldsymbol{b}/\boldsymbol{t}\cdot\boldsymbol{b})^2}} \\ \frac{\boldsymbol{e}_z\cdot\boldsymbol{b}/\boldsymbol{t}\cdot\boldsymbol{b}}{\sqrt{1+(\boldsymbol{e}_z\cdot\boldsymbol{b}/\boldsymbol{t}\cdot\boldsymbol{b})^2}} \end{pmatrix} \tag{5.26}$$

Since $\boldsymbol{s}_1$ and $\boldsymbol{s}_2$ given above are expressed in the base tangent to the refracted wavefront surface $(\boldsymbol{c}', \boldsymbol{b})$, they can be expressed by

$$\boldsymbol{s}_1 = \frac{1}{\sqrt{1 + (\boldsymbol{t} \cdot \boldsymbol{b}/\boldsymbol{e}_z \cdot \boldsymbol{b})^2}} \boldsymbol{c}' + \frac{-\boldsymbol{t} \cdot \boldsymbol{b}/\boldsymbol{e}_z \cdot \boldsymbol{b}}{\sqrt{1 + (\boldsymbol{t} \cdot \boldsymbol{b}/\boldsymbol{e}_z \cdot \boldsymbol{b})^2}} \boldsymbol{b} \tag{5.27}$$

$$\boldsymbol{s}_2 = \frac{1}{\sqrt{1 + (\boldsymbol{e}_z \cdot \boldsymbol{b}/\boldsymbol{t} \cdot \boldsymbol{b})^2}} \boldsymbol{c}' + \frac{\boldsymbol{e}_z \cdot \boldsymbol{b}/\boldsymbol{t} \cdot \boldsymbol{b}}{\sqrt{1 + (\boldsymbol{e}_z \cdot \boldsymbol{b}/\boldsymbol{t} \cdot \boldsymbol{b})^2}} \boldsymbol{b} \tag{5.28}$$

Once the two principal curvatures (Eq.(5.19)) and directions (Eq. (5.27) and (5.28)) of a refracted ray are known at one point, these properties of the refracted ray when it arrives at the second interface (as incident ray) can be deduced. The curvature matrix of wavefront is given by

$$Q_1 = \begin{bmatrix} \frac{1}{R'_{11}+d} & 0 \\ 0 & 0 \end{bmatrix} \tag{5.29}$$

where d is the distance between the two successive interaction points. The two principal directions of refracted wavefront remain the original directions ($\boldsymbol{b}$ and $\boldsymbol{c}'$). Similarly to the refraction at the first point, the curvature matrix of incident wave Q at the second point is the curvature matrix before the second refraction Q_1. The matrix of dioptric surface at this point is noted by the matrix C_1. According to the properties of an infinite cylinder, one of the principal directions is still parallel to z axis ($\boldsymbol{e}_z$), the other is tangent to the dioptric surface ($\boldsymbol{t}_1$).

The projection matrix Θ of the base of the incident wavefront $(\boldsymbol{s}_1, \boldsymbol{s}_2)$ and the dioptric surface is computed by

$$\Theta = \begin{pmatrix} \boldsymbol{t}_1 \cdot \boldsymbol{s}_1 & \boldsymbol{t}_1 \cdot \boldsymbol{s}_2 \\ \boldsymbol{e}_z \cdot \boldsymbol{s}_1 & \boldsymbol{e}_z \cdot \boldsymbol{s}_2 \end{pmatrix} \tag{5.30}$$

The projection matrix Θ' of the base of the second refracted wavefront surface $(\boldsymbol{s}'_1, \boldsymbol{s}'_2)$ and the dioptric surface $(\boldsymbol{t}_1, \boldsymbol{e}_z)$

$$\Theta' = \begin{pmatrix} \boldsymbol{t}_1 \cdot \boldsymbol{b}_1 & \boldsymbol{t}_1 \cdot \boldsymbol{c}_1 \\ \boldsymbol{e}_z \cdot \boldsymbol{b}_1 & \boldsymbol{e}_z \cdot \boldsymbol{c}_1 \end{pmatrix} \tag{5.31}$$

Like for the first refraction, we define $(\boldsymbol{b}_1, \boldsymbol{c}_1)$ to represent the directions of the second refracted wavefront.

According to Eq. (3.3), the curvature matrix of the refracted wavefront after the second refraction is given by

$$Q' = \frac{1}{k}[(\boldsymbol{k}' - \boldsymbol{k}) \cdot \boldsymbol{n}\Theta'^{T-1} C \Theta'^{-1} + k\Theta'^{T-1}\Theta^T Q \Theta \Theta'^{-1}] \tag{5.32}$$

Thus, the curvature radius of each refracted and interior reflected wavefront can be obtained by repeating calculation detailed in Eq. (5.17) to Eq. (5.29).

5.1.3 Polarization

When a cylinder is illuminated by a wave at diagonal incidence, the cross polarization will occur. Lock has examined the scattering of a circular infinite cylinder with diag-

onal incidence of the plane wave by GO [86]. Two polarizations are considered for the incident wave. In case 1, the electric vector of incident wave vibrates along y direction, and its electric field is expressed by $\boldsymbol{E}_0 = \boldsymbol{e}_y$. In case 2, the electric vector of incident wave vibrates in the xz plane, and is given by $\boldsymbol{E}_0 = \cos\zeta\boldsymbol{e}_x + \sin\zeta\boldsymbol{e}_z$. Zouros [51] has studied the scattering of an elliptical cylinder by a method of separation of variable and considered an incident wave polarized in z direction. It seems unreasonable to us for the polarization of a diagonal incident wave has only z component. Here we follow the procedure initially introduce by Lock which consider two kinds of polarizations: one is perpendicular to the plane defined by the incident wave $\boldsymbol{k}$ and z axis (ϵ), the other is parallel to this plane (μ). The electric field of ϵ polarization is given by

$$\boldsymbol{E}_0 = \frac{\boldsymbol{e}_z \times \boldsymbol{k}}{||\boldsymbol{e}_z \times \boldsymbol{k}||} = -\sin\xi\boldsymbol{e}_x + \cos\xi\boldsymbol{e}_y \tag{5.33}$$

If the incident ray is μ polarized, its electric field is expressed by

$$\boldsymbol{E}_0 = \cos\zeta(\cos\xi\boldsymbol{e}_x + \sin\xi\boldsymbol{e}_y) + \sin\zeta\boldsymbol{e}_z \tag{5.34}$$

To apply Fresnel formulae, the two different polarization states of the incident rays should be projected perpendicularly and parallel on the incident plane, i.e in directions $\boldsymbol{b}$ and $\boldsymbol{c}$. This leads for the amplitude of the refracted wave to

$$\begin{cases} E_\perp^{t0} = t_\perp \boldsymbol{E}_0 \cdot \boldsymbol{b} \\ E_\parallel^{t0} = t_\parallel \boldsymbol{E}_0 \cdot \boldsymbol{c} \end{cases} \tag{5.35}$$

and for the amplitude of the reflected wave to,

$$\begin{cases} E_\perp^{r0} = r_\perp \boldsymbol{E}_0 \cdot \boldsymbol{b} \\ E_\parallel^{r0} = r_\parallel \boldsymbol{E}_0 \cdot \boldsymbol{c} \end{cases} \tag{5.36}$$

where $t_\perp$, $t_\parallel$, $r_\perp$ and $r_\parallel$ are the refraction and reflection Fresnel coefficients respectively. The emergent electric field for the reflection ($p = 0$) is therefore given by

$$\boldsymbol{E}_0 = E_\perp^{r0}\boldsymbol{b} + E_\parallel^{r0}\boldsymbol{c}^l \tag{5.37}$$

The refracted electric field is given by

$$\boldsymbol{E}_{t0} = E_\perp^{t0}\boldsymbol{b} + E_\parallel^{t0}\boldsymbol{c}' \tag{5.38}$$

The refracted wave continues to propagate inside the cylinder and it will be considered as the incident wave for the next interaction. In the same manner, we can obtain the

refracted and reflected electric fields for $p = 1$ by using Eq. (5.35) and Eq. (5.36) with $\boldsymbol{E}_0$, $\boldsymbol{b}$ and $\boldsymbol{c}$ replaced by $\boldsymbol{E}_{t0}$, $\boldsymbol{b}_1$ and $\boldsymbol{c}_1$:

$$\begin{cases} E_{\perp}^{t1} = t_{\perp} \boldsymbol{E}_{t0} \cdot \boldsymbol{b}_1 \\ E_{\parallel}^{t1} = t_{\parallel} \boldsymbol{E}_{t0} \cdot \boldsymbol{c}_1 \end{cases} \tag{5.39}$$

and ,

$$\begin{cases} E_{\perp}^{r1} = r_{\perp} \boldsymbol{E}_{t0} \cdot \boldsymbol{b}_1 \\ E_{\parallel}^{r1} = r_{\parallel} \boldsymbol{E}_{t0} \cdot \boldsymbol{c}_1 \end{cases} \tag{5.40}$$

It is worth to point out that Fresnel coefficients of an elliptical cylinder are different at each interaction point. The amplitude of the electrical field of each refraction and reflection proceeds in the similar way, the polarization sates of p order of ray is hereby

$$\boldsymbol{E}_p = \begin{cases} E_{\perp}^{r0} \boldsymbol{b} + E_{\parallel}^{r0} \boldsymbol{c}^l & p = 0 \\ E_{\perp}^{tp} \boldsymbol{b}_p + E_{\parallel}^{tp} \boldsymbol{c}'_p & p \geq 1 \end{cases} \tag{5.41}$$

5.1.4 Amplitude

Since the cross polarization occurs at diagonal incidence, the energy factor $\varepsilon_{X,p}$ of refracted and reflected fraction is no longer suitable to denote the amplitude. The same effect can be described for $\boldsymbol{E}_p$. The total field in far zone at a given angle θ is calculated by the summation of the complex amplitude of all order rays arriving at the same angle :

$$S_{X,p} = \begin{cases} A|E_{\perp}^{tp}| & X = 1 \\ A|E_{\parallel}^{tp}| & X = 2 \end{cases} \tag{5.42}$$

where $A = \sqrt{\frac{\pi}{2}\mathcal{D}}|S_G| \exp(i\phi_p)$. Note that $E_{\perp}^{tp}$ and $E_{\parallel}^{tp}$ should be replaced by $E_{\perp}^{r0}$ and $E_{\parallel}^{r0}$, when $p = 0$.

5.2 Numerical results and discussion

We first consider a circular cylinder of radius $a = 50\mu m$ and refractive index $m = 1.484$ illumined by a diagonal plane wave with $\zeta = 39.28°$ and $\xi = 0$ by setting the same parameters as in Fig. 4 in the reference [86]. The trajectories for $p = 1$ to $p = 6$ are illustrated the Fig. 5.2. We found an agreement between Fig. 5.2(a-e) and the Fig. 4 in the reference [86]. Moreover, the trajectories of order $p = 6$ are also given. According to the notation of Lock [86], varying the tilt angle of plane wave with respect to the cylinder is equivalent to varying the cylinders's refractive index

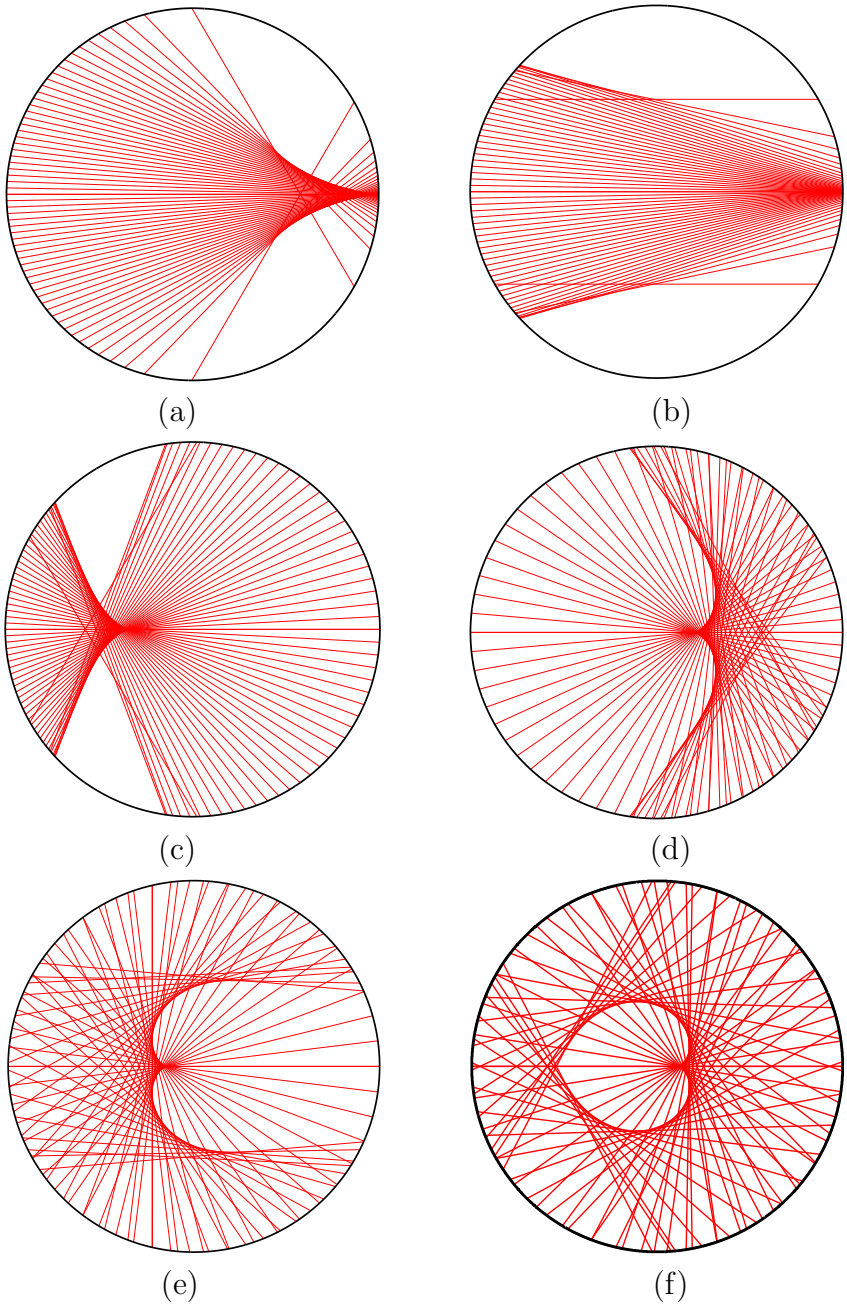

Figure 5.2: Ray trajectories and interior cusp caustics for $m' = 2$ for (a) $p = 1$, (b) $p = 2$, (c) $p = 3$, (d) $p = 4$, (e) $p = 5$ and (f) $p = 6$.

at normal incidence. So the projection of ray tracing in xy plane for a plane wave with $\zeta = 39.28°$ by a cylinder of refractive index $m = 1.484$ is identical to ray tracing for a cylinder of refractive index $m' = 2$ at normal incidence. The position of interior

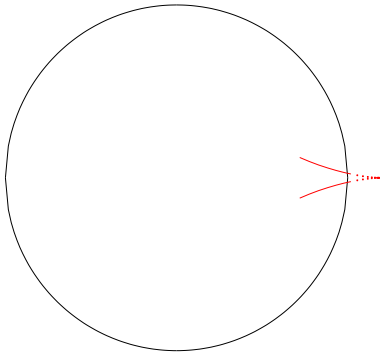

(a)

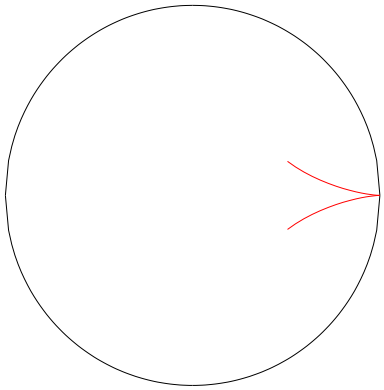

(b)

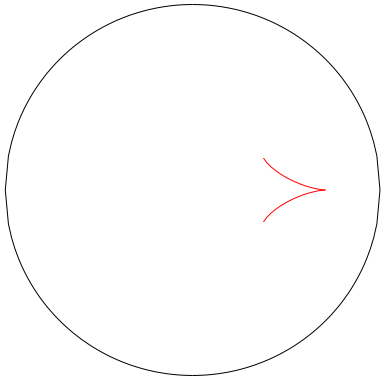

(c)

Figure 5.3: $p = 1$ focusing caustic for (a) $m' = 1.845$, (b) $m' = 2$, and (c) $m' = 2.41$.

caustics on the axis (y=0) can be calculated by [89]

$$x = \frac{(-1)^p}{2p - 1 - n'} a \tag{5.43}$$

Except for $p = 2$ whose the caustics locates at the exterior of the cylinder, the others all locates in the interior of cylinder. The caustics for $p = 1$ occurs at the boundary

of cylinder. From Eq. 5.43 and Fig. 5.2, we find the cusp of different orders are consistent and more close to the axis of the cylinder as the ray order increase.

In VCRM, the curvature radii of wavefront is introduced to described the divergence/convergence of wavefront. So the caustics position of rays can be described by the center of wavefront. Fig. 5.3 shows the center of curvature radii for $p = 1$ by setting the refractive indices $m' > 2$, $m' = 2$ and $m' < 2$. Those figures are also chosen to compare with the conclusions of reference [86], where the cusp points for $p = 1$ locates outsider of the cylinder surface for $m' < 2$, touches the surface for $m' = 2$ and lies within the cylinder for $m' > 2$.

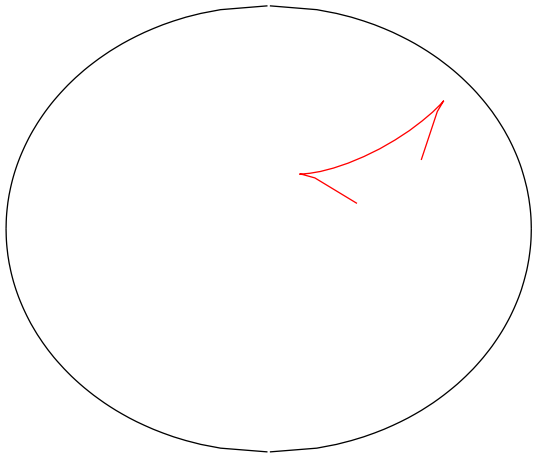

Figure 5.4: $p = 1$ focusing caustic for an elliptical cylinder of $a = 50\mu$m, $b = 40\mu$m and $m = 1.33$ illuminated by a diagonal plane wave making an angle $\zeta = 30°$ with z axis and an angle $\xi = 20°$ with x axis.

Fig. 5.4 illustrates the center of wavefront curvature after the first refraction ($p = 1$) for an elliptical cylinder of $a = 50\mu$m, $b = 40\mu$m and $m = 1.33$ illuminated by a diagonal plane wave with $\zeta = 30°$ and $\xi = 20°$. In Fig. 5.4, the centers of wavefront curvature are no longer symmetric and become more complicate relative to the case of circular cylinder. The refractive index $m = 1.33$ of cylinder at diagonal incidence ($\xi = 30°$) is equivalent to the refractive index $m' = 2.02$ at the normal incidence. To validate its results, the ray tracing for an elliptical cylinder of $a = 50\mu$m, $b = 40\mu$m and $m = 2.02$ is given in Fig. 5.5. The trajectories of curvature center in the Fig. 5.4 are the same as the position of focusing cusp points in Fig. 5.5.

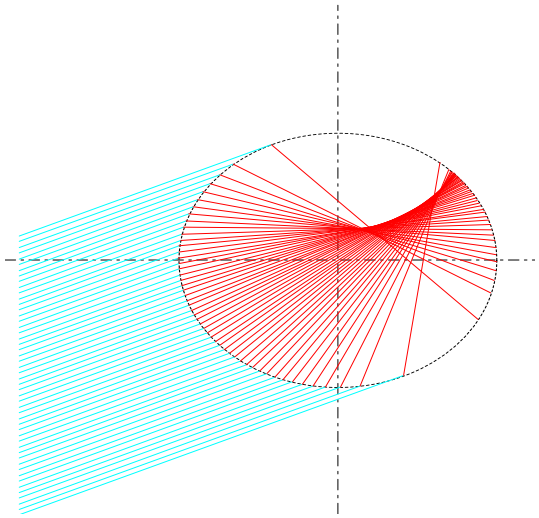

Figure 5.5: $p = 1$ focusing caustic for an elliptical cylinder of $a = 50\mu$m, $b = 40\mu$m and $m' = 2.02$ illuminated by a plane wave making an angle $\xi = 20°$ relative to x axis.

5.3 Conclusion

In this chapter, VCRM is applied to deal with the scattering of an elliptical cylinder illuminated by a diagonal plane wave. To validate our theory, the ray trajectories and the cusp point described by the curvature radii of wavefront for circular cylinders are given. Due to light scattering of a diagonally incident plane wave by an elliptical cylinder has rich in phenomena, the cusp points of the elliptical cylinder are then described. Due to the difficulty to deal with the polarization and the calculation of the Fresnel coefficients in the three dimensional coordinate transformation, the work on the prediction of the scattering diagram has not yet completed.

Chapter 6

Conclusions and perspectives

This thesis is devoted to the development of Vectorial Complex Ray Model(VCRM) to describe the interaction of an infinite elliptical cylinder with a plane wave or a Gaussian beam. In this chapter we draw the conclusions of presented work and give perspectives in further studies.

6.1 Conclusions

The light scattering theories are essential to the particle and particle system characterization which concerns many research and industrial domains, such as the environmental control, the fluid mechanics, the combustion, the micro fluidics and the telecommunication. The most used models of particles in the optical metrology are sphere and infinite circular cylinder for simplicity and the theories have been well developed. However, the shape of the particles in practice are often not so simple. The liquid jet generated from the injection, for example, is not a perfect circular cylinder and the droplets produced in the atomization are not spherical. Some theories and numerical methods have also been developed for regular shape particle, such as spheroid, ellipsoid, or elliptical cylinder to take into account the deformation of the particles. Nevertheless, the sizes of the particles are often limited because of the numerical difficulty. The Vectorial Complex Ray Model(VCRM) recently developed in the laboratory permits to deal with the scattering of large irregularly shaped particles. One of the significant merits of the VCRM is that the concept of wavefront curvature is introduced to the ray model to describe the divergence/convergnece of the wave it presents. In such way, the phase shift due to the focal line can also be counted easily

for complex shape particles. This new property makes a big step in improving the precision of ray model in the scattering theory.

After a brief recall of the fundamental models and concepts in light scattering, the general principle of the VRCM is presented. The novel model has been applied firstly to deal with the scattering of an infinite cylinder of elliptical section illuminated by a plane wave propagating perpendicularly to the cylinder axis. The incident direction can be oblique relative to the axes of the ellipse. By comparison of the scattering diagrams of VCRM for a circular cylinder with that of LMT - a rigorous theory, we have shown that the precision of VCRM is very good for the cylinder of diameter larger than tens of wavelength if all the properties of the rays, i.e. propagation direction, polarization, phase, amplitude and curvature of wavefront, are correctly counted. Since we have not found any results in the literature for the scattering of large elliptical cylinders, the scattered intensities have also been compared to the results of the code VCRM for a long ellipsoid to validate our code for elliptical cylinder.

The scattering diagrams as function of the incident angle and the aspect ratio of the ellipse have been studied. The structure of rainbow is very sensible to the size, the refractive index and the ellipticity of the particle. the refractometry of rainbow is a common technique in optical metrology. A special attention has been paid to the rainbow phenomena of an infinite elliptical cylinder. It is found that if the aspect ratio is important certain orders of rainbows may disappear while the others are doubled for certain incident angles.

Moreover, our model and code have also been used to calculate the diagrams of bubble cylinders (the relative refractive index of the cylinder to the surrounding medium is less than unity) and absorbing cylinder. We observed a special rainbow phenomenon occurred in the elliptical bubble cylinder at certain incident angles which is impossible to happen in the circular cylinder.

VCRM has then been extended to predict the scattering of a shaped beam by an elliptical cylinder also at normal incidence. Three types of Gaussian beams (two dimensional Gaussian beam, circular Gaussian beam and astigmatic elliptical Gaussian beam) have been considered. In case of two dimensional Gaussian beam incidence, the code is validated by comparison of the scattering diagram of a capillary to the numerical and experimental results found in the literature. For the circular Gaussian beam, the focusing effect in the plane containing the cylinder axis is observed and studied extensively. This effect can be explained by the wavefront equation in VCR-

M. We have shown that the scattered wave from an elliptical cylinder is, in general, not cylindrical nor spherical. The astigmatic elliptical Gaussian beam is a Gaussian beam with a elliptical section and its two beam waists may locate at different position along the beam axis, so it is a general form of the two dimensional and the circular Gaussian beams. Furthermore, by choosing the two waist positions, different forms of beam can be obtained. The effect of beam shape on the light scattering is then studied.

When the direction of the incident wave is not perpendicular to the axis of the cylinder, the scattering becomes a problem of three dimensions. The ray tracing, the change of polarization state and the divergence/convergence of the wave through the surface of the particle as well as the calculation of the amplitudes of the waves are very difficult, even impossible, in the context of the classical geometric optics. The thesis presents a very elegant formalism and easy to apply to three-dimensional scattering under VCRM. The code developed on this basis has been validated in comparison with the results found in the literature for the particular case - the prediction of the caustic of a homogeneous circular cylinder. The code was then used to predict the caustic of an elliptic cylinder.

6.2 Perspective

Though the scattering of light by an infinite cylinder at normal incidence is a special case and theoretically easy, it is important for the optical metrology since it corresponds to conventional configurations in experimental setup. What we have developed in the thesis can be applied to the study of the deformation and the measurement of the ellipticity of elliptical cylinder. A systematic study on the relation between the scattered diagram profiles at different angles and the form of the particle could provide practical information for the measurement of the deformation of a optical fibers in production, for example.

Furthermore, other shaped beams, i.e the bessel beam and higher order Hermite-Gaussian beam can be considered. A further extension of VCRM to other irregular particles, coated circular or elliptical cylinder and cylinder with inclusions, also could be done.

The formalism for the scattering of a plane wave by an infinite elliptical cylinder at diagonal incidence has been well developed in the thesis. The code has been also

validated by comparison with the results in the literature for the prediction of caustics. This is an important advance in VCRM to 3 dimensional scattering. The calculation of the scattering intensity is to be finished and should be direct. A extension to the scattering of other shaped beams should not be too difficult.

All the ray models for the light scattering have the same intrinsic problem: the singularities appear where the amplitude (intensity) or its derivative is not continuous. There are three kinds of singularity: 1). in the rainbow angle where the intensity tends to infinite, 2). at the border of the particle where the variation of the amplitude of the incident wave is abrupt, 3). in the critical angle where the total reflection occurs, so the amplitude of the reflected wave is not continuous. In these regions, the ray models themselves fail to predict correctly the scattering intensity. A supplementary theory or model are to be used to correct the prediction of the ray models. The first one is solved by Airy theory for a spherical particle or a circular infinite cylinder. The second singularity is often compensated by the diffraction theory. But this is possible or relatively simple only for plane wave illumination on a particle of simple form. The third one has been studied by Marston [80] for spherical particle and Onofri for spheroid. The fundamental idea in these supplementary theories is to take into account the wave effect near the singularity point or caustics by analytical or semi-analytical expression. To profit the advantage of the VCRM to deal with the scattering of shaped beams by particles of arbitrary shape, the problem near the singularity point must be solved. In fact, this may be realized by numerical simulation since we know all the properties of all the rays in VCRM.

Bibliography

[1] Descartes. *Discourse de la method*. GF-Flammarion, Paris, 1992.

[2] D. Lebrun, S. Belaid, C. Özkul, K. F. Ren, and G. Gréhan. Enhancement of wire diameter measurements: comparison between Fraunhoferdiffraction and Lorenz-Mie theory. *Opt. Eng.*, 35(4):946–950, 1996.

[3] H. C. van de Hulst. *Light scattering by small particles*. Dover Publications, New York, 1957.

[4] C. F. Bohren and D.R. Huffman. *Absorption and scattering of light by small particles*. J. Wiley and sons, New York, 1983.

[5] N. Gauchet, T. Girasole, K. F. Ren, G. Gréhan, and G. Gouesbet. Application of generalized Lorenz-Mie theory for cylinders to cylindrical characterization by phase-Doppler anemometry. *Optical Diagnostic in Engineering*, 2(1):1–10, 1997.

[6] X. Han, K. F. Ren, Z. Wu, F. Corbin, G. Gouesbet, and G. Gréhan. Characterization of initial disturbances in liquid jet by rainbow sizing. *Appl. Opt.*, 37(36):8498–8503, 1998.

[7] N. Vago, A. Spiegel, P. Couty, F. R. Wagner, and B. Richerzhagen. New technique for high-speed microjet breakup analysis. *Exp. Fluids*, 35:303–309, 2003.

[8] T. Ménard, S. Tanguy, and A. Berlemont. Coupling level set/vof/ghost fluid methods: Validation and application to 3d simulation of the primary break-up of a liquid jet. *Intern. J. Multiphase Flow*, 33:510–524, 2007.

[9] J. Wilms, N. Roth, S. Arndt, and B. Weigand. Determination of the composition of multicomponent droplets by rainbow refractometry. *12th International Symposium on Applications of Laser Techniques to Fluid Mechanics. Lisbon*, 2004.

[10] F. Durst, A. Melling, and J.H. Whitelaw. *Principles and Practice of laser-Doppler-Anemometry*. Academic Press, 1981.

[11] T. Girasole, H. Bultynck, G. Gouesbet, G. Gréhan, F. Le Meur, J.N. Le Toulouzan, J. Mroczka, K. F. Ren, C. Rozé, and D. Wysoczanski. Cylindrical fibre orientation analysis by light scattering. part 1: Numericalaspect. *Part. Part. Syst. Charact.*, 14:163–174, 1997.

[12] T. Girasole, G. Gouesbet, G. Gréhan, J.N. Le Toulouzan, J. Mroczkaand K. F. Ren, and D. Wysoczanski. Orientation analysis by light scattering from cylindrical fibres. part 2: Experimental aspect. *Part. Part. Syst. Charact.*, 14:211–218, 1997.

[13] Seker S.S and G Apaydin. Light scattering by thin curved dielectric surface and cylinder. *Geoscience and Remote Sensing Symposium,2009 IEEE International,IGARSS 2009*, 1:I–29–I–32, 2009.

[14] C.A. Valagiannopoulos. Electromagnetic scattering of the field of a metamaterial slab antenna by an arbitrarily positioned cluster of metallic cylinders. *Progress In Electromagnetics Research*, 114:51–66, 2011.

[15] M Yamada, A. Tomoe, and H. Takara. Light scattering characteristics of hole formed by fibre fuse. *Electronics Letters*, 48:519–520, 2012.

[16] G. Martin, S. Hoath, and I. Hutchings. Inkjet printing-the physics of manipulating liquid jets and drops. In *Journal of Physics: Conference Series, 105*, 2008.

[17] C. Yeh. Backscattering cross section of a dielectric elliptical cylinder. *JOSA*, 55(3):309–312, 1965.

[18] J. J. Bowman, Thomas B. A. Senior, and P.L. E. Uslenghi. *Electromagnetic and acoustic scattering by simple shapes*. Taylor & Francis Inc, 1988.

[19] A. K. Hamid and F. R. Cooray. Scattering by a perfect electromagnetic conducting elliptic cylinder. *PIER Lett.*, 10:59–67, 2009.

[20] V. V. Varadan. Scattering matrix for elastic waves. II. Application to elliptic cylinders. *J. Acoust. Soc. Am.*, 63(4):1014–1024, 1978.

[21] J. B. Keller. Geometrical theory of diffraction. *J. Opt. Soc. Am.*, 52(2):116–130, 1962.

[22] M. I. Mishchenko, J. W. Hovenier, and L. D. Travis. *Light Scattering by Non-spherical Particles: Theory, Measurements, and Applications*. Academic Press, 2000.

[23] J. R. Wait. Scattering of a plane wave from a circular dielectric cylinder at obliqueincidence. *J. Phys.*, 33:189–195, 1955.

[24] P. W. Barber and S. C. Hill. *Light scattering by particles: Computational methods*. World Scientific, Singapore, 1990.

[25] A. Sebak and L. Shafai. Generalized solutions for electromagnetic scattering by elliptical structures. *Comput. Phys Commun*, 68:315–330, 1991.

[26] G. Tsogkas, J. Roumeliotis, and S. Stylianos. Scattering by an infinite elliptic metallic cylinder. *Electromagnetics*, 27:159–182, 2007.

[27] C. Adler, J. Lock, J. Nash, and K. Saunders. Experimental observation of rainbow scattering by a coated cylinder: twin primary rainbows and thin-film interference. *Appl. Opt.*, 40:1548–1558, 2001.

[28] R. Li, X. Han, H. Jiang, and K. F. Ren. Debye series of normally incident plane wave scattering by an infinite multi-layered cylinder. *Appl. Opt.*, 45(24)(24):6255–6262, 2006.

[29] R. Li, X. Han, and K. F. Ren. Generalized Debye series expansion of electromagnetic plane wave scattering by an infinite multilayered cylinder at oblique incidence. *Phy. Rev. E.*, 79:036602, 2009.

[30] Shogo Kozaki. A new expression for the scattering of a gaussian beam by a conducting cylinder. *IEEE Transact. Anten. Propag.*, 30(5):881–887, 1982.

[31] Shogo Kozaki. Scattering of a gaussian beam by a homogeneous dielectric cylinder. *J. Appl. Phys.*, 53(11):7195–7200, 1982.

[32] Toshitaka Kojima and Yoichi Yanagiuchi. Scattering of an offset two-dimensional gaussian beam wave by a cylinder. *J. Appl. Phys.*, 50(1):41–46, 1979.

[33] E. Zimmermann, R. Dändliker, N. Souli, and B. Krattiker. Scattering of an off-axis gaussian beam by a dielectric cylinder compared with a rigorous electromagnetic approach. *J. Opt. Soc. Am. A*, 12:398–403, 1995.

[34] G. Gouesbet. Interaction between an infinite cylinder and an arbitrary shaped beam. *Appl. Opt.*, 36(18):4292–4304, 1997.

[35] K. F. Ren, G. Gréhan, and G. Gouesbet. Scattering of a Gaussian beam by an infinite cylinder in GLMT-framework, formulation and numerical results. *J. Opt. Soc. Am. A.*, 14(11):3014–3025, 1997.

[36] L. Mees, K. F. Ren, G. Gréhan, and G. Gouesbet. Scattering of a Gaussian beam by an infinite cylinder with arbitrary location and arbitrary orientation, numerical results. *Appl. Opt.*, 38(9):1867–1876, 1999.

[37] J. A. Lock. Scattering of a diagonally incident focused Gaussian beam by an infinitely long homogeneous circular cylinder. *J. Opt. Soc. Am. A.*, 14:640–652, 1997.

[38] J. A. Lock. Morphology-dependent resonances of an infinitely long circular cylinderilluminated by a diagonally incident plane wave or a focused Gaussian beam. *J. Opt. Soc. Am. A*, 14(3):653–661, 1997.

[39] G. Gouesbet and L. Mees. Generalized Lorenz-Mie theory for infinitely long elliptical cylinders. *J. Opt. Soc. Am. A*, 16(6):1333–1341, 1999.

[40] G. Gouesbet, L. Mees, G. Gréhan, and K. F. Ren. Localized approximation for Gaussian beams in elliptical cylinder coordinates. *Appl. Opt.*, 39(6):1008–1025, 2000.

[41] G. Gouesbet, L. Mees, G. Gréhan, and K. F. Ren. Description of arbitrary shaped beams in elliptical cylinder coordinates,by using a plane wave spectrum approach. *Opt. Commun.*, 161:63–78, 1999.

[42] Shi Chun Mao and Zhen-Sen Wu. Scattering by an infinite homogenous anisotropic elliptic cylinder in terms of Mathieu functions and fourier series. *J. Opt. Soc. Am. A*, 25(12):2925–2931, 2008.

[43] S. C. Mao, Z. S. Wu, and H. Y. Li. Three-dimensional scattering by an infinite homogeneous anisotropic elliptic cylinder in terms of Mathieu functions. *J. Opt. Soc. Am. A*, 26(11):2282–2291, 2009.

[44] S. Caorsi, M. Pastorino, and M. Raffetto. Electromagnetic scattering by a multilayer elliptic cylinder under transverse-magnetic illumination: series solution in terms of Mathieu functions. *IEEE Trans. Anten. Propag*, 45(6):926–935, 1997.

[45] G. Gouesbet, L. Mees, and G. Gréhan. Partial wave description of shaped beams in elliptical cylinder coordinates. *J. Opt. Soc. Am. A*, 15(12):3028–3038, 1998.

[46] G. Gouesbet, L. Mees, and G. Gréhan. Partial wave expansions of higher-order Gaussian beams in elliptical cylindricalcoordinates. *J. Opt. A: Pure and Appl. Opt.*, 1:121–132, 1999.

[47] G. Gouesbet, L. Mees, G. Gréhan, and K. F. Ren. The structure of generalized Lorenz-Mie theory for elliptical infinitecylinders. *Part. Part. Syst. Charact.*, 16:3–10, 1999.

[48] C. Yeh. Scattering of obliquely incident light waves by elliptical fibers. *J. Opt. Soc. Am. A.*, 54:1227–1231, 1964.

[49] J. Yan, R. Gordon, and A. Kishk. Electromagnetic scattering from impedance elliptic cylinders using finite difference method (oblique incidence). *J. Opt. Soc. Am. A.*, 15:157–173, 1995.

[50] J. Tsalamengas. Exponentially converging nystro/spl uml/m's methods for systems of singular integral equations with applications to open/closed strip-or slot-loaded 2-d structures. *Anten Propag, IEEE Transactions*, 54:1549–1558, 1995.

[51] G. P. Zouros. Electromagnetic plane wave scattering by arbitrarily oriented elliptical dielectric cylinders. *J. Opt. Soc. Am. A.*, 28:2376–2384, 2011.

[52] D. Marcuse. Light scattering from elliptical fibers. *Appl. Opt*, 13(8):1903–1905, 1974.

[53] J. Holoubek. Light scattering from unclad fibers: approximate ray theory of backscattered light. *Appl. Opt.*, 15:2751–2755, 1976.

[54] A. R. Steinhardt and L. Fukshansky. Geometrical optics approach to the intensity distribution in finite cylindrical media. *Appl. Opt*, 26(18):3778–3789, 1987.

[55] C. L. Adler, J. A. Lock, and B. R. Stone. Rainbow scattering by a cylinder with a nearly elliptical cross section. *Appl. Opt.*, 37(9):1540–1550, 1998.

[56] P. Yang and K.N. Liou. Geometrics-optics-integral-equation method for light scattering by non-spherical ice crystals. *Appl. Opt.*, 35(33):6568–6584, 1996.

[57] P. Yang and K. N. Liou. An exact geometric-optics approach for computing the optical properties of large absorbing particles. *J. Quant. Spectrosc. Radiat. Transfer*, 110:1162–1177, 2009.

[58] P. Yang, H. Wei, H.-L. Huang, B. A. Baum, Y. X. Hu, M. I. Mishchenko G. W. Kattawar, and Q. Fu. Scattering and absorption property database for nonspherical ice particles in the near- through far-infrared spectral region. *Appl. Opt.*, 44:5512–5523, 2005.

[59] Z. Zhang, P. Yang, G. W. Kattawar, and W. J. Wiscombe. Single scattering properties of platonic solids in geometric-optics regime. *J. Quant. Spectros. Rad. Transfer*, 106:595–603, 2007.

[60] L. Bi, P. Yang, G. W. Kattawar, Y. Hu, and B. A. Baum. Scattering and absorption of light by ice particles: Solution by a new physical-geometric optics hybrid method. *J. Quant. Spectrosc. Radiat. Transfer*, 112:1492–1508, 2011.

[61] E. A. Hovenac. Calculation of far-field scattering from nonspherical particles using a geometrical optics approach. *Appl. Opt.*, 30(33):4739–4746, 1991.

[62] F. Xu, K. F. Ren, and X. Cai. Extension of geometrical-optics approximation to on-axis gaussian beam scattering. I. by a spherical particle. *Appl. Opt.*, 45(20):4990–4999, 2006.

[63] Y. Yuan. *Diffusion de la lumiére par un objet irrgulier et application l'imagerie des spray.* Thesis, 2012.

[64] F. Xu, K. F. Ren, X. Cai, and J. Shen. Extension of geometrical-optics approximation to on-axis gaussian beam scattering II. By a spheroidal particle with end-on incidence. *Appl. Opt.*, 45(20):5000–5009, 2006.

[65] B. Krattiger, A. Bruno, H. Widmer, M. Geiser, and R. Dandliker. Laser-based refractive-index detection for capillary electrophoresis: ray-tracing interference theory. *Appl. Opt.*, 35(6):956–965, 1993.

[66] K. F. Ren, F. Onofri, C. Rozé, and T. Girasole. Vectorial complex ray model and application to two-dimensional scattering of plane wave by a spheroidal particle. *Opt. Lett.*, 36(3):370–372, 2011.

[67] K. F. Ren, C. Rozé, and T. Girasole. Scattering and transversal divergence of anellipsoidal particle by using vectorial complex raymodel. *J. Quant. Spectrosc. Radiat. Transfer*, 113:2419–2423, 2012.

[68] L. Benckert, L. Forsberg, and N. E. Molin. *Fresnel diffraction of a Gaussian laser beam by polished metal cylinders*, volume 29. 1990.

[69] L. Miguel and S. Brea. *Diameter estimation of cylinders by the rigorous diffraction model*, volume 22. 2005.

[70] E. A. Hovenac and J. A. Lock. Assessing the contributions of surface waves and complex rays to far-field scattering by use of the Debye series. *J. Opt. Soc. Am. A*, 9(5):781–795, 1992.

[71] J. A. Lock and C. L. Adler. Debye-series analysis of the first-order rainbow produced in scatteringof a diagonally incident plane wave by a circular cylinder. *J. Opt. Soc. Am. A*, 14(6):1316–1328, 1997.

[72] Haitao Yu, Jianqi Shen, and Yuehuan Wei. Geometrical optics approximation for light scattering by absorbing spherical particles. *J. Quant. Spectroscopy Radiative Transfer*, 110:11781189, 2009.

[73] G. A. Deschamps. Ray techniques in electromagnetics. *Proc. IEEE*, 60(9):1022–1035, 1972.

[74] A. Ghatak. *Optics*. Tata McGraw-Hill Pubishiling Company Limited, 1977.

[75] K. F. Ren, X. Han, and K. Jiang. Scattering of an arbitrary shaped object by using vectorial complex ray model. In *2012 10th International Symposium on Antennas. Propagation & EM Theory (ISAPE),*, 2012.

[76] M. Born and E. Wolf. *Principles of optics, 7th ed.* Cambridge University Press, 1999. Pergamon Press, 3rd edition.

[77] J. Shen, H. Yu, and J. Lu. Light propagation and reflection-refraction event in absorbing media. *Chines Optics Letters*, 8:111–114, 2010.

[78] H. He, W. Li, X. Zhang, M. Xia, and K. Yang. Light scattering by a spheroidal bubble with geometrical optics approximation. *J. Quant. Spect. Rad. Trans.*, 113:1467–1475, 2012.

[79] G. Gouesbet and L. Mees. Validity of the elliptical cylinder localized approximation for arbitraryshaped beams in generalized Lorenz-Mie theory for elliptical cylinders. *J. Opt. Soc. Am. A*, 16(12):2946–2958, 1999.

[80] P. L. Marston. Critical angle scattering by a bubble: physical-optics approximation and observations. *J. Opt. Soc. Am.*, 69:1205–1211, 1979.

[81] F. Onofri, R. Stefan, S. Matthias, and B. Séverine. Physical-optics approximation of near-critical-angle scattering by spheroidal bubbles. *Optics letters*, 37(22):4780–4782, 2012.

[82] R. Goldman. Curvature formulas for implicit curves and surfaces. *Com. Aid. Geo. Des.*, 22:632–658, 2005.

[83] L. W. Davis. Theory of electromagnetic beams. *Phys. Rev. A*, 19:1177–1179, 1979.

[84] James A Lock. Calculation of the radiation trapping force for laser tweezers by use of generalized lorenz-mie theory. i. localized model description of an on-axis tightly focused laser beam with spherical aberration. *Applied optics*, 43(12):2532–2544, 2004.

[85] K. F. Ren. *Diffusion des faisceaux feuille laser par une particule sphérique et applications aux écoulements diphasiques.* PhD thesis, Rouen University, France, May 1995.

[86] C. L. Adler, J. A. Lock, B. R. Stone, and C. J. Garcia. High-order interior caustics produced in scattering of a diagonally incident plane wave by a circular cylinder. *J. Opt. Soc. Am. A*, 14(6):1305–1315, 1997.

[87] M. Kerker, D. Cooke, Z. Farone, and R. Jacobsent. Electromagnetic scattering from an infinite circular cylinder at oblique incidence. i. radiance functions for m=1.46. *J. Opt. Soc. Am. A.*, 56:487–491, 1966.

[88] S. W. Lee, M. S. Sheshadri, and V. Jamnejad. Refraction at a curved dielectric interface: Geometrical optics solution. *IEEE Trans. Micro. Theory Tech.*, MTT-30(1):12– 19, 1982.

[89] J. Lock and E. Hovenac. Internal caustic structure of illuminated liquid droplets. *J. Opt. Soc. Am. A.*, 8:1541–1552, 1991.

Résumé

Cette thèse est dédiée à l'étude théorique et numérique de diffusion de la lumière par un cylindre infini de section elliptique éclairé par une onde plane ou un faisceau gaussien avec le Model de Tracé de Rayons Vectoriels Complexes (TRVC) développé au laboratoire.

La prédiction théorique et numérique de l'interaction de la lumière avec des particules est essentielle pour la caractérisation de systèmes particulaires par la métrologie optique. Ceci concerne un domaine très large tant pour la recherche fondamentale que pour des applications industrielles, comme l'atomisation, la combustion, la mécanique des fluides, le contrôle environnemental, la micro fluidique, la télécommunication ... Les modèles de particules les plus utilisés dans les techniques de mesure optique sont la sphère et le cylindre circulaire et les théories correspondantes sont aussi bien développées. Cependant, les formes de particules rencontrées dans la pratique ne sont pas aussi simples. Les jets liquides générés par l'atomisation, par exemple, ne sont pas tout à fait cylindriques. Le contrôle de la circularité de fibres optiques à la production est aussi important pour garantir sa qualité de transmission des signaux. Des théories et des méthodes numériques ont développés pour des particules de forme régulières comme sphéroïde, ellipsoïde ou cylindre infini de section elliptique, afin de prendre en compte la déformation, mais la taille de particules est très limitée à cause de difficulté de calcul numérique.

Contrairement aux méthodes citées ci-dessus, l'optique géométrique est valide pour des objets de tailles très grandes devant la longueur d'onde. Elle est, sur le principe, facile à utiliser pour la diffusion de la lumière par des particules de forme quelconques. Par contre elle est rarement utilisée à prédire quantitativement l'interaction de la lumière par des particules, car d'une part elle n'est pas aussi simple pour des particules de forme complexe, et d'autre part sa précision n'est pas très satisfaisante. Afin de surmonter ces difficultés, Ren et al ont développé le Tracé de Rayons Vectoriels Complexes (TRVC) en introduisant la propriété de forme du front d'onde dans le model de rayon. TRVC est bien adapté à l'étude de diffusion d'une onde de forme quelconque par un objet de forme complexe de surface lisse afin de prédire la diffusion de particule avec une précision très satisfaisante.

Dans cette thèse, après un rappel des fondamentaux de diffusion de la lumière et les modèles de bases à utiliser, TRVC est d'abord appliqué à la diffusion d'une onde plane par un cylindre infini de section elliptique à incidence normale. Afin de

valider notre code de calcul et de tester la précision de TRCV, les diagrammes de diffusion prédits par TRVC ont été comparés avec ceux de la Théorie de Lorenz-Mie - théorie rigoureuse de référence. Il a été montré que la précision de TRVC est très satisfaisante pour des particules de tailles au-delà d'une dizaine de longueurs d'onde. Le code développé a été ensuite appliqué à l'étude de diffusion d'un cylindre elliptique. On a trouvé que les diagrammes de diffusion d'un cylindre elliptique sont sensibles à son ellipticité et l'angle d'incidence de l'onde plane par rapport aux axis de l'ellipse du cylindre. Une étude approfondie a été menée sur la relation entre les positions d'arcs-en-ciel et l'ellipticité ainsi que l'angle d'incidence de l'onde plane. Contrairement à un cylindre circulaire ou une sphère, certains ordres d'arcs-en-ciel d'un cylindre elliptique disparaissent, d'autres doublent en fonction de son ellipticité et l'angle d'incidence de la lumière. Notre code peut être aussi appliqué à la diffusion d'un cylindre absorbant et d'une bulle cylindrique (indice de réfraction inférieur à celui du milieu environnant).

Les faisceaux laser d'extension finie sont largement utilisés dans la métrologie optique. Pour répondre à ces besoins, TRVC a été appliqué à l'étude de diffusion d'un faisceau de forme quelconque. Ici encore, pour simplifier le problème et mettre en évidence des paramètres principaux sur les phénomènes physiques, on se limite à l'incidence normale. Après une présentation générale du formalisme - détermination de la courbure du front d'onde et la direction de propagation d'un rayon dans un faisceau, la méthode développée a été appliquée à la diffusion de trois types de faisceau gaussien : faisceau gaussien en deux dimensions, faisceau gaussien circulaire et faisceau gaussien elliptique astigmatique. Les effets de l'éclairage localisé, la focalisation du faisceau à travers le cylindre, ainsi que l'ellipticité et l'angle incidence ont été étudiés. Un accent a été mis à l'interprétation physique des phénomènes. Par exemple, lorsque la dimension du faisceau est petite devant le diamètre du cylindre, la diffusion de différents ordres sont bien isolés. Les positions des pics et l'intensité relative permet d'identifier la contribution de différents paramètre et donc très utile pour la conception de technique de mesure dédiée.

Lorsque la direction de l'onde incidente n'est pas perpendiculaire à l'axe du cylindre, la diffusion devient un problème de trois dimensions. Le tracé de rayons, le changement de l'état de polarisation et la divergence/convergence de l'onde à travers la surface de la particule ainsi que le calcul des amplitudes des ondes sont très difficiles voire impossibles dans le cadre de l'optique géométrique. La thèse présente dans le cadre de TRVC un formalisme très élégant et facile à appliquer à la diffusion en trois dimensions. Le code développé sur cette base a été validé en comparaison avec les

résultats trouvés dans la littérature pour le cas particulier - la prédiction de la caustique d'un cylindre circulaire homogène. Le code a été ensuite utilisé pour prédire la caustique d'un cylindre elliptique.

Mots clés: *Diffsion de la lumière, Tracé de Rayons Vectoriels Complexes, Cylindre elliptique, Faisceau gaussien, Incidence diagonal*

Abstract

Theoretical and numerical prediction of light scattering by particles is essential for the optical metrology in basic research and in industrial applications such as atomization, combustion, mechanics of fluids, environmental control, micro-fluidics and telecommunication. The sphere and the circular cylinder are the models the most used in optical measurement techniques, but the particles encountered in practice are not so simple. Some theories and numerical methods have developed for non spherical particles but the particle size is very limited due to difficulty of numerical calculation.

The geometrical optics is just valid for objects of size much larger than the wavelength. It is, in principle, can be applied to any shaped particles. However it is rarely used to predict quantitatively the light scattering of particles, because it is not so simple for complex shaped particles and its accuracy is not very satisfactory. In order to overcome these difficulties, Ren et al. have developed the Vectorial Complex Ray Model (VCRM) by introducing the wavefront curvature.

In this thesis, VCRM is applied to the scattering of a plane wave by an infinite elliptical cylinder at normal incidence. By comparison with Lorenz-Mie theory, it is shown that VCRM can predict the scattering of particles of size more than tens of wavelengths with good precision. The scattering diagrams of an elliptic cylinder are sensitive to its ellipticity and the incident angle with the axis of the ellipse. The rainbow structures are very sensitive to the ellipticity of the cylinder and the incident angle of the wave plane, some orders of rainbows may disappear and others are doubled. The scattering of an absorbing and bubble ($m < 1$) cylinder are also studied.

VCRM is then applied to the scattering of shaped beam, also at normal incidence. After a general presentation of the formalism for determining the curvature of the wavefront and the direction of a ray in the beam, the developed code has been applied to the prediction of three types of Gaussian beam: 2 dimensional Gaussian, circular Gaussian beam and astigmatic elliptical Gaussian beam. The focusing effects of the beam through the cylinder is studied and interpreted in term of VCRM. When the beam is small, the positions of the peaks and the relative intensity allows to identify the contribution of different parameter and therefore very useful for the design of dedicated measurement technique.

At diagonal incidence, the scattering problem becomes 3D. A very elegant formalism is derived. A code is developed and validated by comparison with the results in the literature for a homogeneous circular cylinder. It is then used to predict the caustic of an elliptic cylinder.

KeyWord: *light scattering, geometrical optics, Vectorial Complex Ray Model, elliptical cylinder, Gaussian beam, diagonal incidence*